ABSTRACT

PRICE, TIMOTHY KEITH. Permeation Testing of Mechanically Deformed Thin Chemical Protective Clothing Material. (Under the direction of Timothy Gladstone Clapp and Juan Paulo Hinestroza).

This research work presents a comprehensive analysis of permeation testing of mechanically deformed thin films. Specifically this research includes permeation testing of single component, binary, and ternary organic mixtures through virgin and radially deformed neoprene to obtain a better understanding of the material barrier properties under realistic use conditions.

A standardized ASTM D2000BC neoprene rubber was used in all experiments to evaluate the permeation behavior of samples under virgin and uniform radial deformation when exposed to single component, binary and ternary chemical mixtures. 2-Chloro-1,3-butadiene (neoprene) was used as a representative chemical protective clothing and liquid acetone, toluene, and p-xylene were used to create single component, binary, and ternary mixtures for the challenging agent. The challenge agents were chosen to have different characteristic FTIR peaks in order compare experimental data with previous experimental reports. Uniform radial mechanical deformation was induced to the material using a novel deformation apparatus.

Steady state permeation rate results from experiments performed under radial deformation do not agree qualitatively with previously reported biaxial and uniaxial experiments on stress enhanced transport as an initial decrease in SSPR then increase with increasing deformation was observed in the majority of experiments. Previous studies on uniaxial deformation in the elastic region of the polymeric material increased permeation and higher deformations in the inelastic region decreased permeation. Initial

observation indicates that radial deformation is causing morphological changes in the material differing from that seen in biaxial and uniaxial deformation. A unified BT for each component was observed with mixtures and a decrease in BT with increased deformation was evident in all experiments. Interesting observations were made about the challenging agents. Xylene has elevated SSPRs in all experiments and chemical combinations. Chemical reactions between solvent and material appear to be the cause of higher permeation rates. In single component experiments, toluene has the highest SSPR and shortest BT with the exception of xylene as a result of the similarity of solubility parameters. Acetone exhibits the same behavior as toluene in single component experiments and in binary experiments acetone transport was facilitated by toluene as it was the higher permeating component.

PERMEATION TESTING OF MECHANICALLY DEFORMED THIN CHEMICAL PROTECTIVE CLOTHING MATERIAL

by
TIMOTHY KEITH PRICE

A thesis submitted to the Graduate Faculty of
North Carolina State University
in partial fulfillment of the
requirements for the Degree of
Master of Science

TEXTILE ENGINEERING

Raleigh, NC

2007

APPROVED BY:

_____
Dr. Timothy G. Clapp
Chair of Advisory Committee

_____ _____
Dr. Jeffrey Ray Thompson Dr. Marian G. McCord

BIOGRAPHY

Timothy Keith Price was born July 28, 1982 to Tony and Joan Price in Kinston, North Carolina. He grew up in Pink Hill and attended East Duplin High School where he graduated in June of 2000.

In August of 2000, Tim moved to Raleigh, North Carolina to attend North Carolina State University. Tim studied Textile Engineering at State University. Outside of class, Tim performed with the NCSU Wolfpack Clogging Team. During his senior year, Tim along with Senior Design teammates began work with Dr. Hinestroza on a novel mechanical deformation device. The device induces uniform radial deformation to thin films while accompanying the ASTM F739 permeation cell. Tim graduated with Honors from North Carolina State University with a Bachelor of Science in Textile Engineering in June 2004. That fall Tim began working towards a Master of Science in Textile Engineering at North Carolina State University under the direction of Dr. Timothy Clapp and Dr. Juan Hinestroza.

Tim will graduate with the Degree of Master of Science in May 2007.

ACKNOWLEDGEMENTS

I would like to gratefully acknowledge my advisors Dr. Timothy Clapp and Dr. Juan Hinestroza for their vast knowledge and guidance.

I would like to thank my committee members Dr. Marian McCord and Dr. Jeffrey Thompson for their guidance and support.

I am grateful to all of my fellow graduate and undergraduate students who have helped me along the way to completing my thesis as well as lending an hear to listen when I needed it. I am especially thankful to Brian Shiels for his guidance and teaching on conducting permeation experiments and Michael Crouch for his knowledge of Omnic and collecting data from the experiments conducted.

I am especially grateful to all of my friends for giving me support when it seemed as though completing my graduate work was impossible and all the great times we have shared.

Most importantly I would like to thank my close and loving family. My parents have always been there for me and ever so through graduate school. Encouraging words, emotional support, and just being there for whatever I needed, has helped me through this experience along my professional path.

TABLE OF CONTENTS

LIST OF FIGURES ..... **vi**

LIST OF TABLES ..... **ix**

CHAPTER 1: INTRODUCTION **1**

1.1 PURPOSE 1
1.2 NEED 1
1.3 CHALLENGES 4
1.4 RESEARCH OBJECTIVES 5

CHAPTER 2: LITERATURE REVIEW **6**

2.1 FUNDAMENTALS 6
2.1.1 Permeation 6
2.1.2 Theoretical 11
2.1.3 Deformation 12
2.2 EXISTING TECHNIQUES IN PERMEATION 13
2.2.1 ASTM F-739 13
2.2.2 Other Permeation Methods 18
2.3 PERMEATION UNDER STRESS 22
2.4 PERMEATION OF MIXTURES 29
2.5 DESIGN OF EXPERIMENTS MIXTURES 31

CHAPTER 3: EXPERIMENTAL **34**

3.1 PERMEATION TESTING 34
3.2 PERMEATION UNDER UNIFORM RADIAL DEFORMATION 34
3.2.1 Design of Experiments 37
3.2.2 Materials 38
3.2.3 Methods 41

CHAPTER 4: RESULTS AND DISCUSSION **48**

4.1 PERMEATION UNDER UNIFORM RADIAL DEFORMATION 48
4.2 INITIAL RESULTS 48
4.2.1 Single Component Permeation 51
4.2.2 Binary Mixture Permeation 60
4.2.3 Ternary Mixture Permeation 72
4.3 CONFIRMATION RUN 74

CHAPTER 5: FUTURE WORK **81**

5.1 FUTURE EXPERIMENTS 81

REFERENCES.....83

APPENDICES.....91

APPENDIX A Randomized run order of experiments.....92
APPENDIX B FTIR peak area conversion to concentration.....95
APPENDIX C Flux versus time graphs for the 84 experimental combinations....96

LIST OF FIGURES

Figure 1: Permeation Test Cell 15
Figure 2: Fully Flooded Test Cell 21
Figure 3: Apparatus Cycle for Deforming Sample Material and Monitoring Permeation using FTIR 24
Figure 4: Testing Apparatus 25
Figure 5: Modified ASTM F739 permeation cell in deformation apparatus 36
Figure 6: Simplex-lattice containing all mixture combinations 38
Figure 7: Experimental setup 40
Figure 8: Bottom clamping ring and deformation ring 42
Figure 9: Sample in place with clamping and stabilizing ring 43
Figure 10: Full infrared spectrum 45
Figure11: Close-up spectra showing linear increase in peak area with increasing toluene concentration 46
Figure 12: Toluene SSPR trend over increasing deformation 54
Figure 13: Xylene SSPR trend over increasing deformation 56
Figure 14: Acetone flux at increasing deformation levels 57
Figure 15: Acetone SSPR trend over increasing deformation 58
Figure 16: Acetone SSPR with increasing deformation and % mixture 64
Figure 17: Toluene SSPR with increasing deformation and % mixture 65
Figure 18: Acetone SSPR with increasing deformation and % mixture 66
Figure 19: Xylene SSPR with increasing deformation and % mixture 67
Figure 20: 20% xylene 80% acetone binary mixture flux at 0% deformation 68
Figure 21: Toluene SSPR with increasing deformation and % mixture 69
Figure 22: Xylene SSPR with increasing deformation and % mixture 70
Figure 23: 20% xylene 60% acetone 20% toluene ternary mixture flux at 0% deformation 74
Figure 24: Confirmation results for SSPR of pure toluene using deformation as a categorical variable 76
Figure 25: Confirmation results for SSPR of pure toluene under 5% deformation increments 77
Figure 26: Confirmation results for BT of pure toluene under 5% deformation increments 78
Figure 27: Change in thickness with increased deformation 78
Figure 28: Decrease in BT with increasing deformation 79
Figure 29: 100% toluene flux 0% deformation 96
Figure 30: 100% toluene flux 20% deformation 97
Figure 31: 100% toluene flux 30% deformation 97
Figure 32: 100% toluene flux 40% deformation 98
Figure 33: 20% acetone 80% toluene flux 0% deformation 98
Figure 34: 20% acetone 80% toluene flux 20% deformation 99
Figure 35: 20% acetone 80% toluene flux 30% deformation 99
Figure 36: 20% acetone 80% toluene flux 40% deformation 100
Figure 37: 40% acetone 60% toluene flux 0% deformation 100
Figure 38: 40% acetone 60% toluene flux 20% deformation 101

Figure 39: 40% acetone 60% toluene flux 30% deformation 101
Figure 40: 40% acetone 60% toluene flux 40% deformation 102
Figure 41: 60% acetone 40% toluene flux 0% deformation 102
Figure 42: 60% acetone 40% toluene flux 20% deformation 103
Figure 43: 60% acetone 40% toluene flux 30% deformation 103
Figure 44: 60% acetone 40% toluene flux 40% deformation 104
Figure 45: 80% acetone 20% toluene flux 0% deformation 104
Figure 46: 80% acetone 20% toluene flux 20% deformation 105
Figure 47: 80% acetone 20% toluene flux 30% deformation 105
Figure 48: 80% acetone 20% toluene flux 40% deformation 106
Figure 49: 100% acetone flux 0% deformation 106
Figure 50: 100% acetone flux 20% deformation 107
Figure 51: 100% acetone flux 30% deformation 107
Figure 52: 100% acetone flux 40% deformation 108
Figure 53: 20% xylene 80% toluene flux 0% deformation.....108
Figure 54: 20% xylene 80% toluene flux 20% deformation.....109
Figure 55: 20% xylene 80% toluene flux 30% deformation.....109
Figure 56: 20% xylene 80% toluene flux 40% deformation.....110
Figure 57: 20% xylene 20% acetone 60% toluene flux 0% deformation 110
Figure 58: 20% xylene 20% acetone 60% toluene flux 20% deformation 111
Figure 59: 20% xylene 20% acetone 60% toluene flux 30% deformation 111
Figure 60: 20% xylene 20% acetone 60% toluene flux 40% deformation 112
Figure 61: 20% xylene 40% acetone 40% toluene flux 0% deformation 112
Figure 62: 20% xylene 40% acetone 40% toluene flux 20% deformation 113
Figure 63: 20% xylene 40% acetone 40% toluene flux 30% deformation 113
Figure 64: 20% xlyene 40% acetone 40% toluene flux 40% deformation 114
Figure 65: 20% xylene 60% acetone 20% toluene flux 0% deformation 114
Figure 66: 20% xylene 60% acetone 20% toluene flux 20% deformation 115
Figure 67: 20% xylene 60% acetone 20% toluene flux 30% deformation 115
Figure 68: 20% xylene 60% acetone 20% toluene flux 40% deformation 116
Figure 69: 20% xylene 80% acetone flux 0% deformation 116
Figure 70: 20% xylene 80% acetone flux 20% deformation 117
Figure 71: 20% xylene 80% acetone flux 30% deformation 117
Figure 72: 20% xylene 80% acetone flux 40% deformation 118
Figure 73: 40% xylene 60% toluene flux 0% deformation.....118
Figure 74: 40% xylene 60% toluene flux 20% deformation.....119
Figure 75: 40% xylene 60% toluene flux 30% deformation.....119
Figure 76: 40% xylene 60% toluene flux 40% deformation.....120
Figure 77: 40% xylene 20% acetone 40% toluene flux 0% deformation 120
Figure 78: 40% xylene 20% acetone 40% toluene flux 20% deformation 121
Figure 79: 40% xylene 20% acetone 40% toluene flux 30% deformation 121
Figure 80: 40% xylene 20% acetone 40% toluene flux 40% deformation 122
Figure 81: 40% xylene 40% acetone 20% toluene flux 0% deformation 122
Figure 82: 40% xylene 40% acetone 20% toluene flux 20% deformation 123
Figure 83: 40% xylene 40% acetone 20% toluene flux 30% deformation 123
Figure 84: 40% xylene 40% acetone 20% toluene flux 40% deformation 124

Figure 85: 40% xylene 60% acetone flux 0% deformation 124
Figure 86: 40% xylene 60% acetone flux 20% deformation 125
Figure 87: 40% xylene 60% acetone flux 30% deformation 125
Figure 88: 40% xylene 60% acetone flux 40% deformation 126
Figure 89: 60% xylene 40% acetone flux 0% deformation 126
Figure 90: 60% xylene 40% acetone flux 20% deformation 127
Figure 91: 60% xylene 40% acetone flux 30% deformation 127
Figure 92: 60% xylene 40% acetone flux 40% deformation 128
Figure 93: 60% xylene 20% acetone 20% toluene flux 0% deformation 128
Figure 94: 60% xylene 20% acetone 20% toluene flux 20% deformation 129
Figure 95: 60% xylene 20% acetone 20% toluene flux 30% deformation 129
Figure 96: 60% xylene 20% acetone 20% toluene flux 40% deformation 130
Figure 97: 60% xylene 40% acetone flux 0% deformation 130
Figure 98: 60% xylene 40% acetone flux 20% deformation 131
Figure 99: 60% xylene 40% acetone flux 30% deformation 131
Figure 100: 60% xylene 40% acetone flux 40% deformation 132
Figure 101: 80% xylene 0% toluene flux 0% deformation.....132
Figure 102: 80% xylene 20% toluene flux 20% deformation.....133
Figure 103: 80% xylene 20% toluene flux 30% deformation.....133
Figure 104: 80% xylene 20% toluene flux 40% deformation.....134
Figure 105: 80% xylene 20% acetone flux 0% deformation 134
Figure 106: 80% xylene 20% acetone flux 20% deformation 135
Figure 107: 80% xylene 20% acetone flux 30% deformation 135
Figure 108: 80% xylene 20% acetone flux 40% deformation 136
Figure 109: 100% xylene flux 0% deformation.....136
Figure 110: 100% xylene flux 20% deformation.....137
Figure 111: 100% xylene flux 30% deformation.....137
Figure 112: 100% xylene flux 40% deformation.....138

LIST OF TABLES

Table 1: Initial experimental results 49
Table 2: Single component experimental results 51
Table 3: BT comparison of Li et al. to Neoprene 52
Table 4: Binary mixture experimental results 61
Table 5: Ternary mixture experimental results 72
Table 6: Confirmation experimental results 75
Table 7: Randomized run order of experimental combinations 92
Table 8: Concentration calculations 95

Chapter 1: Introduction

1.1 Purpose

This research work presents a comprehensive analysis of permeation testing of mechanically deformed protective clothing material. Specifically this research includes permeation testing of single component, binary, and ternary organic mixtures through virgin and radially deformed neoprene.

Materials used in chemical protective clothing (CPC) such as gloves, boots, and body suits are faced with deformation at mobile joints in the body [38, 61]. A current test method, ASTM F739, test a specimen in its virgin undeformed state. This testing condition leaves much to be known about the actual barrier properties of a material under deformation. In actual use conditions the CPC is subject to stresses and deformation which in the presence of organic chemicals have been reported to cause swelling of the material. While some investigators have performed permeation testing under uniaxial and biaxial deformation, this research work is novel as none have incorporated a means of uniform deformation or radial deformation [38, 61]. Furthermore, the study of organic mixtures under these deformation conditions has not been performed.

The current research aims to use experimental conditions similar to actual use to study the effects of uniform radial deformation on permeation and material performance.

1.2 Need

The need for this research work is evident in any environment where chemical protective clothing is a necessity. First, are the professions that require the use of CPC's with a specific example in pesticide application and some studies on CPC.

Representative testing is also necessary to demonstrate that a material is suitable for a particular application depending on the substance that will be in contact. Specifically a material should be tested in several conditions that would be encountered in the working environment including mechanical deformation, mixtures of chemicals, and environmental conditions.

Awareness of risks involved in chemical contamination of the skin is essential for professions such as people applying pesticides, firefighters, surgical and clinical staffs, etc. Therefore, an increasing range of professions choose and are required to wear protective clothing to avoid toxic and harmful chemicals from contacting the skin. Contamination of CPC can result in dermal contact, inhalation, thermal hazards such as freezing of the skin from rapid evaporation of liquefied gases, etc. Chemical protective clothing (CPC) can include gloves, boots, suits, facemasks, and other components depending on the profession. Along with the increasing demand for CPC, there is an increasing need for testing protective clothing and developing new CPC [30, 32, 38].

Pesticides can cause harmful consequences to humans and the environment. Contact with pesticides can result in health problems such as rashes, respiratory ailments, reproductive problems, cancer, Parkinson's disease, etc. The CPC for pesticide applicator professionals include protective goggles preventing vision impairment or blindness and nose and mouth facemasks providing protection from dangerous and possibly fatal respiratory exposure. Gloves must also be worn, but applicator professionals must be aware that pesticides can absorb through skin and possibly protective clothing. A study testing the permeation of solvents and pesticide chemicals

through gloves worn by applicators concluded that within one half hour penetration of the chemicals had occurred. A simulation study conducted for permethrin-based pesticide resulted in absorption through protective gloves in 25 of 30 pilot tests. Another study performed within a greenhouse where applicator professionals wore gloves and facemasks, found exposure to the chemicals through blood testing [65].

Full body protective clothing is extremely important to pesticide applicators. However, applicators should not rely on the clothing preventing penetration from chemical exposure. A study testing the penetration of protective clothing resulted in 95% of samples that pesticides were able to get beneath the protective coveralls. The fabric used in CPC for pesticide applicators also contributes to the amount of pesticide exposure. A study showed that 20 to 30% of concentrated herbicide flowed through untreated polyester fabric, whereas 10 to 20% penetrated cotton/polyester blend. Another study tested four types of water repellant fabrics used for CPC and resulted in penetration of all four fabrics by a concentrated insecticide solution. A study found that herbicide did not penetrate through repellent treated cotton/polyester blends or polyester fabric except for one CPC. The CPC that was penetrated contained the heaviest amount of simulated "wear" [65]. This suggests that deformed protective fabrics are more likely to be penetrated than unworn protective fabrics, where the fabrics are the same indicating that permeation testing needs to be conducted in a manner simulating wear conditions instead of in the virgin state.

An example of the need for representative testing and adequate awareness of proper CPC use is evident in the case of Dr. Karen Wetterhahn who died as a result of

exposure to dimethylmercury. The Material Safety Data Sheets (MSDS) prepared by the manufacturer and supplier of the dimethylmercury did not indicate the correct gloves to wear when handling the compound. Permeation tests were conducted at Dartmouth College using ASTM test method F739 on disposable latex and polyvinyl chloride gloves to determine the permeability. The tests conducted found that the dimethylmercury permeated the material within 15 seconds or less. Modifications to the test method were required to account for the permeation rate [11]. This incident clearly shows that proper testing on the CPC and awareness of CPC use was not employed.

1.3 Challenges

Experimental challenges evident from this work and other work may come from the fact that such testing is expensive and time consuming. The equipment and methods employed in permeation testing are expensive. The glass permeation cells required for testing have to be custom fabricated. Costly analytical techniques are required to identify the permeant and quantity permeated during testing. Furthermore, in order to deform the material, a device has to be used in conjunction with the permeation equipment in order to induce the deformation. This device can also be expensive to fabricate and require computer interface. For these reasons only a few investigators have studied permeation alone or under deformation.

Other challenges may come from the material itself and the chemicals used for testing. Polymer films with uniform thickness are hard to manufacture and therefore present a problem in material evaluation because breakthrough times have been found to be a linear function of material thickness [34, 37, 40, 74, 75]. Also of importance is the

selection of chemicals that do not occupy the same spectral peaks on the infrared absorbance spectrum. Peaks that overlap would make permeant identification and quantity permeated difficult to determine.

1.4 Research Objectives

The basic objective of this work is to conduct permeation testing of single component, binary and ternary chemical mixtures on neoprene rubber under virgin and uniform radial deformation to study the effects on the barrier properties of the material under realistic use conditions. A standardized ASTM D2000BC neoprene rubber was used in all experiments in order to have meaningful comparisons among other studies. The challenge agents were chosen to have different characteristic peaks in order to evaluate the data and compare with previous experimental data.

Specific objectives of this work include:

1. Determine breakthrough times for single component, binary, and ternary mixtures using ASTM F739 in virgin and deformed state.
2. Determine steady state permeation rate for single component, binary, and ternary mixtures using ASTM F739 in virgin and deformed state.
3. Determine effects of uniform radial deformation on the permeation behavior of organic chemicals and mixtures thereof.
4. Determine effects of mixtures of chemicals on permeation behavior.

Chapter 2: Literature Review

2.1 Fundamentals

Developments in permeation testing have been slow. One main aspect of protection associated with protective clothing is permeation. Permeation is a complex process that involves both thermodynamics and kinetics. A second aspect is that of deformation encountered when protective clothing is worn. The combination of the two can have effects on the protective ability of protective clothing.

2.1.1 Permeation

Permeation is defined as the process by which a chemical moves through a protective clothing material on a molecular level [8]. Permeability is the capacity of a porous material for transmitting a fluid [54]. Liquid permeation through a membrane includes three steps, entry on one side of the material, movement through the material, and exit on the other side of the material, or more formally adsorption, diffusion, and desorption respectively [2, 4]. The rate at which permeation occurs is defined as the mass of challenge agent passing through a specified surface area per unit time [33]. Permeation should not be confused with penetration which is another test method outlined by ASTM. Penetration is the bulk flow of chemical through imperfections in the material, not on a molecular level. Permeation testing is normally used to determine the protective ability of a given material and how well it will prevent a chemical from entering. Several factors can have an effect on the three steps previously mentioned and change the protective ability of a given material. Some factors include the molecular structure of the challenge agent and material, ambient temperature, stresses on the

material, and chemical interactions occurring between the material and challenging agent [3, 4, 64].

Permeation of a challenging agent into a material can be broken into two processes: solubility and diffusion. The solubility is characterized by a solubility parameter. From solubility theory, if the solubility parameter or cohesive energy of the solvent and polymer are similar they will have maximum solution and the solvent will diffuse as long as the permeant molecule can enter the lattice network of the polymer. Hildebrand correlated solubility with the cohesive properties of solvents based on the heat of vaporization and molar volume and developed the relation that the square root of cohesive energy density, C, is the solubility parameter, δ, as shown in Equation 1.

$$\delta = \sqrt{C} \qquad (1)$$

Hansen extended the solubility parameter approach to include polar and hydrogen bonding systems resulting in the relationship in Equation 2.

$$C^2 = D^2 + P^2 + H^2 \qquad (2)$$

In Equation 2 the cohesive energy density is composed of three forces that Hansen believed held a liquid together; the dispersion parameter, D, the polar parameter, P, and the hydrogen bonding parameter, H. The thermodynamic criterion of solubility is based on Equations 3 and 4.

$$\Delta G_m = \Delta H_m - T\Delta S_m \qquad (3)$$

$$\Delta G^m_{noncomb} = \varphi_1 \varphi_2 V_m (\delta_1 - \delta_2)^2 \qquad (4)$$

In Equation 3 the classic thermodynamic free energy of mixing is related to the change in enthalpy, ΔH, and entropy, ΔS, of the mixture as well as the temperature, T. From

solubility theory two substances are soluble if upon mixing their free energy of mixing is zero or negative which occurs in Equation 3 when the enthalpy of mixing is less than the entropy. Equation 4 presents the relationship between the solubility parameter and the noncombinatorial free energy of mixing based on the volume fraction of solvent and polymer, φ, and the molar volume, V_m. In this relationship all free energy effects are included except the combinatorial entropy of solution which comes from simply mixing the components. From this equation equal solubility parameters result in zero noncombinatorial free energy of mixing, implying solution, which included with a positive entropy change will ensure solution [35]. Solubility can not be fully explained by the solubility parameters as pointed out earlier because the permeant molecules must be small enough to enter the polymer network. This can be visualized by Flory's model of swelling. In the polymer network the molecular chains take on a more stretched conformation as premeant molecules are absorbed and the network swells until elastic retractive forces develop in opposition to the swelling. Equilibrium is reached when the retractive forces increase to the osmotic pressure. This model is used for cross-linked rubber but it does not explain swelling in semi-crystalline polymers [82, 85].

The kinetic component of permeation in polymers is often based on Fickean diffusion or Case I diffusion. Fickean diffusion is defined by two laws. Fick's first law describes diffusion as a steady state diffusion where the concentration in diffusion volume does not change with respect to time. This relationship can be seen in Equation 5 where J is mass flux in mg/cm^2min, D is the diffusion coefficient in cm^2/min, c is the

solvent concentration in the membrane in mg/cm^3, and x is the distance in cm from the contacted membrane surface.

$$J = -D\frac{dc}{dx} \qquad (5)$$

In Fick's first law J is proportional to the concentration gradient in the membrane. Fick's second law describes diffusion as a change in concentration within the diffusion volume with respect to time and a change in flux with respect to position as seen in Equation 6.

$$\frac{dc}{dt} = D\frac{d^2c}{dx^2} \qquad (6)$$

Fick's second law states that the challenging agent is absorbed at a rate proportional to the square root of time. The main criteria for Fickean diffusion is instantaneous achievement of equilibrium. Most polymer-solvent systems don't follow these models because the assumptions that the medium is isotropic, homogeneous, and has local equilibrium fail [53, 57, 76, 77].

Deviations, categorized as Case II, or non-Fickian diffusion, from Fickian diffusion have been observed. Alfrey characterized the sharp boundaries between swollen and unswollen portions in a penetrant-polymer membrane as Case II diffusion [67]. Deviations from Fickian diffusion result from the finite rate of structure change that every unique polymer possesses during swelling. This is the case instead of instantaneous equilibrium. Anomalous diffusion is a combination of Case I and Case II diffusion. Several other factors have been identified as aspects of non-Fickian diffusion and lead to complicate modeling of permeation behavior. These factors include degree of crystallinity, cross-linking agents, temperature, plasticizers, etc. Some of these factors

are induced by permeant interaction with the polymer as with the case of permeant-induced crystallization. A material made with plasticizers is initially highly permeable but interaction with the permeant may cause leaching effectively forcing the polymer chains closer together reducing permeability causing non-Fickian diffusion [15, 16, 26, 27, 44, 53, 79].

Permeation testing is important in protective equipment like gloves, especially if the protective equipment will be used in any type of hazardous environment. Testing of permeation is dependent on several factors such as: the concentration of chemical, the thickness of material, and contact time. Permeation begins once the material surface absorbs the challenging liquid then continues with diffusion, the movement of contaminate from a high to low concentration. The longer the protective clothing is in contact with contaminant, the higher the concentration of contaminant in the material, and the thinner the protective clothing all result in a higher amounts of permeated chemical. Degradation may occur from a chemical reaction between the protective clothing and contaminate. Degradation from contamination stands only to increase permeation by damaging the protective clothing [69].

Temperature can also affect permeation of the material. Polymers can both stretch and become soft at high temperatures or become rigid in low temperatures, each can effectively decrease the protection associated with the material [69]. Factors such as hydrogen bonding, dipole interactions, molecular size, and shape are influenced by temperature also [1, 78].

2.1.2 Theoretical

To date there are several theoretical frameworks and mathematical models to describe permeation but none have been able to incorporate all aspects [3, 29, 50]. Different theories incorporate aspects previously discussed including Fickean, swelling, and Case II behavior.

Crank proposed a model based on "history-dependent" diffusion coefficient. In this model the surface concentration remains constant during sorption. The diffusion coefficient changes in two stages both instantaneous followed by gradual toward an equilibrium value. The diffusion coefficient is a function of time and concentration. This model was able to predict many aspects of non-Fickean diffusion but failed to predict the plug-like front. The model was able to identify swelling stresses resulting from the swollen and non-swollen areas of the polymer [18].

Long and Richman challenged the sorption process proposed by Crank. The model incorporated a time-dependent surface concentration into the boundary conditions for diffusion resulting in a two stage sorption process, absorption due to initial surface concentration and that due to the time dependence of the surface concentration. This model assumes that molecular relaxation occurs in two stages, first instantaneous molecular rearrangement and then a gradual change to equilibrium, introducing the notion that there is a gradual relaxation of physical processes [46, 63]. Petropolous and Roussis contributed to the previous work with two changes. First, they used an activity term as the driving force for diffusion instead of the concentration gradient because

concentration is affected by the relaxation process. Second they applied the relaxation term to the entire material instead of the surface layer [58].

Thomas and Windle made an advance in predicting non-Fickean diffusion in the late 1970s. The model developed accounted for many non-Fickean behaviors observed in experimental testing. In the model proposed, permeant enters the polymer and creates an osmotic pressure as described earlier. The osmotic pressure, which allows more permeant to enter the polymer, causes the polymer chains to stretch. This model is based on the concentration dependence of the creep response time verifying the process is not instantaneous [70, 71].

All of these models do not consider external stress. Only a few researchers have studied the effects of stress on permeation properties of polymers. The most work has been experimental.

2.1.3 Deformation

Deformation is alteration in the shape or dimensions of an object as a result of the application of stress to it [20]. Deformation of polymers is described by viscoelasticity, in that it is a time dependent deformation. Polymers exhibit this property at room temperature because of their low melt temperature [25]. Viscoelasticity is characterized by crystalline and amorphous regions in that the crystalline regions behave like a spring and the amorphous regions behave like a fluid. Deformation in protective clothing occurs in gloves, boots, and areas such as the knees and elbows where the fabric is stretched. Deformation results from mechanical stresses and dimensional change [38]. Stress is the amount of force per cross-sectional area being applied to cause the material to deform.

At the breaking point, the stress on the material has reached its limit causing a failure in the material structure (rips, breaks, tears). The strength of a material is found by measuring the break point or the max stress a material can withstand.

Tension can be applied uniaxial, biaxial, or radial. Applying tension on a fabric causes stress in the directions of the forces being applied. Ideally, uniform deformation is the result of moving points in Euclidean space a known distance; therefore the change in area of the space, such as a triangle, circle or square, would be completely known. The location of the deformed space would not be known by the change in length of sides [31].

2.2 Existing Techniques In Permeation

Several methods have been developed for the permeation testing of chemical protective materials. The main one accepted by the scientific community is ASTM F739. The gravimetric sorption method also provides a framework for evaluating chemical protective clothing and the parameters associated with permeation.

2.2.1 ASTM F-739

Permeation testing has been developed by the American Society for Testing and Materials (ASTM) titled, *Test Method for Resistance of Protective Clothing Materials to Permeation by Liquids or Gases Under Conditions of Continuous Contact (method F739-99)*. The test method provides specifications for the design of a test cell and for the evaluation of barrier effectiveness of chemical protective clothing under continuous contact with liquids and gases [9]. The method and test cell provide standardized conditions, sample size, collection medium, and analytical limits of detection. The test method specifically calls for the material to be tested in its virgin state. Under this

condition the barrier properties are not fully realized because the test does not emulate actual use conditions. The cell is capable of being tested with gases and liquids, submersion in a liquid bath to maintain temperature control and using gas or liquid as a collection medium to be analyzed [48]. The test is used to measure and graphically analyze the breakthrough detection time (BT), normalized breakthrough detection time, and steady-state permeation rate (SSPR) of chemicals through the replicate sample materials [8]. The BT is the time at which the presence of the challenge chemical is first detected on the inside of the test sample. The BT is dependent upon the analytical method used in the test. The dependence of BT on the analytical method motivated the F23 committee to specify a normalized breakthrough time; defined as the point at which the flux reaches 0.1mg/cm^2/min for open-loop configurations and 0.25mg/cm^2/min for closed-loop configurations [7]. It is well documented that permeation breakthrough times are a linear function of material thickness [34, 37, 40, 74, 75]. The SSPR is the constant rate of permeation once all forces affecting permeation have reached equilibrium. ASTM's establishment of these two parameters provide grounds for comparison of the protective performance of different CPC materials [7]

A dual chambered test cell, shown in Figure1, is used to expose the specimen to the challenge agent. The challenge side of the test cell is equipped with a port for introduction of the challenge agent. The collection side of the test cell is equipped with inlet and outlet ports where collection medium such as nitrogen is passed [7, 80, 81].

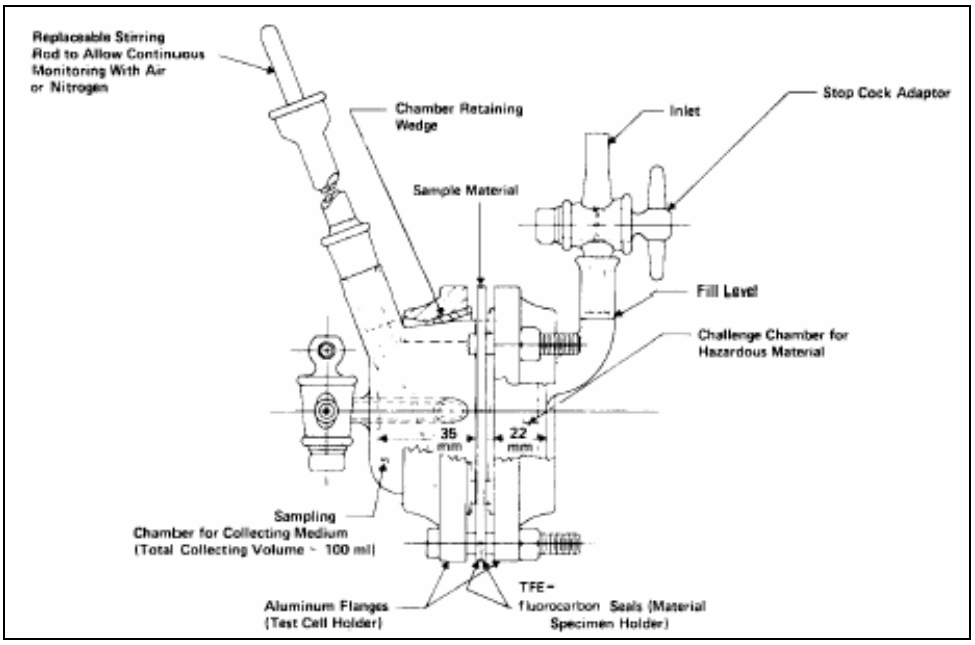

Figure 1: Permeation Test Cell [5]

The collection medium can be flowed in an open-loop or closed-loop configuration. In the open-loop configuration, the collection medium is continually passed through the system and replaced. In the closed-loop system, there is a fixed volume of collection medium that is circulated through the system. The prepared sample, conditioned at ambient room conditions, of material is clamped between the two glass chambers visible in Figure 1. The collection cell is sealed by the protective clothing material. The test temperature, duration, analytical method, and configuration are recorded with the test results [7]. The liquid or gas is analyzed for the concentration of the chemical and amount that permeated the barrier after initial contact with the sample material [8].

In order to use a gaseous collection media it is assumed that the challenge agent is volatile enough to evaporate from the inside surface of the material. The collection medium must be removed from the collection chamber and replenished. If the challenge

agent is allowed to build up in the collection chamber the chemical could saturate the collection medium and affect the concentration gradient across the membrane and/or prevent complete evaporation of the challenge agent from the material. These items can both affect the SSPR [7]. In order to prevent saturation of the collection medium or collection of the challenge agent on the membrane surface a suggested concentration of below 20 percent is suggested for the challenge agent in the collection medium [52,60].

In some experiments if the challenging agent is not volatile enough or has low water solubility, a solid sorption material has been used as the collection medium or a method of dehumidifying and heating the contaminated material [28, 59, 68]. Solid sorbants such as silicon rubber sheets have been used because of its ability to absorb and desorb hydrophobic mixtures [28]. Another method to measure the resistance of materials to low volatility materials are dynamic swelling where change in length of a membrane placed in the chemical is recorded over time [55].

Anna et al. identified that proper flow rate of the collection medium must be attained in order to maintain the desired concentration levels in the collection side of the test cell. The rate used was in the range of 0.050 to 0.150 L/min of collection medium as recommended by ASTM F739. In a study conducted on the ASTM F739 test method by Anna et al. using four glove materials and 44 challenge agents it was discovered that an increased flow rate was needed in ¾ of their experiments in order to obtain a true SSPR. Included in the first set of tests is acetone with butyl, nitrile, neoprene, and natural rubber. The tests were conducted using two ASTM permeation test cells in parallel in an open loop configuration with a nitrogen sweep. A gas chromatograph system was used to

analyze the nitrogen sweep. In order to identify the steady state permeation rate, SSPR, three consecutive points were analyzed to a standard deviation of less than 2%. If passed, the average of the three points was taken as the SSPR, and the flow rate was doubled, if the SSPR didn't change then this was taken as the correct SSPR otherwise the flow rate was doubled again to further analyze SSPR. One finding of this test proving that the proper flow rate needs to be determined for correct identification of SSPR is in the case for acetone. Several low vapor pressure permeates required a flow rate of 0.5 L/min to measure SSPR and higher permeation rates required increased flow rates. Acetone having high vapor pressure stood out in this case requiring a flow rate of 1 L/min as it permeated slowly through natural rubber [7]. From this experiment it is evident that higher permeation rates may be necessary depending on the challenging agent and collection medium as the challenge agent may not be volatile or may have a high permeation rate.

An experiment conducted by Chao, Lee, and Wu used a modified version of the ASTM F739 test method for permeation testing of organic solvents through protective nitrile gloves. Both the permeation cell and the nitrogen were kept at the same temperature by immersion in a water bath at a temperature of 25°C [14]. Anna et al used the same modified test cell in experiments. Immersion in water is a recommendation by the ASTM F739 method in an open loop system.

2.2.2 Other Permeation Methods

An alternative to the ASTM F739 test is the gravimetric sorption method which is accompanied with advantages and disadvantages. The U.S. Army Research has also developed a fully flooded test cell method to evaluate chemical protective clothing.

A method to determine the thermodynamic properties, mutual diffusion coefficient, BT, and SSPR of polymer and solvent systems is the gravimetric method [23, 41, 86]. Differential sorption experiment is an example of utilizing the gravimetric method where the diffusion process has to be Fickian in order to determine the mutual diffusion coefficient. Vrentas et al. developed a Deborah number to determine if an experiment will follow Fickian diffusion. The Deborah number is based on temperature, solvent concentration and sample thickness. If the Deborah number is sufficiently large or small, $10^{-2} <$ Deborah number $< 10^{2}$, the experiment will follow Fickean diffusion [76]. In the gravimetric sorption method, the challenge agent is on one side of a membrane and the opposite side is mounted on a balance. One limitation of this experimental method is that it can only be used with volatile chemicals, as the challenge agent has to evaporate once permeated to the opposite face of the sample. Evaporation of the chemical leads to an overall drop in mass of the system which is recorded as the breakthrough time. The SSPR is reported as the test continues. A second pitfall of the gravimetric method is the inability to analyze the permeant once evaporation has occurred [5, 56]. In this method it is assumed that there is thermal equilibrium between the film and surroundings. A study by Doumenc, Guerrier, and Allain proves this assumption wrong by looking at the mutual diffusion coefficient of polyisobutylene and

toluene for various solvent concentrations at 25°C. During an experiment, the temperature of the film surface changes due to the latent heat of vaporization, causing the film to be out of thermal equilibrium with the surroundings, which is often neglected. It was found that a small change in the sample temperature induces a change in the surface solvent concentration that can be significant compared to the solvent concentration change during the sorption [24].

Another experiment used the gravimetric method to estimate the permeation rate of chemicals through elastomeric materials. Nader and Victor used samples of neoprene, butyl and chlorinated polyethylene from gloves and garments to study the sorption and desorption of ethyl acetate. The experiment was conducted by first soaking the material in the test liquid for 72 hours and then desorbed in a thermogravimetric analyzer. The recording of weight loss against time was automated. The calculated solubility and diffusion coefficients were used to estimate the steady-state permeation rate. The purpose of this estimation technique, even though it is not exact, is to reduce chemical waste and determine the amount of additives removed from a polymer during contact with a chemical. The results of the calculated permeation rates agree with experimental data [73]. Another gravimetric study was conducted on the permeation of linear and branched ketones in biaxially oriented polyethylene terephthalate [21]. It was found that acetone has the highest diffusion coefficient out of the ketones in BPET. Several researchers have determined that sorption and desorption kinetics are described by Fickian diffusion or a two stage model using Fickian diffusion at short times and protracted polymer structural relaxation at long times [22, 41, 86]. It is stated that the

effects of morphology, orientation, and crystallinity on sorption and transport of solvents in PET are complex as they have been studied by many researchers [21].

One study conducted at National Tsing Hua University used the sorption experiment technique to examine the kinetics of acetone transport in polycarbonate under compression and with varying thicknesses. The study is based on the difference in chemical potential of organic solvent in vacuum and in polymer which causes the solvent molecules to diffuse into the polymeric matrix. The stress generated in the medium is relaxed by swelling or rearrangement of the molecular chains. Solvent transport has been classified in three cases: Case 1 transport from the concentration gradient, Case 2 transport from stress relaxation, and anomalous transport is a mixed transport of Case 1 and 2. The experiment was conducted using polycarbonate under compressive deformation and varying thickness. The samples were contained in acetone filled glass bottles until solvent saturation was reached. It was found that the activation energies of D and v for the stress-free PC were greater than those for the compressed samples because acetone is required to overcome a lower energy barrier in the compressed PC than in the stress-free PC. It was also found that acetone transport is more difficult to achieve in a thinner specimen because the activation energies of D and v increased with decreasing thickness [45].

A fully flooded test cell method has been created by the U.S. Army Research, Development and Engineering Command for convenience and ease of use. The test cell can be seen in Figure 2.

Figure 2: Fully Flooded Test Cell [66]

The experiment was conducted to study the permeation resistance of elastomeric materials to chemical warfare agents. A fully flooded test cell was used in order to maintain the maximum concentration differential for a constant permeation rate. The apparatus consists of a two piece metal cell for testing specimens 3 -5 cm in diameter. The upper section screws into the base securing the specimen. The device has an alloy cap to prevent liquid evaporation. The base has an inlet and outlet port for testing. The discussion identifies permeation as being dependent on material properties including solubility and molecular diffusion coefficient. The testing results indicate that CWA and toxic liquid permeation can be estimated using a nontoxic test liquid with a matching permeation curve or normalized kinetic and thermodynamic properties [66].

One study conducted by Pengfei et al. analyzed the change in permeation parameters of chemical protective gloves after repeated exposure to solvents and thermal

decontaminations. The materials used were neoprene, butyl, and nitrile synthetic rubber gloves. The challenging agents were toluene and acetone. The breakthrough time and steady state permeation rate were measured on each combination of material and chemical for 10 cycles. Permeation was studied similar to other experiments using a permeation cell in a closed loop system where the chemical is conserved and accumulated. After each test the material was decontaminated using heat. Thermal decontamination was found to be an effective method of removing solvents after contamination for all combinations of solvent and material except for butyl and toluene. On average, breakthrough time and steady state permeation rate increase were 11.5% and 13.7% after seven cycles of permeation and decontamination. Neoprene and acetone had mean breakthrough times of 34.0, 35.3, and 37.6 min for the new swatch, after 5 cycles, and after 10 cycles respectively. The SSPR was 259.8, 279.6, and 287.1 $\mu g/cm^2/min$ respectively. This shows that permeation remained virtually unchanged after several cycles and demonstrates that multiple reuses of some chemical protective clothing could be safe [32].

2.3 Permeation Under Stress

The drawing of polymers causes orientation which can improve barrier properties of such materials as protective clothing. A fiber that has been stretched undergoes an increase in crystallinity resulting from the elongated conformation that the polymer chains assume allowing them to pack closer. In a study where a film of linear low density polyethylene was stretched biaxially, X-ray diffraction detected increases in crystalline regions [47].

Wolf et al. have studied the effect of stress on the permeation of eight solvents on poly aryl ether ether ketone (PEEK). The study found that applied stress greatly increases the rate of diffusion and solubility for all eight solvents. When the applied stress reaches a critical value, the solubility is increased and the time to reach saturation is decreased. The solubility of toluene in semicrystalline PEEK increased from 9% to nearly 44% under 30 MPa of tensile stress. These samples were only stressed uniaxially, this was the first study to correlate stress-enhanced solubility and swelling with a critical value dependent upon degree of crystallinity, solvent, and temperature [82].

Lee et al. studied the permeation of hydrocarbons through biaxially deformed butyl rubber membranes. The study found that BT is proportional to film thickness and SSPR is dependent on deformation level. Each combination that was studied resulted in a decrease in BT and an increase in SSPR [42].

Dr. Hinestroza, and other engineers developed an apparatus that can be used in parallel with the ASTM F739 method to test permeation of chemicals on deformed sample materials. Permeation rates in real time are calculated quicker and more accurately using an infrared spectroscopic method, which measures downstream chemical concentrations. The infrared method also measures individual component transport rates for upstream drops of chemicals. The main components in the experimental setup are the ASTM F-739 permeation cell, stretching device, and a Mattson Genesis FTIR that is connected to a computer. The stretching device can stretch sample materials in biaxial and uniaxial directions. Figure 3 is an illustration of the material flow through the

apparatus beginning with deforming the fabric, conducting permeation testing, and monitoring permeation using the FTIR [38].

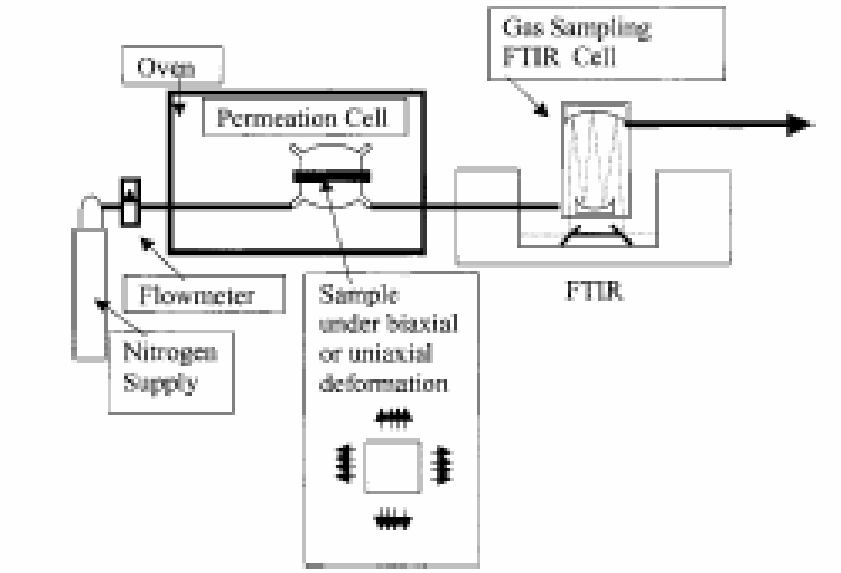

Figure 3: Apparatus Cycle for Deforming Sample Material and Monitoring Permeation Using FTIR [38]

The membrane test sample is loaded into the moveable heads and stretched to a desired deformation measured by a ruler mounted on the apparatus. The deformation, either uniaxially or biaxially, is induced by the manually controlled screw mechanism. Deformation of 200% is possible by this mechanism. The deformation apparatus was designed by the authors in order to induce uniaxial or biaxial deformation by clamping the material in the mobile heads and deforming to the desired amount monitored by ruler measurement. An inherent problem with this method of deformation is that the biaxial deformation may not be uniform in the x and y directions resulting from the fact that one direction is stretched then the perpendicular direction is stretched. The bottom permeation cell is fixed whereas the top permeation cell is attached to a clamping device. The clamping device presses the feed and permeation components to the sample material.

Permeation of the agent is measured by a nitrogen gas sweep through infrared spectroscopy [38]. The apparatus is shown below in Figure 4.

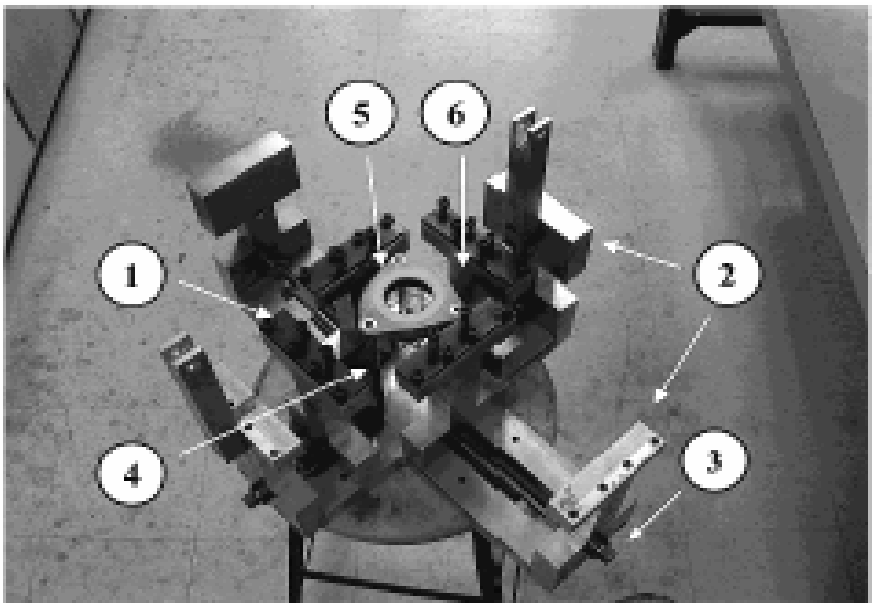

Figure 4: Testing Apparatus; (1. Mobile Heads) (2. Fixed Heads) (3. Screw System) (4. Inlet/Outlet Ports) (5. Bottom Hemisphere of Cell) (6. Test Sample) [38]

The study addressed the issue of permeation of a polymeric film under 0, 20, and 40% uniaxial and biaxial stress. The polymeric film studied was cis-1,4-polyisoprene using pure acetone, pure benzene, and a mixture of hexane, acetone, and benzene as the permeant. The experiment was conducted in real time with FTIR analysis of the downstream nitrogen sweep from the ASTM F-739 permeation cell. Using spectra analysis the breakthrough time and steady state permeation rate were recorded for each test. Flux versus time graphs are also presented. The development in this study is testing of the film under deformation, as the ASTM F-739 test method calls for testing of a material in the virgin state. The results indicate that changes in flux and breakthrough time are the result of morphological changes in the material rather than thinning resulting from deformation. The thinning was found to be negligible enough that it could not

account for changes in diffusion as seen with acetone flux increasing with small biaxial deformation then decreasing with larger biaxial deformation. This is also evident between the nonelongated, uniaxial, and biaxial deformation as steady state permeation increases by 100% under 40% uniaxial deformation but decreased by 25% when deformed 40% biaxially. The authors suggest further studies will need to be done to understand the interaction between morphological changes of the membrane under deformation and interaction with permeate [38].

Another study conducted by Hinestroza and De Kee, culminated in similar results with elongated geomembranes made of linear low-density polyethylene [39]. In this study, the membranes were challenged with methylene chloride, trichloroethylene, and a mixture of both using the same experimental technique explained previously. As with previous papers this study found that the swelling of the material and the solubility of polymer and solution effect permeation. TCE having a higher swelling value also had a lower breakthrough time. The experiments show the same results. The polymer-solution combination with similar solubility values result in higher permeation as with the LLDPE-TCE combination compared to LLDPE-MEC. It was also found that the transport of the solution mixtures had different breakthrough times in the present study because of the crystalline and amorphous structure of the material as compared to a rubbery material. Of the 50 different experimental conditions, stress-enhanced transport was found by reduction in breakthrough time by 38-45% and an increase in SSPR by 300-400% [39].

In parallel with this experimental work, Hinestroza et al. conducted a theoretical study to develop a mathematical procedure and flux versus time equation to model and predict the effect of mechanical deformation on the transport of molecules through polymeric membranes [61]. Experimental data reveal similar results with the model. The theoretical model assumes that the concentration on the downstream side of the material is not zero but a flux that is a function of the concentration and stress. Three parameters γ_1, γ_2, and γ_3 were varied to study the effect on the prediction equation. These parameters are related to molecular diffusion coefficient, D, elastic diffusion coefficient, E, and the reciprocal of the relaxation time, β, respectively as listed below:

$$\gamma_1 = \frac{D}{l^2\beta} \qquad \gamma_2 = \frac{E\upsilon_1}{l^2\beta} \qquad \gamma_3 = \frac{\upsilon_2\beta}{\upsilon_1}$$

Membrane thickness is represented by l, υ_1 and υ_2 are constants. These parameters are used in Equations 7 and 8, which relate concentration and stress, and subsequently are used to create the model equation for flux on the exit side of the membrane that is proportional to concentration.

$$\frac{\partial c}{\partial t} = \gamma_1 \frac{\partial^2 c}{\partial x^2} + \gamma_2 \frac{\partial^2 \sigma}{\partial x^2} \qquad (7)$$

$$\frac{\partial \sigma}{\partial t} + \sigma = \frac{\partial c}{\partial t} + \gamma_3 \frac{\partial^2 c}{\partial t^2} \qquad (8)$$

The article presents correlation between the theoretical and empirical results by referencing past experiments to show that varying a parameter has direct effect on flux and breakthrough time. The parameter γ_1 was increased showing an increase in flux and decrease in time to maximum flux agreeing with experimental evidence found with

increased diffusion coefficients. The parameter γ_2 was increased showing an increase in flux and time to maximum flux as a result of localized crystallinity also agreeing with experimental evidence where stressed transport resulted in an increase in time to maximum flux. Varying the parameter γ_3 shows the same results as varying γ_2 [61].

Other studies have been conducted on the transport of organic contaminants through geomembranes. These studies include permeation under biaxial and uniaxial deformation as well as with mixtures of penetrants. The results of one of the studies found that extension enhances the permeation rate through polyvinyl chloride and decreases the permeation rate in high-density polyethylene. This result is believed to be due to the structural changes resulting from extension. An example is if the extension is within the elastic region the diffusive properties of the material increase whereas if the extension causes irreversible change then the barrier properties are increased [83, 84].

De Kee et al. conducted a study on the influence of uniaxial deformation on the barrier properties of natural, bromobutyl, and nitrile rubber using dichloromethane, acetone, benzene, and toluene as challenging agents. In this study, ASTM test method F-739 was used in combination with deformations in the range of 0 to 20%. Most studies conducted in the past dealt only with residual stress and not actual testing while the material is deformed. Several results were found in this study including a relationship between molecular size of permeate, degree of swelling, and polarity. The size of the molecules affects permeation in that the larger molecules will permeate slower as found in the study between benzene and toluene where benzene had higher flux. A higher flux was found with benzene than acetone, indicative of the higher equilibrium swelling found

in benzene. Polarity was also found to play a role in permeation behavior as both polar solutions and materials had higher permeation. A decrease in breakthrough time was found with increased mechanical elongation, thought to be due to a decrease in thickness of the material. Little change was observed in the steady state permeation flux as this may increase or decrease depending on the solvent-rubber combination. The diffusion of permeate was found to increase with stress increase due to an increase in free volume [43]. Treloar, in a study conducted in 1950 observed the same effect of tensile stress on the swelling of rubber long before this experiment. Treloar found that when stress is applied to rubber, it tends to absorb more fluid than in the unstrained state [72].

Another study looked at the effect of temperature and elongation on the barrier properties of these rubbers. The diffusive properties were studied in the range of temperatures between 273 and 313 K with uniaxial elongation between 0 and 40% using the same experimental technique described previously. The study found that as temperature and elongation increase; the SSPR increases and the BT decreases [19].

2.4 Permeation of Mixtures

Permeation testing of mixtures can be conducted in the same manner as single components. A primary difficulty is measuring the time and quantity of each challenging agent. In the case of organic chemicals, gas chromatography, FTIR or GC-mass spectrography can be used as downstream detection to identify and quantify chemical permeants [51, 62]. The primary reason care needs to be taken in measuring how much and when a chemical component is permeating is because many materials are selectively

permeable [36]. This will result in the chemical components permeating at different rates.

An example of the different methods used in permeation testing of mixtures is evident in a study of permeation through a 1 mm membrane of high density polyethylene (HDPE). August and Tatzky measured transmission rates of six solvents in an equivolume mixture [10]. A dual compartment apparatus, where the compartments were separated by the HDPE membrane, was used in the experiments. The upper compartment was filled with the mixture of the six solvents and the permeant vapors were removed from the lower compartment. These vapors were frozen in a cooling trap, and analyzed using gas chromatography [10]. Britton et al. estimated the partition coefficients and diffusion coefficients of eight compounds in an HDPE membrane using the ASTM F739 method. The eight compounds were mixed in a solution with equimolar concentrations. A method of immersing the samples then weighing them was used to estimate the solubility coefficient of the permeants [13].

Nelson et al. performed studies on the permeation of bi-component mixtures through polymers. In one experiment the permeation of a mixture of toluene and chloroform through neoprene was evaluated. The permeation rates were found to be directly proportional to the relative concentrations of each solvent. In a separate experiment, a pentane and tri-chloroethylene mixture was permeated through a polyethylene glove. The permeation rate of the mixture exceeded the sum of its parts, illustrating the difficulty in accurately predicting the permeation behavior of mixtures [49].

In a study, by Xiao et al., mentioned earlier on the transport of organic contaminants through PVC and high density polyethylene geomembranes it was found that the flux of the components in a mixture was enhanced compared to single component permeation. This is believed to result from swelling caused by one or more of the components in the mixture, such as trichloroethylene, as the component with the closest solubility to the polymer will have greater solution [83, 84]. In a similar study by Hinestroza et al., also mentioned earlier on the permeation of organics through linear low density polyethylene geomembranes, facilitated transport is observed in mixtures of trichloroethylene with other chemicals, as TCE causes larger swelling [39]. Similar results were found by Georgoulis et al. in an experiment on permeation of methyl ethyl ketone (MEK) and toluene through natural rubber and nitrile gloves [33]. They observed that material swelling was a key factor in permeation of the mixture. Based on the chemical composition of material and solvent they observed that the nonpolar solvent toluene permeates more readily through natural rubber which has a nonpolar monomer. In effect the toluene swells the natural rubber more, enhancing the permeation of MEK [33]. Ultimately the permeation behavior is dependent on the mixture, solvent-solvent interaction, and can not be extrapolated from pure solvent permeability [33, 55].

2.5 Design of Experiments Mixtures

The design of experiments for mixtures is different from factorial design in that the measured response is assumed to depend only on the proportions, such as by volume, of the ingredients in the mixture and not on the amount of the mixture [6, 17]. Therefore the levels of each factor or component are not independent of the levels of other factors.

The proportions are expressed as fractions of the total mixture which must sum to unity. In a mixture design, if the proportion of one of the components is 1 it is considered a single component mixture based on the previous assumption of a fixed total volume. The mixture can be composed of 1 or many components. Each mixture design is defined by a simplex-lattice. Simplex is a term for a figure that has one more vertex than dimensions and a lattice is an ordered arrangement of uniformly spaced distribution points. The simplex-lattice can be described by {q,m}. The number of components is represented by q, with m+1 equally spaced values from 0 to 1. In the case of a three component mixture the simplex factor space is an equilateral triangle. The factor space contains 3 components consisting of all points on or inside the boundaries based on the number of proportions, such as for 2 proportions there would be 6 points. This can be visualized by,

$$X_i = 0, 1/m, 2/m, \ldots, 1$$

where X_i is the proportion for each component. The simplex lattice points would be,

$$(x1, x2, x3) = (1, 0, 0), (0, 1, 0), (0, 0, 1), (½ , ½, 0), (½, 0, ½), (0, ½, ½)$$

creating the equilateral triangle. After the experimental responses have been recorded from randomly run experiments to reflect normal process variation, a model is created to represent the response surface. The model is normally tested for adequacy to determine if the prediction tool is applicable. The purpose of the model is to measure the dependence of the response variables on the relative proportions of the components by an equation. This allows the influence, of each component alone or combined with other components, on the response to be measured. From the model equation, predictions of the response can be made and mixtures can be identified with desired results.

Interactions can be observed as either synergistic or antagonistic where components act to increase or decrease the response variable respectively [6, 17].

Chapter 3: Experimental

3.1 Permeation Testing

The experimental setup on the permeation testing of thin films of standardized neoprene, virgin and deformed, with single component, binary, and ternary mixtures are outlined. First, the setup of the entire system is presented with all the experimental and analytical equipment defined. The particular Design of Experiments conducted is also presented and outlined. Last, the materials used and the methods employed are defined so the entire experiment can be reproduced.

3.2 Permeation Under Uniform Radial Deformation

The ASTM F739 standard test method, with some modifications, and a novel deformation device was used in all permeation tests. Some modifications to the test were in the permeation cell itself. The other modifications involve the state of the material being tested. First, the orientation of the test cell was changed from its typical design, in which the barrier fabric is held in a horizontal orientation instead of the standard vertical orientation.

For this project, a deformation apparatus had been previously designed to accommodate the ASTM F739 permeation cell. The apparatus holds the test cell in the horizontal position, rotated 90 degrees from the typical orientation, as described previously and as seen in Figure 5. Note that the top chamber of the test cell in Figure 5 has two ports. This allows evaluation of both liquid and gaseous permeants using the same experimental setup. This design of the top chamber also allows it to be more easily filled with liquid challenge agents.

The ASTM F739 standard test method states the sample is to be tested in its virgin state. The deformation device was used to apply uniform radial deformation to the sample thereby allowing permeation testing of a sample under deformation up to 40 percent.

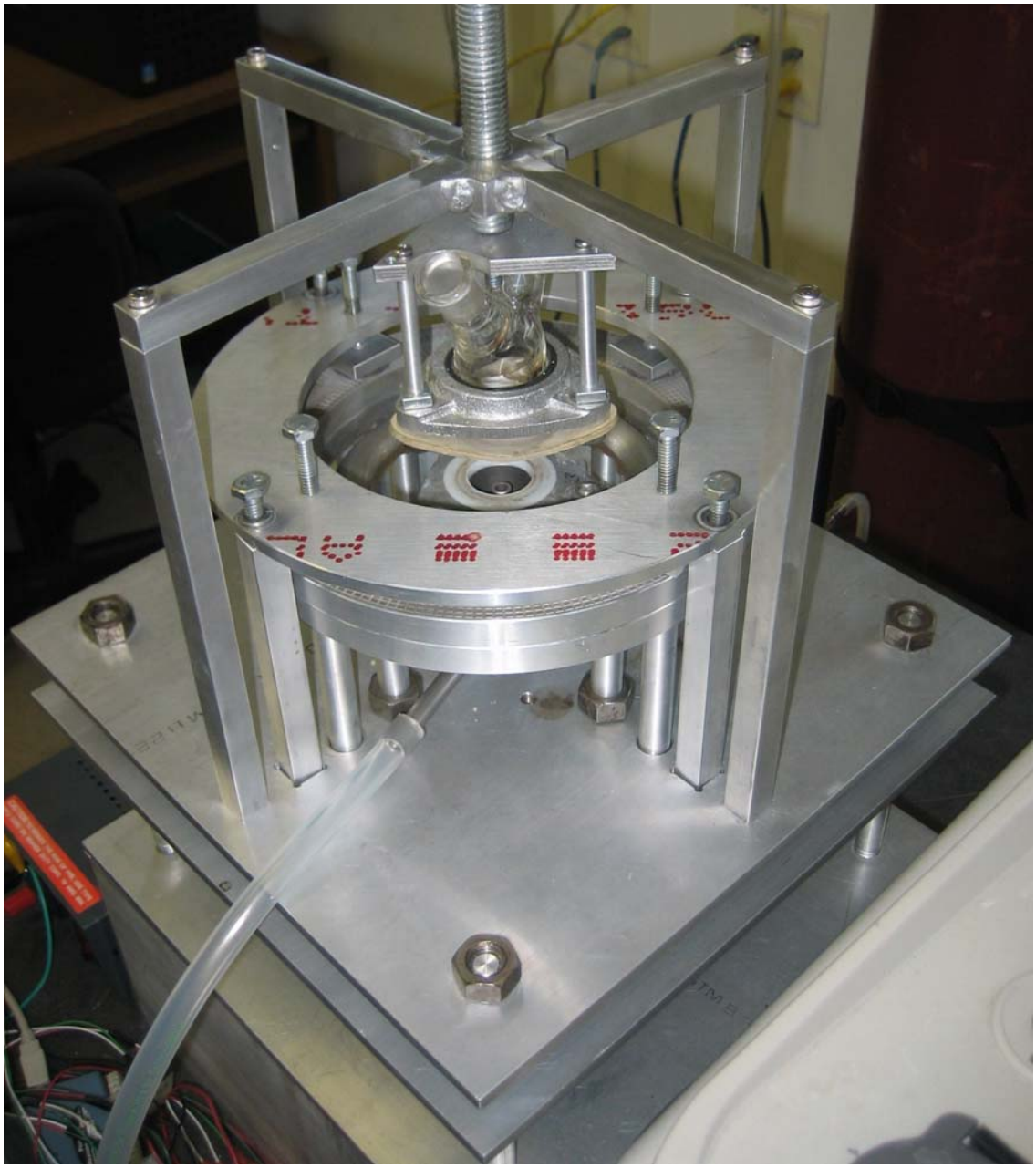

Figure 5: Modified ASTM F739 permeation cell in deformation apparatus

3.2.1 Design of Experiments

The Design of Experiments, DOE, is used to answer practical questions about the system being studied. The specific practical question is how does varying the independent factors of barrier deformation and chemical mixture composition effect the response variables BT and SSPR. The DOE is used to create an expression to answer this question based on the experimental results input into the model. The DOE was made based on a full factorial in which every possible combination of factors and levels was used. This design was used in order to have a complete representation of any main effects and interactions occurring between the chosen factors and levels. The two factors chosen were barrier deformation and chemical mixture. The deformation levels were 0, 20, 30, and 40 percent. The chemical mixtures were composed of acetone, toluene, and p-xylene. There were 21 mixtures total including all possible ternary mixtures of 0, 20, 40, 60, 80, and 100 percent. The DOE layout and random test run order of the 84 experiments can be seen in Appendix A. The simplex-lattice design can be seen in Figure 6, each mixture combination is represented by a square marker.

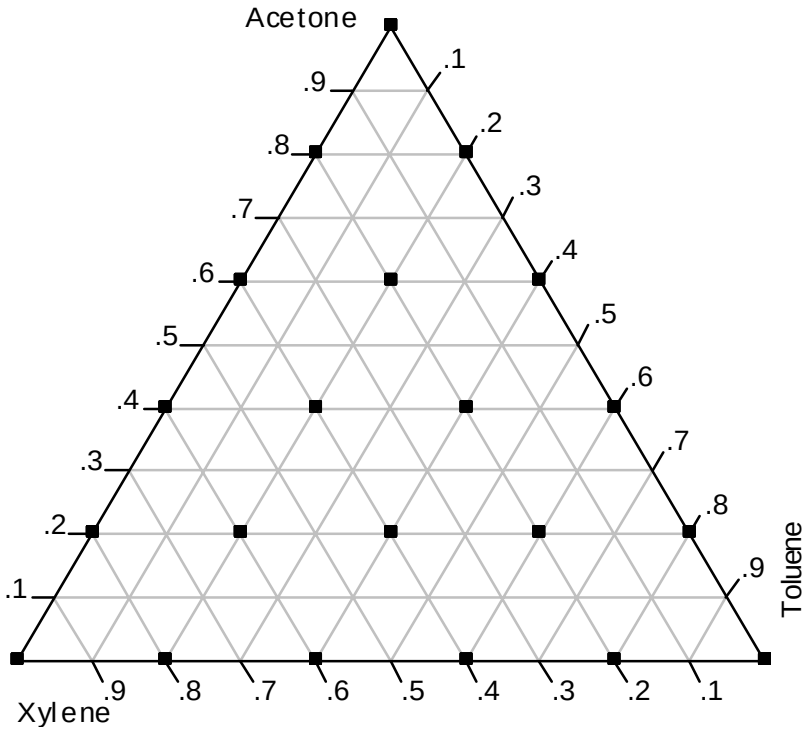

Figure 6: Simplex-lattice containing all mixture combinations

3.2.2 Materials

The liquid challenge agents for all permeation tests were 99.9% pure acetone (CAS: 67-64-1) from Sigma-Aldrich (St. Louis, MO), 99.5% pure toluene (CAS: 108-88-3) from Sigma-Aldrich (St. Louis, MO), and 99.9% pure p-xylene (CAS: 106-42-3) purchased from Fisher Scientific (Fair Lawn, NJ). The acetone, toluene, and p-xylene were received as a bulk liquid and used as received. The 21 single component, binary, and ternary chemical mixtures were made by dispensing the liquids using measuring volumetric pipettes. The mixtures were created from all possible combinations of a single component, binary, and ternary mixture in increments of 20% as follows 0, 20, 40, 60, 80, and 100 percent.

Neoprene in 0.5 mm thickness sheet form was purchased from McMaster Carr and used for the permeation tests.

The permeation cell used was designed by Brian Shiels and fabricated by the campus glass blower, Janice Singhass (Raleigh, NC). The cell meets ASTM design specifications except for the orientation of the ports. Standard aluminum flanges, chamber retaining wedges, and PTFE gaskets were used from the A.A. Pesce Glass Company (Kennett Square, PA).

All plumbing for the collection medium was made from ¼" Tygon tubing from Cole-Parmer (Vernon Hills, IL). Industrial nitrogen purchased from Machine and Welding Supply Company (Dunn, NC) was used as the collection medium.
Flow rates of the collection medium were controlled using Omega Engineering, Inc. (Stanford, CT) mass flow controllers, model FMA 1820 ST and a standard pin valve.

Quantitative and qualitative analysis of the collection medium was performed using a Thermo-Nicolet (Madison, WI) Nexus 670 FT-IR e.s.p. in conjunction with its supplied integration software. The FTIR was equipped with a variable path-length IR gas cell, model 7.2-V, from Infrared Analysis, Inc. (Anaheim, CA). The gas cell allowed for continuous sampling of the collection medium throughout the duration of the test.

The deformation device was previously designed and built by the author, and Design Project Teammates; James Damon, and Katrina Swaney. The deformation device is interfaced with Softwire for automated control of deformation. The entire system is shown in Figure 7.

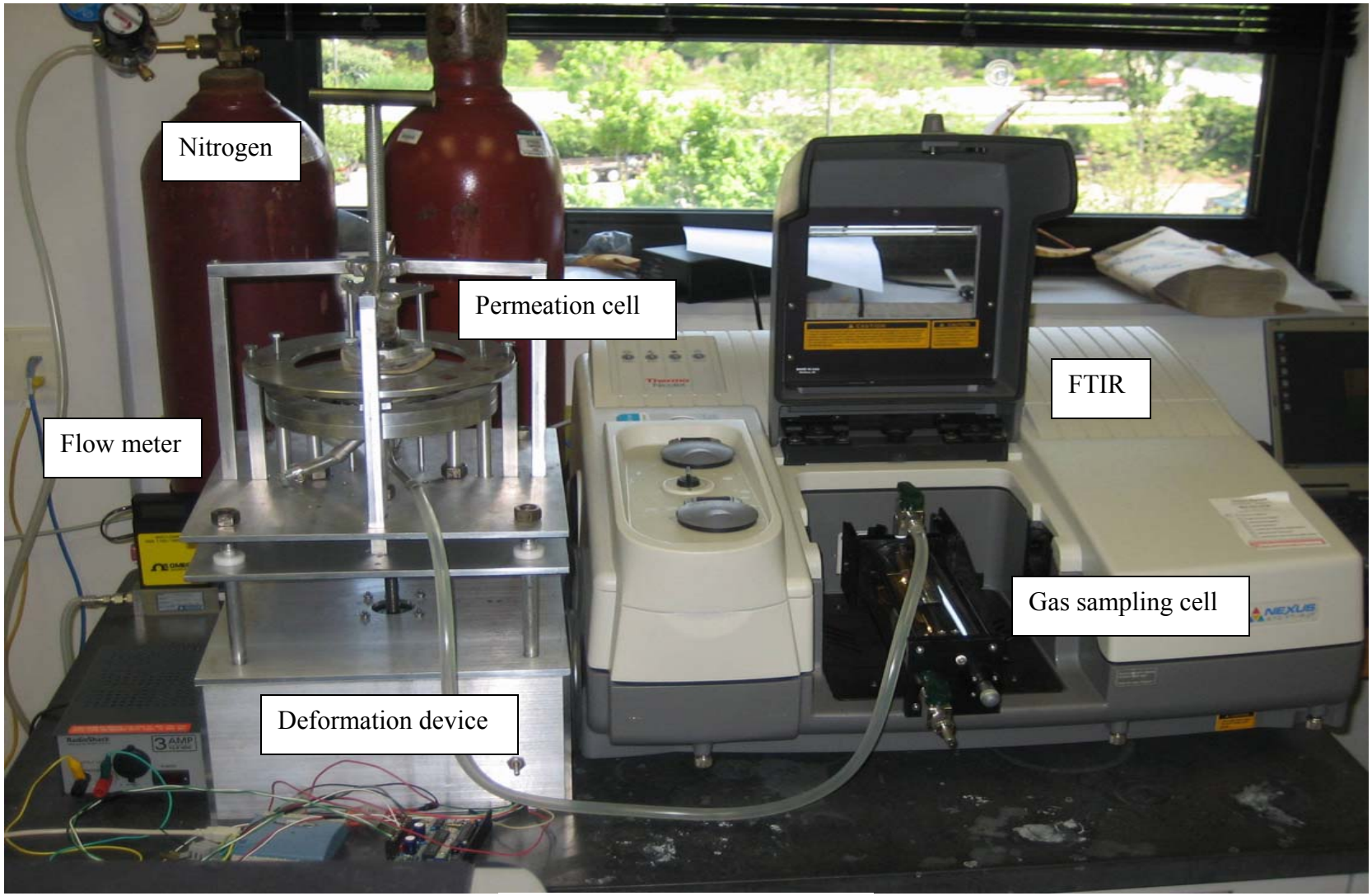

Figure 7: Experimental setup

3.2.3 Methods

The deformation apparatus was setup with the bottom-clamping ring level with the inner deformation ring as seen in Figure 8. Samples were cut from the Neoprene sheet in 8" by 8" squares to accommodate the deformation apparatus clamps and a 1" circle drawn in the center of the square with a marker. The thickness of each neoprene sample was measured to the nearest 0.001 mm using a Model II Electronic Thickness Tester from the Thwing-Albert Instrument Company (Philadelphia, PA). The sample was then centered onto the bottom-clamping ring so that material was hanging off of the sides of the bottom-clamping ring. The top-clamping ring was then placed on top of the sample and lined up with the bottom-clamping ring. Next, the stabilizing clamping ring, which is bigger than the clamping rings, was screwed into the rods and another set of screws are used to screw into shoes. The clamping and stabilizing rings can be seen in Figure 9.

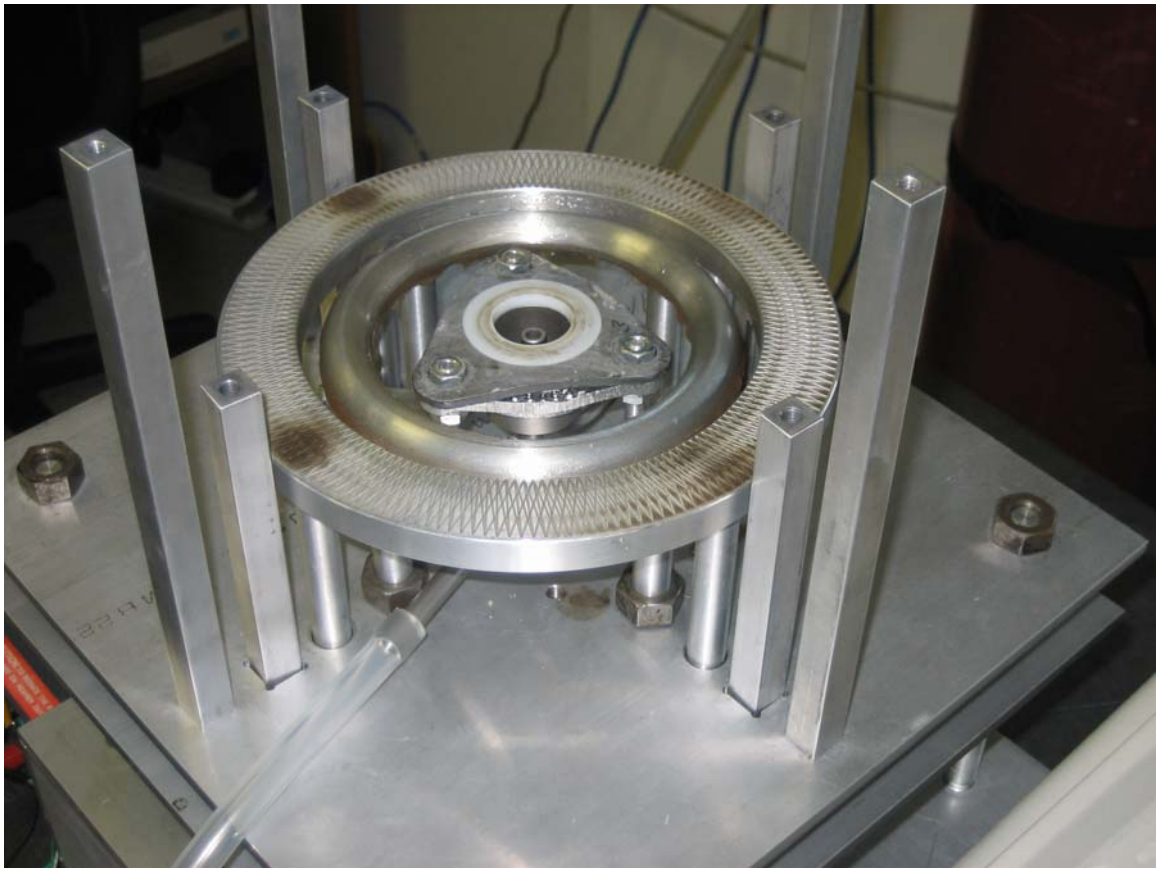

Figure 8: Bottom clamping ring and deformation ring

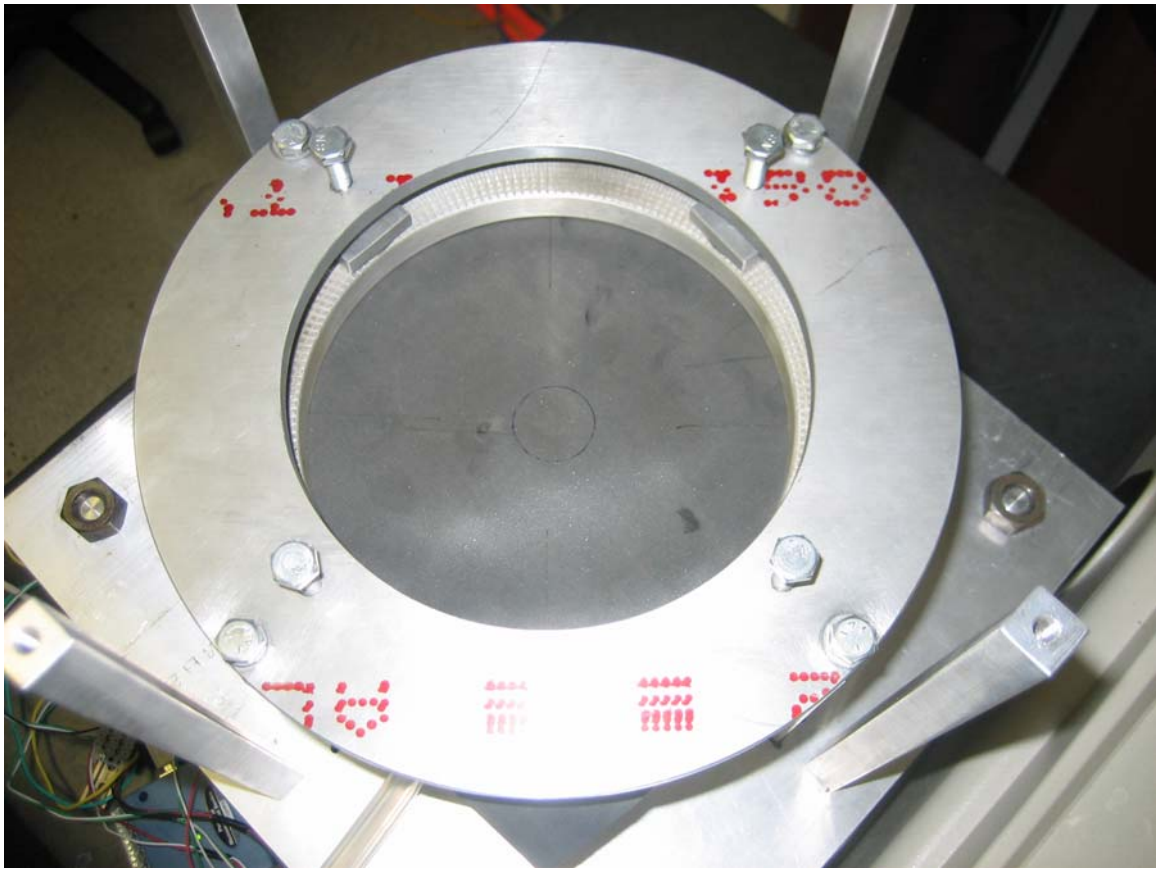

Figure 9: Sample in place with clamping and stabilizing ring

Once the sample was secured in the deformation device, the sample was deformed to 20, 30, or 40% radially depending on the experiment. The experiment conducted was selected from the randomized list of 84 experiments outlined in the Design of Experiments. The amount of deformation was determined by measuring the diameter of the circle on the sample to the nearest 0.001 mm using a Model II Electronic Calipers. Once the correct deformation was attained, the top permeation cell was screwed down onto the apparatus. This places the deformed sample between the two PTFE gaskets on test cell. Once properly sealed, flow of the collection medium was commenced at 0.7 standard liters per minute (SLPM) as controlled by mass flow. Nitrogen was allowed to flow for at least ten minutes to allow for any air or other non-collection medium gases to escape the system. After this period, a background measurement of 32 scans was collected. A new background was recorded each day. The background was saved into the Macros Basic command to be referenced throughout the duration of the test. The Macros used in all experiments were created by Michael Crouch.

The Macro was programmed to initiate a new 32-scan analysis every minute for 120 minutes. The wavenumber regions were selected based on characteristics peaks of each chemical and to prevent overlapping of peaks in order to correctly account for the type and amount of each permeant. The wavenumber regions for toluene, acetone, and p-xylene are 696-692, 1709-1685, and 799-787 respectively. The Macro was programmed to integrate the area under each peak and report the peak area into a spreadsheet in Microsoft Excel. A full infrared spectrum is illustrated in Figure 10 while Figure 11 shows the linear increase in area under the specified peak for toluene.

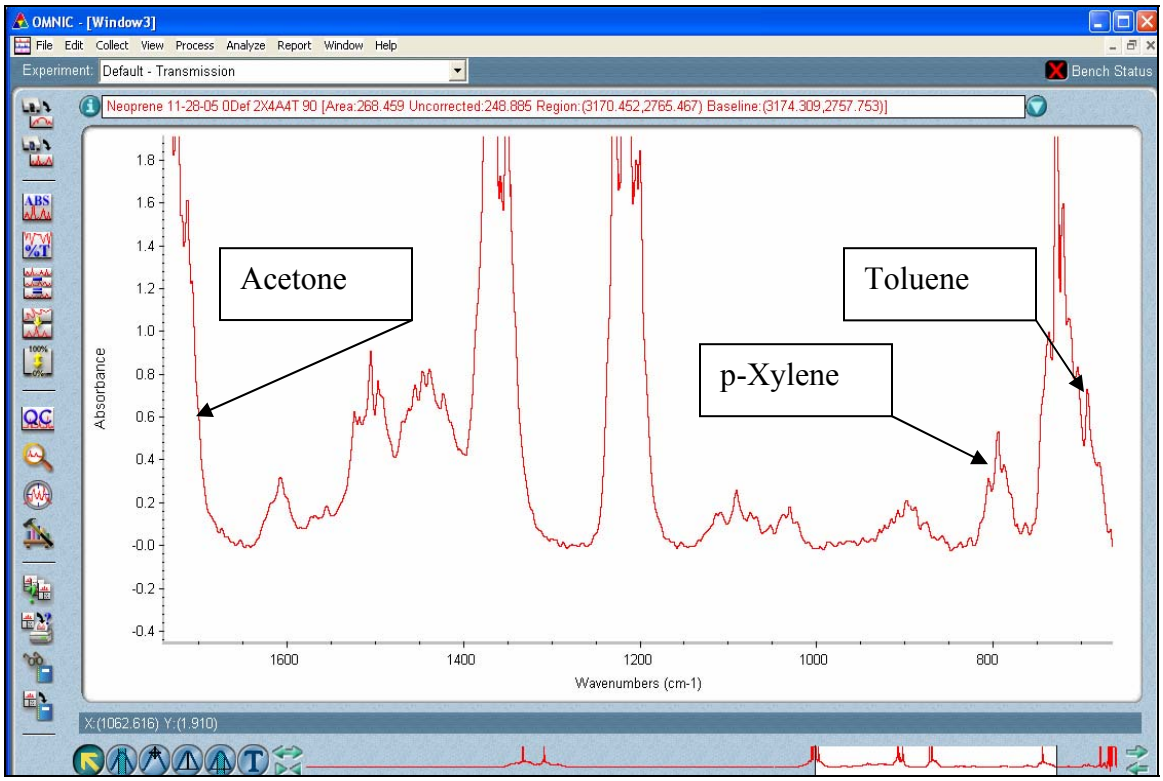

Figure 10: Full infrared spectrum

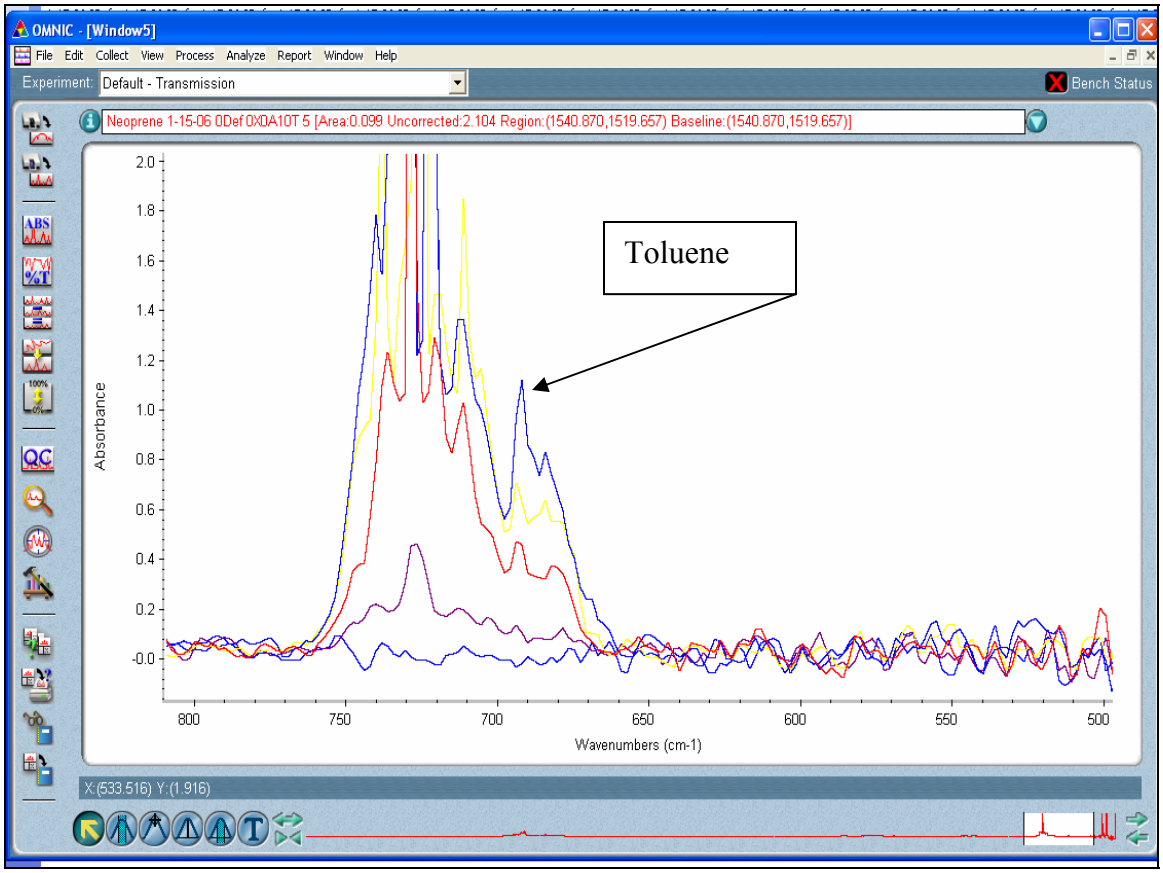

Figure11: Close-up spectra showing linear increase in peak area with increasing toluene concentration

The test was terminated after 120 data points had been collected or 2 hours had passed. After the test was complete, the remaining chemical was removed from the challenge chamber with a pipette and disposed. The deformation in the sample was removed and each sample was catalogued.

Peak area data that was recorded in the spreadsheet was correlated to concentration. Absorbance measurements in the excel data files were converted to concentration using a saturated vapor for each chemical. A saturation bubbler was used in combination with a pure nitrogen gas flow line to create varying percent mixtures. The

mixture was analyzed using the same FTIR device and macro to report the area into an Excel spreadsheet. A linear regression was fitted to area and percent mixture data in order to calculate the area for the 100 percent mixture. The value for 100% concentration was reported by Dr. Hinestroza using Aspen chemical mixture simulation software following the same experimental conditions reported earlier. The relationship between concentration and area is proportionate; therefore a multiplication factor was used to calculate the concentration that corresponds to the reported area for the saturation experiments. Another linear regression was then fitted to this data. The linear regression of concentration to area is the equation used for converting area reported in the Excel spreadsheet to concentration. Appendix B contains a table relating percent mixture to concentration for each chemical as well as the linear regression equations used to convert reported area data to concentration.

Given the known membrane area (5.067075 cm^2) for the nominal one-inch cell, the known flow rate of the collection medium (700 cm^3/min), and the measured concentration ($\mu g/cm^3$), the flux in units of $\mu g/cm^2$/min can be calculated using Equation 9. This flux is plotted against time for establishment of BT and SSPR.

$$flux = \frac{(flowrate)(concentration)}{area} \qquad (9)$$

BT in minutes was determined from the flux versus time graphs where the linear portion of the flux curve intersects the x axis. SSPR for each chemical in an experimental run was calculated based on an average of 20 flux readings after the experiment had ran for 60 minutes and the flux had equilibrated.

Chapter 4: Results and Discussion

4.1 Permeation Under Uniform Radial Deformation

Initial results for the permeation testing of single component, binary, and ternary mixtures on virgin and deformed films are presented and discussed. Each experiment ran 60 minutes. A total of 84 experiments were run under these conditions. Confirmation runs were conducted on pure toluene permeation through deformed films in increments of 5% from 0 to 40% to verify a trend visible in the SSPR of toluene with increased deformation and repeatability of experiments.

4.2 Initial Results

The initial results include the BT and SSPR for all 84 experiments conducted. All results are presented in Table 1.

Table 1: Initial experimental results

	Mixture Component						
Percent Deformation	Xylene	Acetone	Toluene	BT (min)	SSPR Xylene ($\mu g/cm^2 min$)	SSPR Acetone ($\mu g/cm^2 min$)	SSPR Toluene ($\mu g/cm^2 min$)
0	0.0	0.0	1.0	4	0	0	783
0	0.0	0.2	0.8	5	0	373	782
0	0.0	0.4	0.6	5	0	758	696
0	0.0	0.6	0.4	5	0	759	390
0	0.0	0.8	0.2	5	0	689	150
0	0.0	1.0	0.0	6	0	648	0
0	0.2	0.0	0.8	7	1713	0	540
0	0.2	0.2	0.6	6	2565	421	581
0	0.2	0.4	0.4	5	3342	713	540
0	0.2	0.6	0.2	5	2838	1022	235
0	0.2	0.8	0.0	5	2498	978	0
0	0.4	0.0	0.6	6	3026	0	312
0	0.4	0.2	0.4	5	4059	231	303
0	0.4	0.4	0.2	5	7113	748	327
0	0.4	0.6	0.0	5	6531	1061	0
0	0.6	0.0	0.4	7	4065	0	226
0	0.6	0.2	0.2	6	7248	267	215
0	0.6	0.4	0.0	5	11667	925	0
0	0.8	0.0	0.2	8	6343	0	166
0	0.8	0.2	0.0	5	15022	255	0
0	1.0	0.0	0.0	6	6238	0	0
20	0.0	0.0	1.0	4	0	0	617
20	0.0	0.2	0.8	3	0	246	611
20	0.0	0.4	0.6	4	0	345	388
20	0.0	0.6	0.4	3	0	837	395
20	0.0	0.8	0.2	4	0	335	76
20	0.0	1.0	0.0	4	0	506	0
20	0.2	0.0	0.8	5	1644	0	560
20	0.2	0.2	0.6	4	2128	209	455
20	0.2	0.4	0.4	3	2545	642	400
20	0.2	0.6	0.2	3	2731	825	235
20	0.2	0.8	0.0	4	2096	821	0
20	0.4	0.0	0.6	5	2624	0	331
20	0.4	0.2	0.4	4	3649	329	310
20	0.4	0.4	0.2	4	3681	392	156
20	0.4	0.6	0.0	4	4066	514	0
20	0.6	0.0	0.4	3	5726	0	355
20	0.6	0.2	0.2	4	5069	194	164

Table 1 (continued)

	Mixture Component						
Percent Deformation	Xylene	Acetone	Toluene	BT (min)	SSPR Xylene ($\mu g/cm^2 min$)	SSPR Acetone ($\mu g/cm^2 min$)	SSPR Toluene ($\mu g/cm^2 min$)
20	0.6	0.4	0.0	3	8131	656	0
20	0.8	0.0	0.2	7	4206	0	118
20	0.8	0.2	0.0	4	8385	192	0
20	1.0	0.0	0.0	4	10232	0	0
30	0.0	0.0	1.0	2	0	0	841
30	0.0	0.2	0.8	2	0	248	735
30	0.0	0.4	0.6	2	0	573	586
30	0.0	0.6	0.4	3	0	849	490
30	0.0	0.8	0.2	3	0	1241	212
30	0.0	1.0	0.0	4	0	231	0
30	0.2	0.0	0.8	2	2367	0	601
30	0.2	0.2	0.6	2	2285	222	554
30	0.2	0.4	0.4	2	3356	567	430
30	0.2	0.6	0.2	2	3132	1042	255
30	0.2	0.8	0.0	2	2186	577	0
30	0.4	0.0	0.6	3	2836	0	375
30	0.4	0.2	0.4	3	4851	273	427
30	0.4	0.4	0.2	2	4663	535	201
30	0.4	0.6	0.0	2	6347	1242	0
30	0.6	0.0	0.4	4	4042	0	259
30	0.6	0.2	0.2	3	5917	232	205
30	0.6	0.4	0.0	2	7351	704	0
30	0.8	0.0	0.2	2	10823	0	216
30	0.8	0.2	0.0	2	11218	220	0
30	1.0	0.0	0.0	3	10671	0	0
40	0.0	0.0	1.0	2	0	0	657
40	0.0	0.2	0.8	2	0	360	910
40	0.0	0.4	0.6	2	0	622	656
40	0.0	0.6	0.4	2	0	738	387
40	0.0	0.8	0.2	2	0	1381	267
40	0.0	1.0	0.0	2	0	366	0
40	0.2	0.0	0.8	3	2106	0	655
40	0.2	0.2	0.6	2	2892	322	670
40	0.2	0.4	0.4	2	3528	743	530
40	0.2	0.6	0.2	2	3640	1251	320
40	0.2	0.8	0.0	3	1921	571	0
40	0.4	0.0	0.6	3	4185	0	565
40	0.4	0.2	0.4	2	5880	318	464
40	0.4	0.4	0.2	2	6173	633	227
40	0.4	0.6	0.0	2	7212	1333	0
40	0.6	0.0	0.4	3	4989	0	333

Table 1 (continued)

	Mixture Component						
Percent Deformation	Xylene	Acetone	Toluene	BT (min)	SSPR Xylene ($\mu g/cm^2 min$)	SSPR Acetone ($\mu g/cm^2 min$)	SSPR Toluene ($\mu g/cm^2 min$)
40	0.6	0.2	0.2	2	8161	267	231
40	0.6	0.4	0.0	2	9524	595	0
40	0.8	0.0	0.2	2	11800	0	197
40	0.8	0.2	0.0	2	9794	175	0
40	1.0	0.0	0.0	3	9305	0	0

4.2.1 Single Component Permeation

The BT and SSPR for each single component experiment are presented in Table 2. Each challenging agent has a unique permeation behavior at each deformation level.

Table 2: Single Component Experimental Results

	Mixture Component						
Percent Deformation	Xylene	Acetone	Toluene	BT (min)	SSPR Xylene ($\mu g/cm^2 min$)	SSPR Acetone ($\mu g/cm^2 min$)	SSPR Toluene ($\mu g/cm^2 min$)
0	0	0	1	4	0	0	783
0	0	1	0	6	0	648	0
0	1	0	0	6	6238	0	0
20	0	0	1	4	0	0	617
20	0	1	0	4	0	506	0
20	1	0	0	4	10232	0	0
30	0	0	1	2	0	0	841
30	0	1	0	4	0	231	0
30	1	0	0	3	10671	0	0
40	0	0	1	2	0	0	657
40	0	1	0	2	0	366	0
40	1	0	0	3	9305	0	0

BT for each experiment decreases or remains the same with increased deformation regardless of the challenging agent. This qualitatively agrees with previous experimental evidence [19, 38, 43, 84]. Toluene has the shortest breakthrough time at 4 minutes, followed by xylene and acetone at 6 minutes under zero deformation. This is

also the case for each higher level of deformation, where Toluene either has the smaller BT or is tied with another chemical having the shortest BT. The smaller BT of toluene will be evident in the discussion of SSPR for single components; in each experiment the higher SSPR is associated with a lower BT as a result of similarity in solubility parameters.

In a similar study the breakthrough times of acetone, toluene, benzene, and dichloromethane (DCM) through natural (NR), bromobutyl (BIIR), and nitrile (NBR) rubber were found to decrease as elongation increased [43]. In this study by Li et al. the actual breakthrough times for acetone and toluene through NR, BIIR, and NBR are 4 and 3 times, 113 and 8, 3 and 10 times larger respectively than in the present study at 0 deformation. The experimental values of the study by Li compared to the present study can be seen in Table 3.

Table 3: BT comparison of Li et al. to Neoprene

			Acetone	Toluene
	Material Thickness (mm)	Solubility Parameter	20.3	18.2
			BT (min)	
NR	0.75	16.6	26	13
BIIR	0.8	-	680	31
NBR	0.8	20.2	19	43
Neoprene	0.5	16.6-19.2	6	4

The higher BT values in the study by Li et al. can be the result of several factors. First, different rubbers are being tested than in the present study with a thickness 0.25 to 0.3 mm greater. The increase in material thickness would act to increase the BT as seen with the results by Li. The chemical structure as well as the physical properties of the rubber

is different than neoprene resulting in different permeation characteristics and longer BTs. The solubility parameters for the rubbers in the study by Li are similar to the range seen for neoprene of 16.6-19.2 ($MPa^{1/2}$). The inconsistency in BT should not arise from this aspect. The difference in monomers of the rubbers is another possible source affecting the transport of acetone and toluene, essentially slowing the permeation. The molecules are not able to move through the lattice work as readily in the materials used by Li compared to the present study resulting in higher BTs

A study by De Kee et al. with the same challenging agents and materials had similar results quantitatively to Li. The same general trend in decrease of BT with increase in deformation is evident between the studies using different rubbers. Similar results were also found in experiments with acetone and polyisoprene under uniaxial and biaxial deformation where breakthrough times decrease with increasing deformation [38]. This study by Hinestroza et al. also had higher breakthrough times than the present study at deformations of 0, 20, and 40 percent both uniaxial and biaxial. The samples used in the experiments were polyisoprene and had a dry thickness of 0.1 mm greater than the samples in the present study. The same factors identified in the previous study can be stated as causing the higher BTs. The BT is heavily dependent upon the affinity of challenging agent and material, swelling induced by the solvent, cohesive energies of both, and the elongation induced.

Of the three chemicals used in the experiments, xylene has the highest SSPR followed by toluene then acetone for each level of deformation. The SSPR elicits a different behavior for each level of deformation and chemical. In the case of toluene a

deformation of 20% decreases the flux by 21% of the observed SSPR for no deformation. The flux then increases to 1037 µg/cm^{2}min under 30% deformation, an increase in flux of 32% from the case for no deformation. The behavior seen by toluene is studied further to substantiate the decrease, increase, decrease trend in SSPR. The trend in SSPR over increasing deformation can be seen in Figure 12. Each SSPR value in Figure 12 is an average of 20 successive readings as explained in the experimental section.

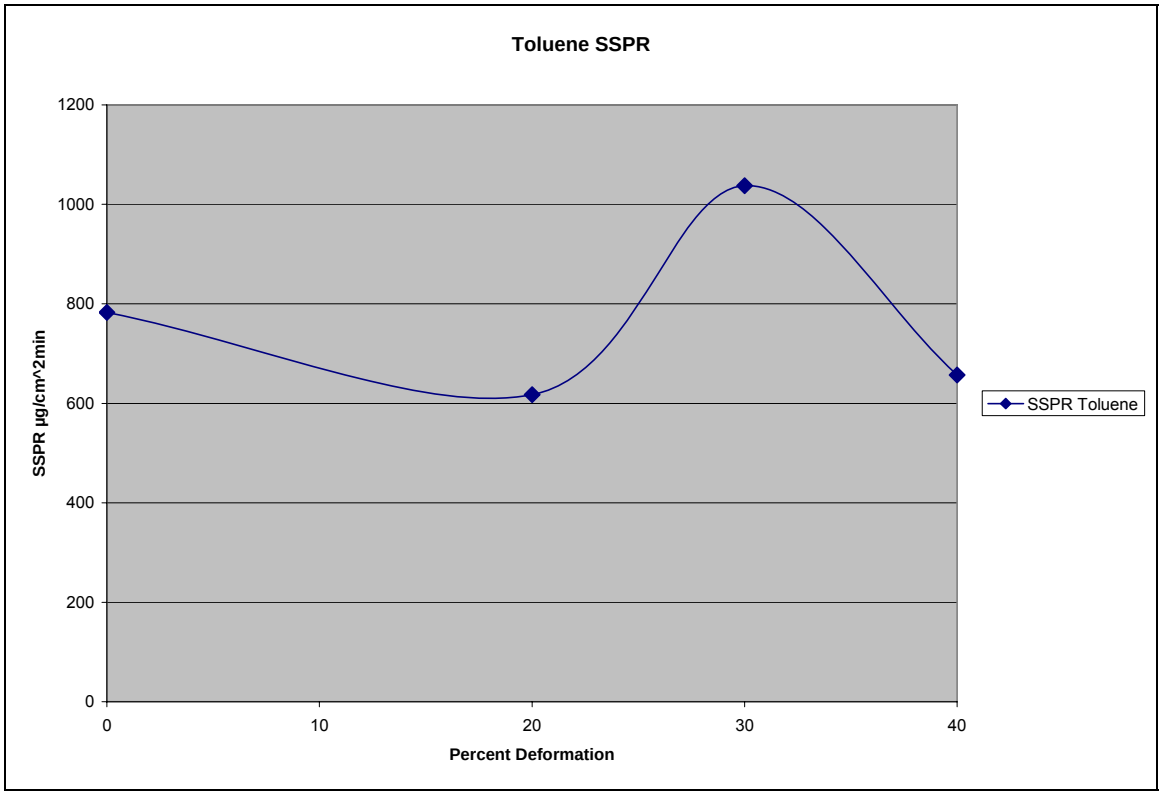

Figure 12: Toluene SSPR trend over increasing deformation

The preferential solubility of toluene can be explained by Hildebrandt's solubility parameter as discussed earlier in the thermodynamic component of permeation. The solubility parameters for acetone, toluene, and xylene are 20.3, 18.2, and 18.0 (MPa$^{1/2}$) respectively. The solubility parameter for polychloroprene or neoprene ranges from

16.6-19.2 from observed experiments or calculations [12]. In the present case the solubility parameter for neoprene would appear to be closer to that of toluene as it has the shortest breakthrough time and the highest SSPR with the exception of xylene. In the study by Li et al. mentioned previously, the solubility parameters, δ, for NR and toluene are 16.6 and 18.8 respectively. The pairing of NR and toluene results in a shorter BT and higher SSPR than NR and acetone which has a solubility parameter of 20.3. The similarity of results with the study by Li using NR and the present study using neoprene support the rule that the closer the values of δ for a material and solvent the higher the permeation properties. The comparison between solubility parameters can be seen in Table 3 where polymer and solvent pairings with similar solubility parameters results in shorter BTs.

For xylene a different behavior is observed. The sample with no deformation has the lowest SSPR followed by a jump to 10232 μg/cm^{2}min with 20% deformation. A continued increase is visible in SSPR to 10671 μg/cm^{2}min for 30% deformation then a decrease to 9305 μg/cm^{2}min for 40% deformation. Regardless of deformation, xylene has an elevated SSPR compared to the other chemicals. The trend in SSPR over increasing deformation can be seen in Figure 13.

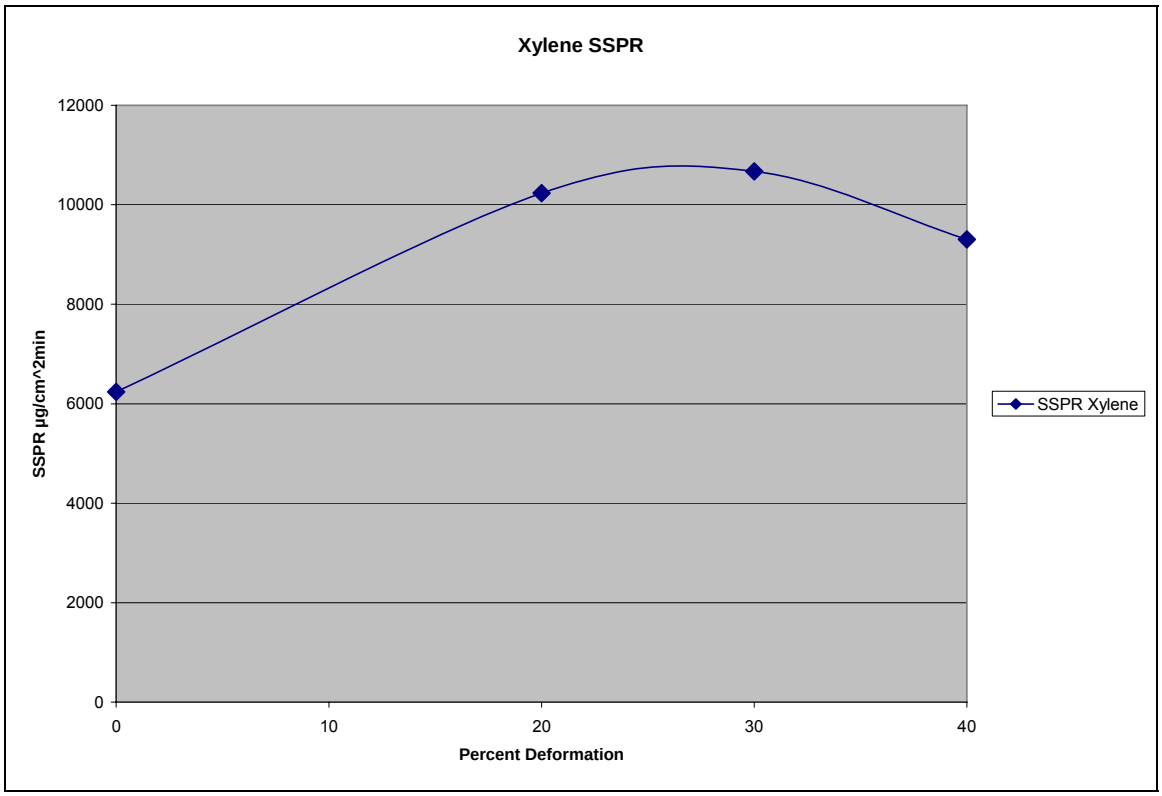

Figure 13: Xylene SSPR trend over increasing deformation

Li et al. had similar results in her study between DCM and two materials NBR and BIIR which were attributed to a chemical reaction between DCM and the material. The SSPR for DCM continually increased with each increase in deformation level up to 20 percent similar to the case with xylene in the present study except the SSPR began to decrease at 40% deformation. Li et al. did not conduct permeation experiments at higher levels of deformation so the behavior with DCM is uncertain. A change in solvent color was noted with all experiments. In the case of xylene, additives in the rubber might have dissolved or the possibility of a chemical reaction between the sample and challenge agent resulting in larger swelling and the elevated SSPR.

The behavior of acetone is similar to that of toluene except the increase in SSPR is seen at 40% deformation instead of 30% deformation. The virgin sample has the highest flux followed by decreasing flux with each successive deformation level until 40%. At 40% the flux increases to 366 from 232 µg/cm^{2}min as seen with 30% deformation. The trend in acetone flux with increasing deformation can be seen in Figure 14 and 15. Figure 14 contains all data points for the 2 hour permeation experiment, showing the increase to an equilibrium permeation rate. The negative SSPR visible in Figure 14 can be attributed to noise in the system. Figure 15 shows the average of 20 successive points in the steady state permeation region for each deformation level. The lower SSPR of acetone at 0 deformation is also supported by the study completed by Li et al. in that the δ difference of chemical and material is greater than that of toluene and neoprene.

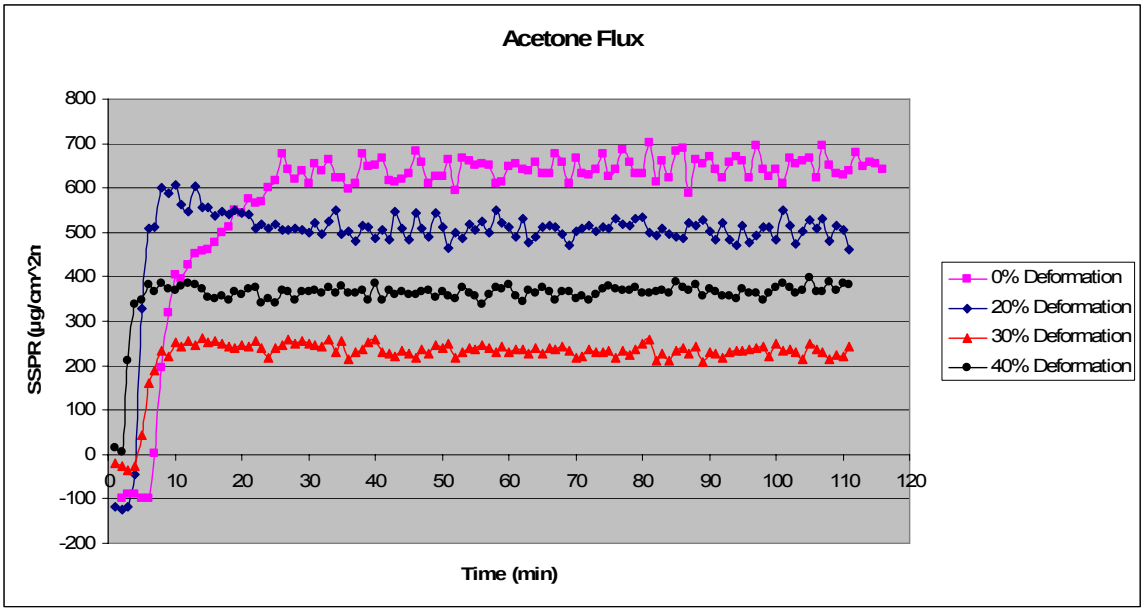

Figure 14: Acetone flux at increasing deformation levels

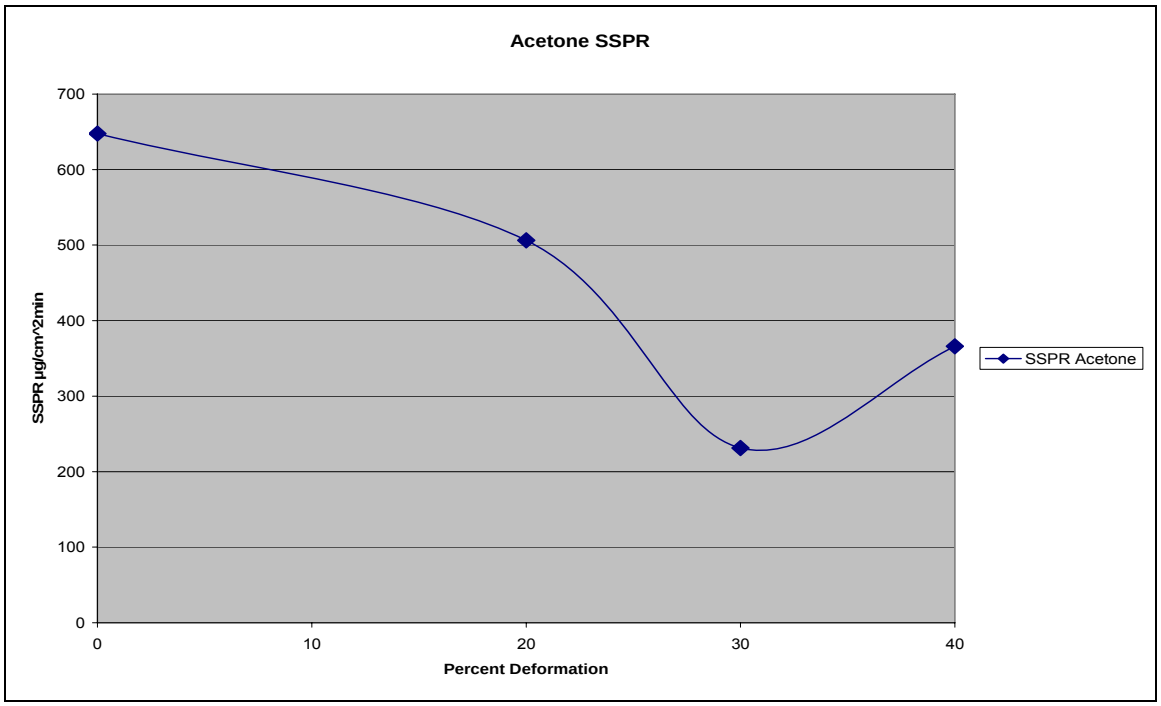

Figure 15: Acetone SSPR trend over increasing deformation

The trend in SSPRs with changing elongation for the present study, with the exception of xylene, does not occur often in the results from any previous studies whether the material is amorphous or semicrystalline. The study by Li et al. identified three common cases observed in permeation experiments with increasing elongation. They are:

- A continual increase in flux with increasing elongation
- An increase then decrease in flux with increasing elongation
- A decrease then increase in flux with increasing elongation

In the present study, SSPR rate decreases initially then increases with elongation for toluene and acetone but xylene increases initially then decreases as seen in Figures 12, 13, and 15. The study by Li identified only two cases where an initial decrease then

increase in SSPR occurred, which were DCM through NR and Acetone through NBR. The majority of other studies exhibit an initial increase then decrease in steady state flux over increasing elongation. These studies include toluene in poly aryl ether ether ketone, MEC and TCE through LLDPE, acetone through polyisoprene , DCM, TCE, benzene through HDPE and PVC, and those by Li et al. [38, 39, 43, 82, 84]. The primary explanation for this permeation behavior is explained by Xiao et al. Xiao states that stressing a polymer causes deformation and crystallization depending on the chemical properties of the polymer, how much stress is applied, and the rate. Deformation that is elastic and not permanent upon stress release results in increased permeation whereas stress that causes permanent deformation or crystallization and chain alignment results in decreased permeation. At lower elongations in the previous studies the deformation is not permanent therefore the SSPRs increase with increasing elongation until the point where the deformation is no longer elastic, then the SSPRs decrease. In these studies the deformation is either uniaxial or biaxial. None of the studies incorporate a uniform radial means of deformation as in the present study which appears to be one cause of the different permeation behavior observed. These results appear to be originating from morphological changes occurring in the material with radial deformation as well as each chemical's interaction with the material. The permeation behaviors observed with radial deformation are profound in that increased protective properties are evident at lower permeations; these properties are decreased at higher deformations. The behavior seen in the present study is opposite that seen in other experiments as stated earlier. The standard

test methods will be greatly affected if radial deformation is indeed observed in real use applications, ultimately swaying material selection for a particular application.

4.2.2 Binary Mixture Permeation

The BT and SSPR for each binary mixture experiment are presented in Table 4.

Table 4: Binary Mixture Experimental Results

	Mixture Component						
Percent Deformation	Xylene	Acetone	Toluene	BT (min)	SSPR Xylene ($\mu g/cm^2 min$)	SSPR Acetone ($\mu g/cm^2 min$)	SSPR Toluene ($\mu g/cm^2 min$)
0	0.0	0.2	0.8	5	0	373	782
0	0.0	0.4	0.6	5	0	758	696
0	0.0	0.6	0.4	5	0	759	390
0	0.0	0.8	0.2	5	0	689	150
0	0.2	0.0	0.8	7	1713	0	540
0	0.2	0.8	0.0	5	2498	978	0
0	0.4	0.0	0.6	6	3026	0	312
0	0.4	0.6	0.0	5	6531	1061	0
0	0.6	0.0	0.4	7	4065	0	226
0	0.6	0.4	0.0	5	11667	925	0
0	0.8	0.0	0.2	8	6343	0	166
0	0.8	0.2	0.0	5	15022	255	0
20	0.0	0.2	0.8	3	0	246	611
20	0.0	0.4	0.6	4	0	345	388
20	0.0	0.6	0.4	3	0	837	395
20	0.0	0.8	0.2	4	0	335	76
20	0.2	0.0	0.8	5	1644	0	560
20	0.2	0.8	0.0	4	2096	821	0
20	0.4	0.0	0.6	5	2624	0	331
20	0.4	0.6	0.0	4	4066	514	0
20	0.6	0.0	0.4	3	5726	0	355
20	0.6	0.4	0.0	3	8131	656	0
20	0.8	0.0	0.2	7	7387	0	165
20	0.8	0.2	0.0	4	8385	192	0
30	0.0	0.2	0.8	2	0	248	735
30	0.0	0.4	0.6	2	0	573	586
30	0.0	0.6	0.4	3	0	849	490
30	0.0	0.8	0.2	3	0	1241	212
30	0.2	0.0	0.8	2	2367	0	601
30	0.2	0.8	0.0	2	2186	577	0
30	0.4	0.0	0.6	3	2836	0	375
30	0.4	0.6	0.0	2	6347	1242	0
30	0.6	0.0	0.4	4	4042	0	259
30	0.6	0.4	0.0	2	7351	704	0
30	0.8	0.0	0.2	2	10823	0	216
30	0.8	0.2	0.0	2	11218	220	0
40	0.0	0.2	0.8	2	0	360	910

Table 4 (continued)

Mixture Component							
Percent Deformation	Xylene	Acetone	Toluene	BT (min)	SSPR Xylene ($\mu g/cm^2 min$)	SSPR Acetone ($\mu g/cm^2 min$)	SSPR Toluene ($\mu g/cm^2 min$)
40	0.0	0.4	0.6	2	0	622	656
40	0.0	0.6	0.4	2	0	738	387
40	0.0	0.8	0.2	2	0	1381	267
40	0.2	0.0	0.8	3	2106	0	655
40	0.2	0.8	0.0	3	1921	571	0
40	0.4	0.0	0.6	3	4185	0	565
40	0.4	0.6	0.0	2	7212	1333	0
40	0.6	0.0	0.4	3	4989	0	333
40	0.6	0.4	0.0	2	9524	595	0
40	0.8	0.0	0.2	2	11800	0	197
40	0.8	0.2	0.0	2	9794	175	0

Binary mixture permeation incorporates not only the effect of each chemical on the material but also that of the mixture. An observed trend with all binary mixtures was a decrease in BT with increased deformation. Neoprene is an amorphous material having a different transport behavior than semicrystalline materials. The crystalline regions in a semicrystalline material are impermeable to the challenge agents, therefore the chemicals travel a longer path than that in an amorphous material. In contrast to independent breakthrough times observed for mixtures through semicrystalline materials, amorphous materials exhibit a unified breakthrough time. A study by Hinestroza et al. on the hexane, acetone, benzene ternary mixture permeation through polyisoprene is an example of a unified BT for each chemical present through an amorphous material regardless of the deformation induced [38]. The present study exhibits a unified BT for binary mixtures of solvents. There is relatively no difference in BT of pure solvents at 0 deformation and the binary mixtures of acetone and toluene, and acetone and xylene.

The binary mixture of xylene and toluene has a longer BT at zero defomation than either of the pure components. The combination of xylene and toluene resulted in an increase in BT of 2 to 3 minutes over the pure component BT. The increase in BT may be associated with a lower degree of swelling associated with the mixture or there is a large difference in the cohesive energy of the mixture and the components. An example of independent BTs is evident in experiments on the permeation of methylene chloride and trichloroethylene through low-density polyethylene geomembranes. Independent breakthrough times were observed for each chemical in the mixture resulting from the semicrystalline nature of the material [39]. A decrease in BT with increased deformation was observed in this study as well.

Binary mixtures of acetone and toluene at 0 deformation resulted in increased SSPR of acetone with decreased percent volume of acetone until 40 percent volume of acetone is reached, the SSPR of acetone then begins to decrease. The toluene acts to facilitate transport of acetone as the 80% binary mixture of acetone with 20% toluene has a higher SSPR then pure acetone. Toluene SSPR at 0 deformation appears proportionate to the mixture compositions. The same facilitated transport of acetone is observed at 20% deformation. The results of facilitated transport of mixtures are similar to experimental results on mixture transport of benzene, dichloromethane, and trichloroethylene through HDPE and PVC [83,84]. It is evident from the results that percent volume of each component in the mixture drives the SSPR above deformations of 20%, as SSPR increases and decreases relative to mixture composition for each component within a deformation level. The facilitated transport of acetone by toluene is

overridden by the effect of deformation at 30 and 40%. The SSPR behaviors can be seen in Figures 16 & 17 for acetone and toluene.

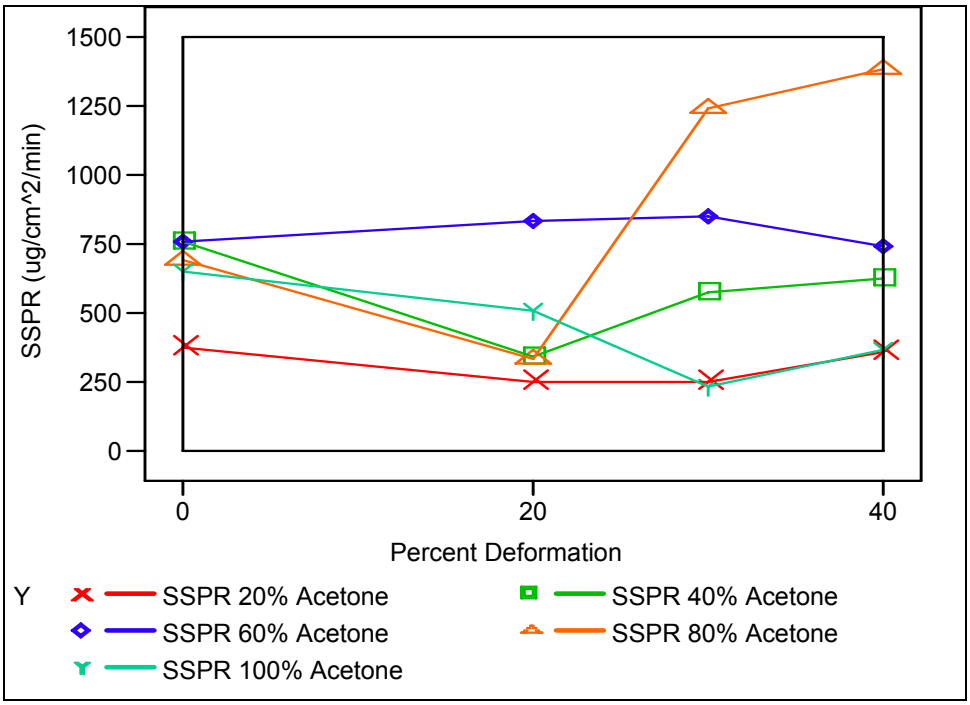

Figure 16: Acetone SSPR with increasing deformation and % mixture

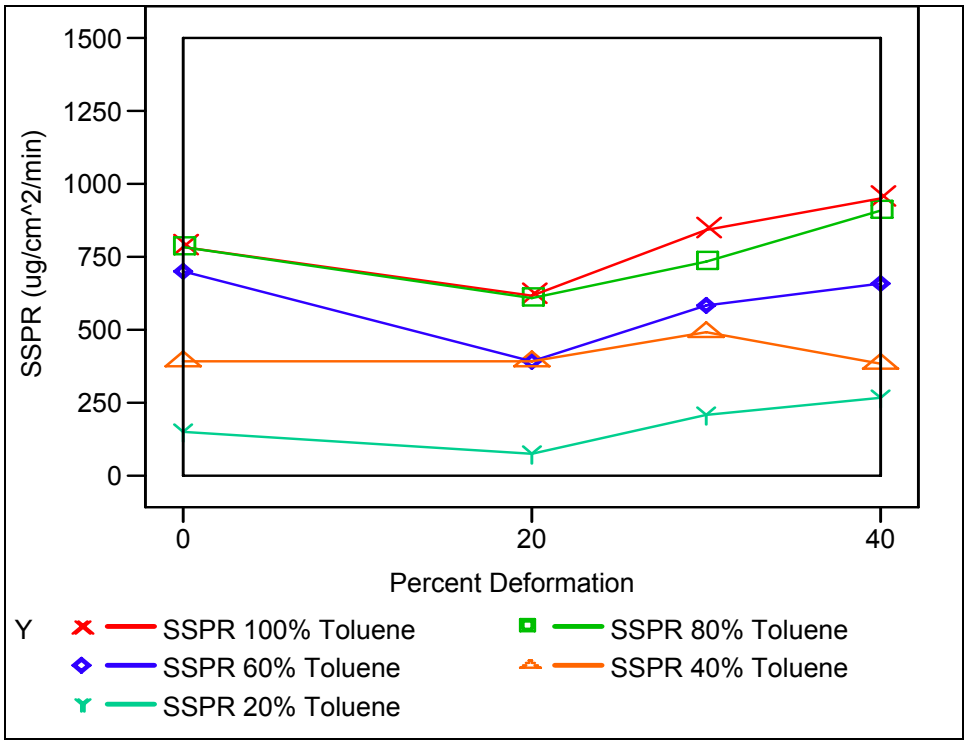

Figure 17: Toluene SSPR with increasing deformation and % mixture

Binary mixtures of acetone and xylene at all deformations resulted in elevated SSPR of xylene, the same as seen with the single component xylene permeation. A graph of 20% xylene 80% acetone binary mixture flux at 0 deformation can be seen in Figure 20. Xylene SSPR increases with increasing percent xylene in mixture for each deformation. Acetone has the same behavior except at 80% acetone level the SSPR for acetone decreases. Xylene is the higher permeating solvent, increasing the acetone permeation as part of a mixture, at 80%, over the SSPR of 648 µg/cm^{2}min seen with just the single component acetone. From this observation, xylene will be analyzed to see the effect of deformation on permeation. Three different behaviors were observed with xylene and acetone at different deformations. The behaviors were:

- Continued decrease in SSPR with deformation

- Initial decrease then continued increase in SSPR with deformation
- Decrease, increase, and decrease in SSPR with deformation

These behaviors can be seen in Figures 18 & 19.

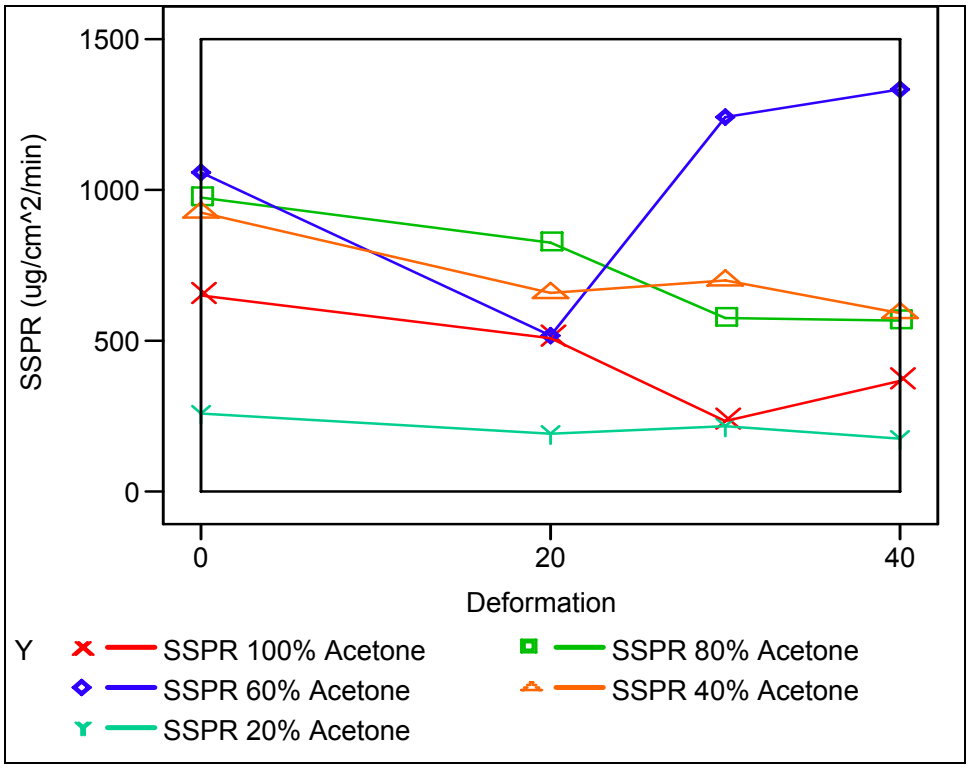

Figure 18: Acetone SSPR with increasing deformation and % mixture

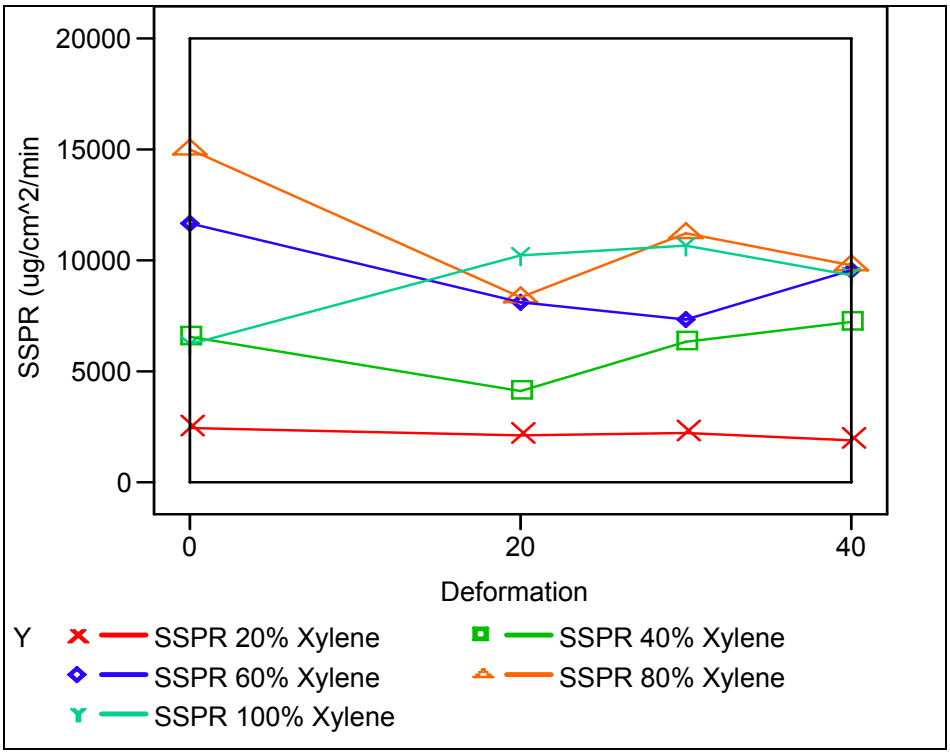

Figure 19: Xylene SSPR with increasing deformation and % mixture

Xylene and acetone mixtures of 60% acetone 40% xylene and 20% acetone and 80% xylene exhibit the same behavior at lower deformations. 60% acetone 40% xylene exhibits an initial decrease then continued increase in SSPR. 20% acetone 80% exhibits a decrease, increase, decrease behavior in SSPR with increased deformation up to 40%. The 80% acetone 20% xylene and 40% acetone 60% xylene combinations follow different behaviors in SSPR.

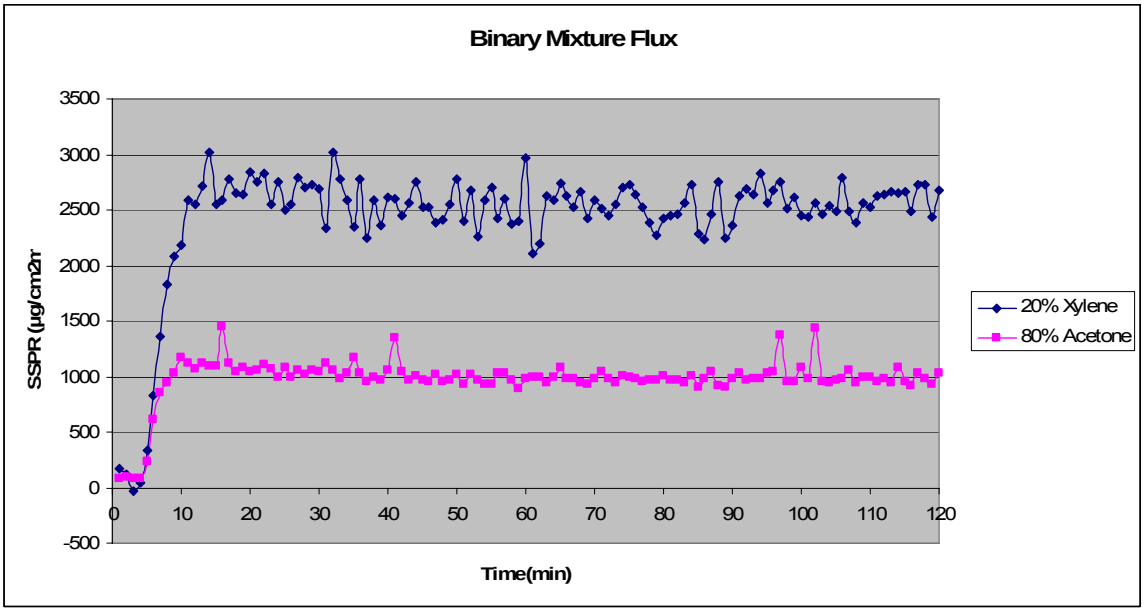

Figure 20: 20% xylene 80% acetone binary mixture flux at 0 deformation

Binary mixtures of toluene and xylene at all deformations resulted in elevated SSPR of xylene, the same behavior seen with single component xylene permeation and binary mixture acetone and xylene. Xylene SSPR increases with increasing percent xylene in mixture for each deformation. Toluene SSPR also increases with increasing percent toluene in the mixture for each deformation. Xylene does not appear to have the same effect on toluene as seen with acetone. The SSPR of toluene as part of a mixture at 80% with xylene at 20 % is not greater than the SSPR seen with single component permeation of toluene. Four different behaviors were observed with xylene and toluene. The behaviors were:

- Continued increase in SSPR with deformation
- Decrease initially then a continued increase in SSPR with deformation
- Decrease, increase, and decrease in SSPR with deformation

- Increase, decrease, and increase in SSPR with deformation

Theses behaviors can be seen in Figures 21 & 22.

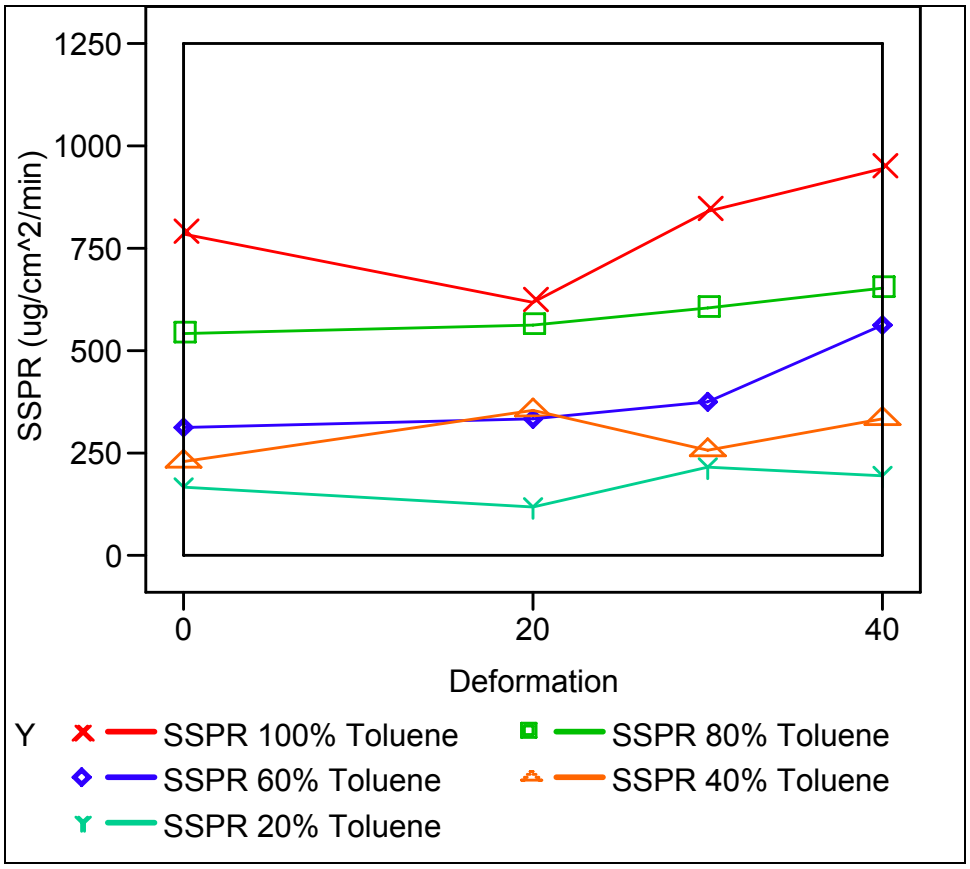

Figure 21: Toluene SSPR with increasing deformation and % mixture

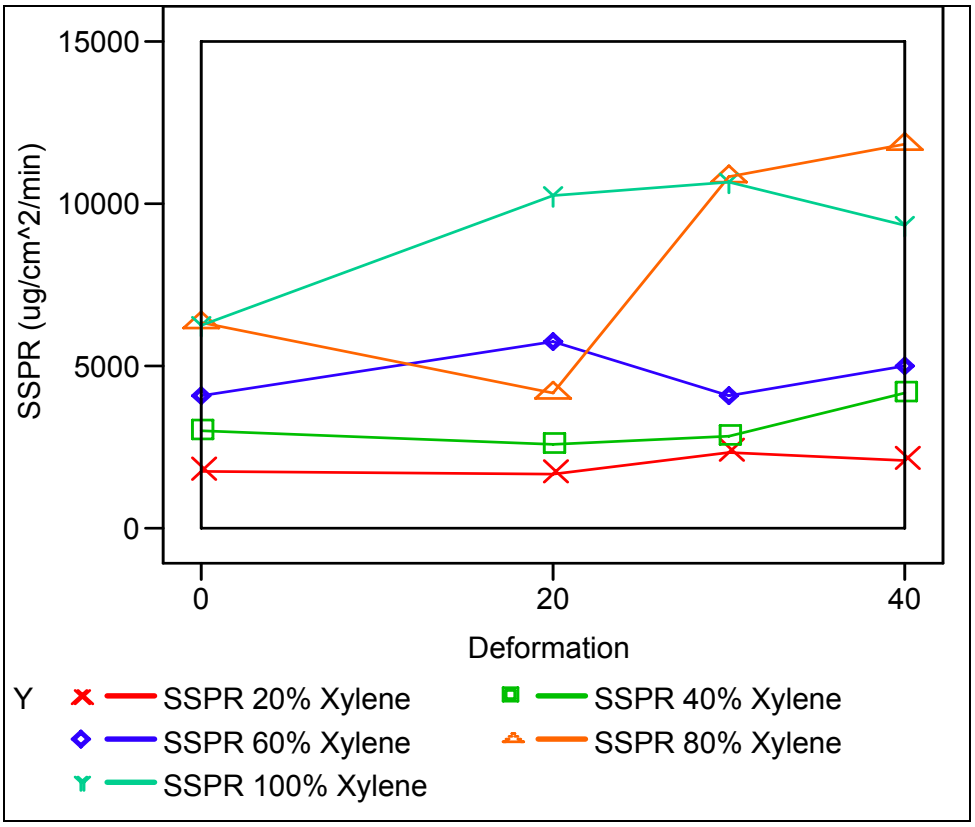

Figure 22: Xylene SSPR with increasing deformation and % mixture

No apparent trends are evident as permeation rates increase and decrease with each deformation level. Several factors appear to be inducing variation in the results, such as the varying percent toluene-xylene mixtures, mixture-material interaction, deformation induced, and swelling of the material.

Some components of the results match previous studies. In a study on natural rubber and nitrile gloves using different mixture combinations of toluene and MEK, the higher permeating solvent facilitated the permeation of the lower permeating solvent. The composition of the mixture was also proportionate to the permeation. The same effect as seen with acetone and toluene in the present study. The effect of deformation on the permeation is not known, as only unstressed experiments were conducted on natural

rubber and nitrile gloves [33]. Another study on MEC and TCE mixture permeation through linear low-density polyethylene geomembranes resulted in increased SSPR with increased deformation both uniaxial and biaxial, which was attributed to an increase in the amorphous regions of the polymer. The SSPR of MEC through LLDP increased with decreasing percent MEC in the mixture with all deformations. This behavior was seen with toluene and acetone in the present study for all mixture combinations except 20% acetone. The major difference with the present study is the application of radial deformation.

4.2.3 Ternary Mixture Permeation

The BT and SSPR for each ternary mixture experiment are presented in Table 5.

Table 5: Ternary Mixture Experimental Results

	Mixture Component						
Percent Deformation	Xylene	Acetone	Toluene	BT (min)	SSPR Xylene ($\mu g/cm^2 min$)	SSPR Acetone ($\mu g/cm^2 min$)	SSPR Toluene ($\mu g/cm^2 min$)
0	0.2	0.2	0.6	6	2565	421	581
0	0.2	0.4	0.4	5	3342	713	540
0	0.2	0.6	0.2	5	2838	1022	235
0	0.4	0.2	0.4	5	4059	231	303
0	0.4	0.4	0.2	5	7113	748	327
0	0.6	0.2	0.2	6	7248	267	215
0	0.6	0.2	0.2	6	4268	19	122
20	0.2	0.2	0.6	4	2128	209	455
20	0.2	0.4	0.4	3	2545	642	400
20	0.2	0.6	0.2	3	2731	825	235
20	0.4	0.2	0.4	4	3649	329	310
20	0.4	0.4	0.2	4	3681	392	156
20	0.6	0.2	0.2	4	5069	194	164
30	0.2	0.2	0.6	2	2285	222	554
30	0.2	0.4	0.4	2	3356	567	430
30	0.2	0.6	0.2	2	3132	1042	255
30	0.4	0.2	0.4	3	4851	273	427
30	0.4	0.4	0.2	2	4663	535	201
30	0.6	0.2	0.2	3	5917	232	205
40	0.2	0.2	0.6	2	2892	322	670
40	0.2	0.4	0.4	2	3528	743	530
40	0.2	0.6	0.2	2	3640	1251	320
40	0.4	0.2	0.4	2	5880	318	464
40	0.4	0.4	0.2	2	6173	633	227
40	0.6	0.2	0.2	2	8161	267	231

Complex interactions occur in ternary mixture interactions with neoprene. An observed trend with all ternary data is a decrease in BT with increased deformation regardless of mixture combination. The same unified breakthrough of all chemicals in the mixture as seen with binary mixtures is also seen with ternary mixtures

Within a deformation level the SSPR of each chemical does not correspond to the percent mixture. The SSPR of xylene is again elevated in all of the ternary mixture experiments. Four out of the six chemical mixtures follow the same decrease, increase, increase in SSPR with each successive deformation level. The 20% xylene, 40% acetone, 40% toluene, and the 40% xylene, 20% acetone, 40% toluene exhibit a different behavior in permeation. Overall the ternary mixtures exhibit an initial decrease in SSPR with 20% deformation then a continued increase in SSPR with 30 and 40% deformation. The flux trend for the 20% xylene 60% acetone 20% toluene ternary mixture at 0 deformation can be seen in Figure 23. In a study on the permeation of an aqueous mixture of DCM, TCE, and benzene through PVC and HDPE geomembranes, the mixture permeation continually increases up to the highest deformation performed of 80% through PVC. In the HDPE geomembrane a deformation of 60% causes the mixture permeation to decrease to below that seen for zero deformation [84]. The study concludes that PVC did not undergo irreversible changes whereas the HDPE geomembranes did resulting in the permeation behaviors observed. Another study on the acetone, benzene, hexane mixture permeation through polyisoprene found that the SSPR of all components in the mixture increased under 40x40% biaxial deformation from that seen in the nonelongated case [38]. Morphological changes in the polymer were identified as the cause for the increase. In the present study on xylene, acetone, and tolune, the lower permeation at 20% would appear to be the result of a decrease in the free volume of the polymer or due to the radial nature of deformation because irreversible changes in the polymer are not certain at this low of a deformation. The higher elongation acts to decrease the barrier properties of the

material and increase the SSPR indicating that perhaps only reversible changes have occurred in the polymer.

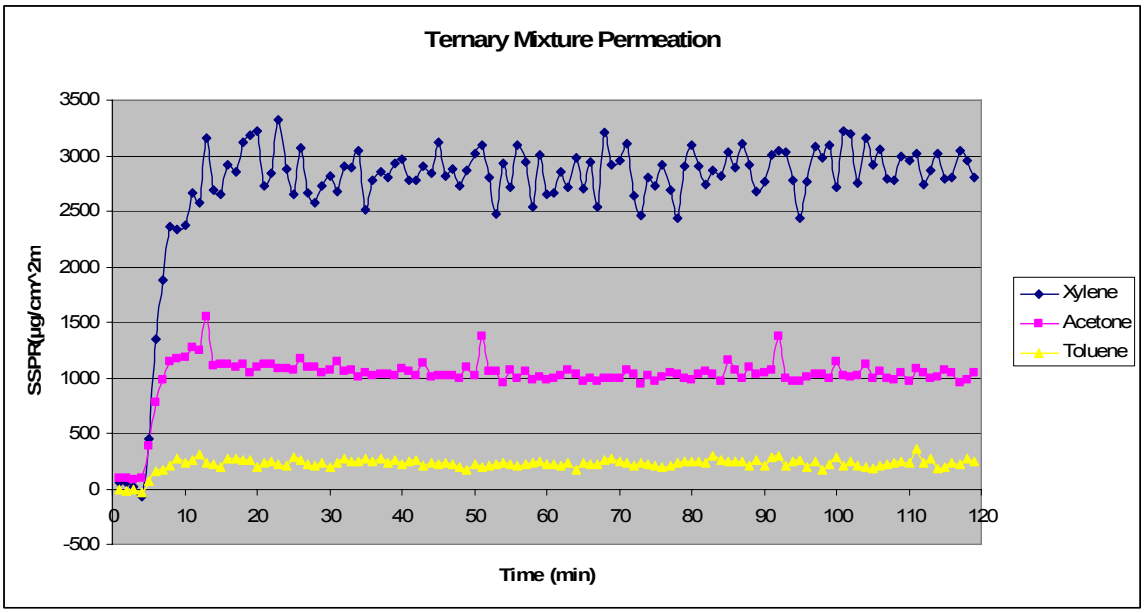

Figure 23: 20% xylene 60% acetone 20% toluene ternary mixture flux at 0 deformation

4.3 Confirmation Run

Confirmation runs were conducted on pure toluene under 0 to 40% deformation in 5% increments to check repeatability of SSPR and characterize and verify a trend visible in the SSPR. The results of the confirmation runs can be seen in Table 6.

Table 6: Confirmation experimental results

	Mixture Component						
Percent Deformation	Xylene	Acetone	Toluene	BT (min)	SSPR Xylene ($\mu g/cm^2 min$)	SSPR Acetone ($\mu g/cm^2 min$)	SSPR Toluene ($\mu g/cm^2 min$)
0	0	0	1	5	0	0	803
5	0	0	1	4	0	0	779
10	0	0	1	4	0	0	711
15	0	0	1	4	0	0	599
20	0	0	1	3	0	0	662
25	0	0	1	3	0	0	714
30	0	0	1	2	0	0	838
35	0	0	1	2	0	0	882
40	0	0	1	2	0	0	947

Figure 24 presents the Matched Pairs Analysis, produced using JMP Software, of SSPR for toluene. The graph shows the difference between the confirmation run and the first run data on the y-axis and the mean of the confirmation run and the first run data on the x-axis for pure toluene at 0, 20, 30, and 40 percent deformation. The mean difference is the center horizontal line, with the 95% confidence interval above and below. The confidence region for the data set includes the horizontal line at zero, implying the experimental runs are not significantly different at the 0.05 level and the process is repeatable. The 40% deformation point lies almost on the 95% confidence interval line. The 40% deformation level would need to be tested again to determine if the result is random error or process related.

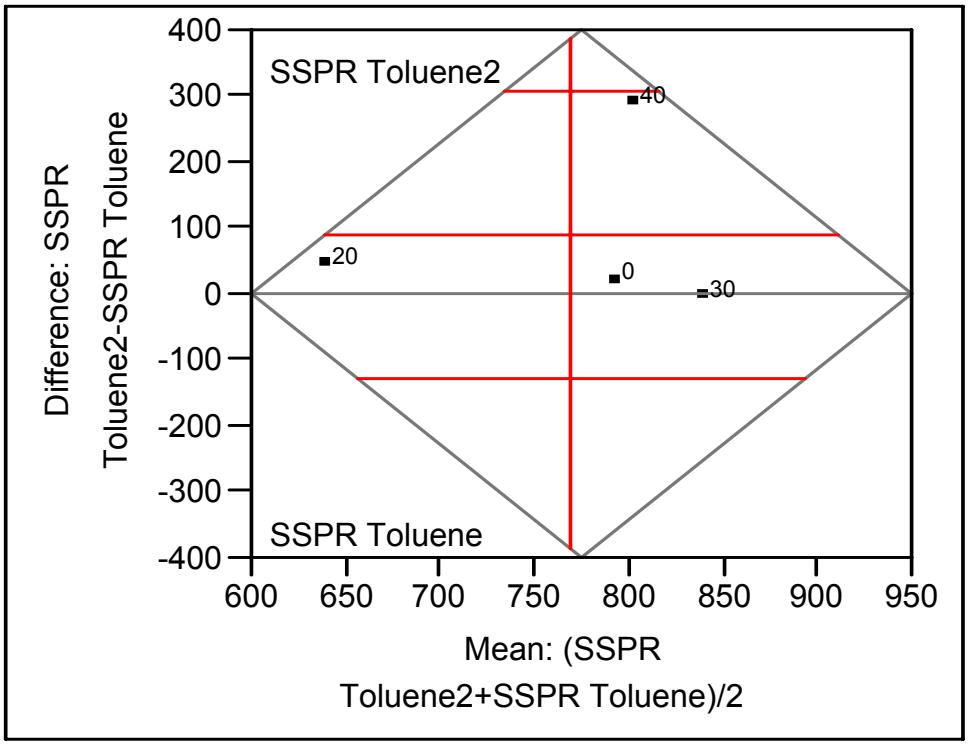

Figure 24: Confirmation results for SSPR of pure toluene using deformation as a categorical variable

As stated earlier the confirmation experiments were conducted in 5% deformation increments to confirm the trend in SSPR of toluene. Figure 25 displays the original, marked with circles, as well as the confirmation results, marked with an x, for pure toluene. Based on the trend visible with the 5% increments in Figure 25 the SSPR would be expected to increase at 40% deformation, indicating that there is an error in the first experimental run. The graph shows that deformations up to 15% act to increase the barrier properties of the material whereas higher deformations increase the SSPR. A cubic polynomial regression with an R-square value of 0.85 was fitted to the data as shown in Figure 25.

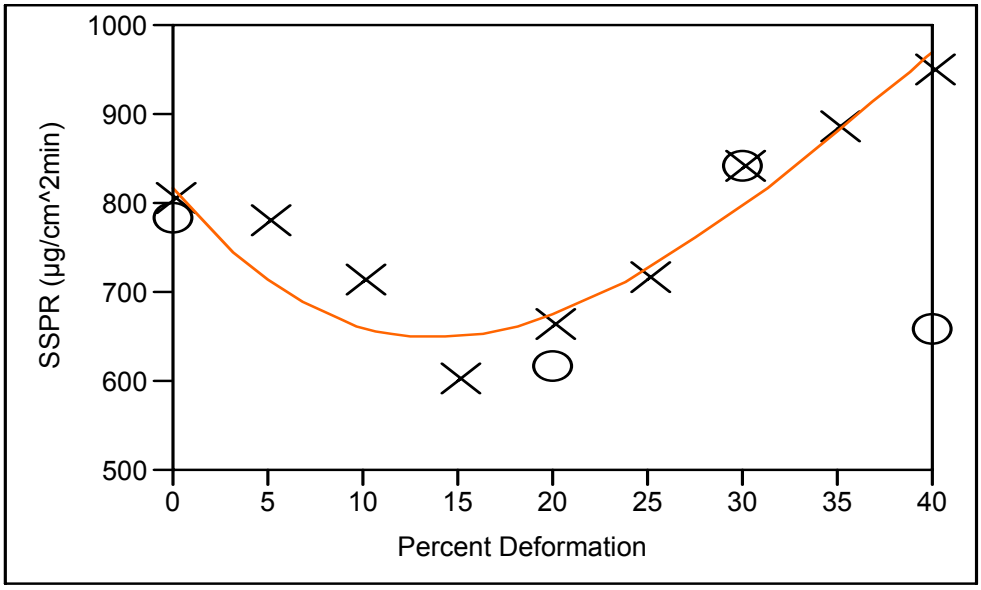

Figure 25: Confirmation results for SSPR of pure toluene under 5% deformation increments

An interesting observation was found regarding BT between the tested deformations of 0-40%. To better visualize the change in BT, a bivariate graph of the original experimental BTs, marked with a circle, and the confirmation BTs, marked with an x, is shown in Figure 26. It is evident from the graph that lower deformations result in a higher BT and this begins to decrease at15% deformation until 30% deformation where BT plateaus again. A cubic polynomial regression with an R-square value of 0.88 was fitted to the data as shown in Figure 26. This behavior can be explained by the decrease in material thickness with increased deformation as can be seen in Figure 27. Material thickness decreases exponentially with increasing deformation assuming a constant volume. Figure 28 is a graph of BT for all experiments with increasing deformation. Here a linear decrease in BT with increasing deformation can be seen.

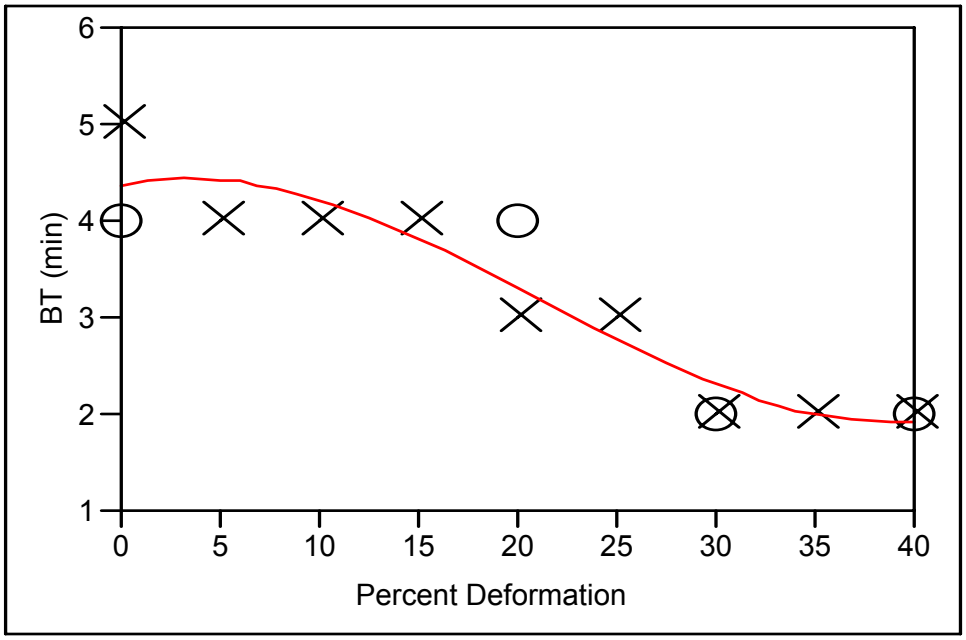

Figure 26: Confirmation results for BT of pure toluene under 5% deformation increments

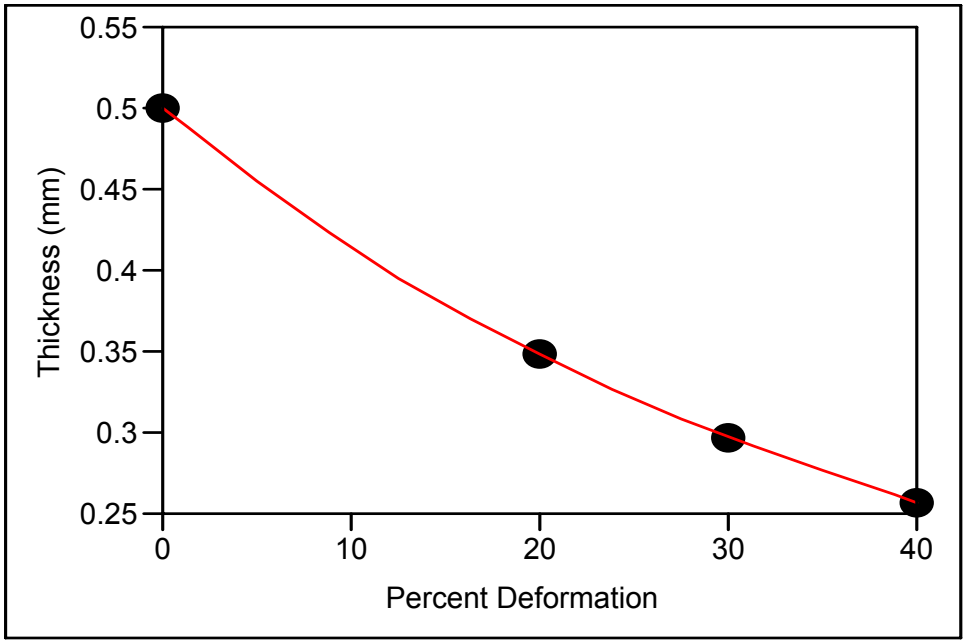

Figure 27: Change in thickness with increased deformation

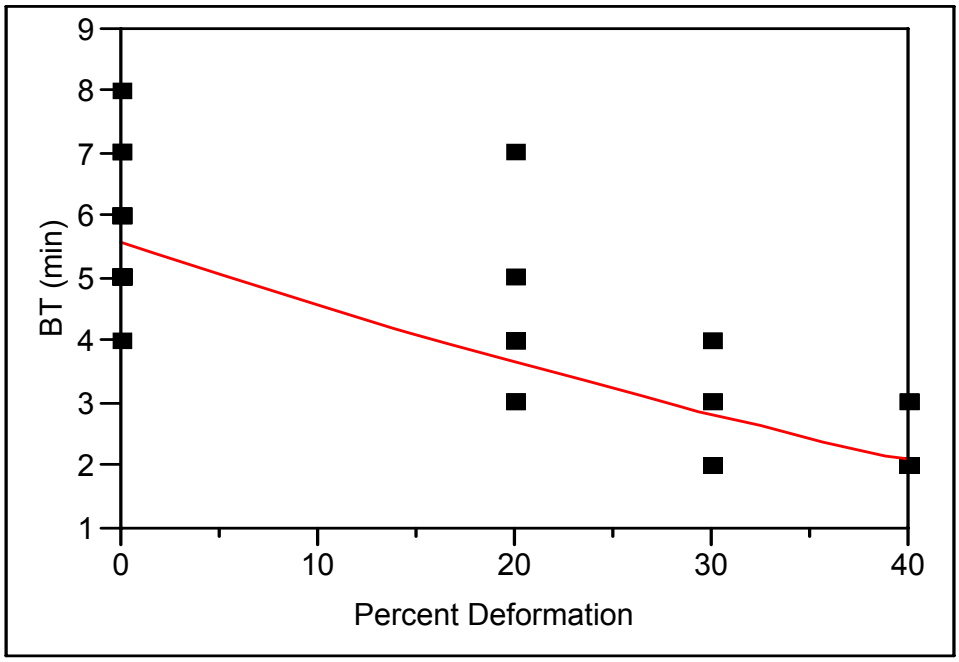

Figure 28: Decrease in BT with increasing deformation

The current research has incorporated experimental conditions similar to actual use to study the effects of uniform radial deformation on permeation and material performance. In actual use conditions, CPC is flexed and stretched at elbows, knees, and joints; therefore a similar deformation mechanism was used in the current study. BT and SSPR values were determined experimentally to evaluate the effects of radial deformation and single component, binary, and ternary mixtures on permeation.

A unified BT for each component was observed with mixtures and a decrease in BT with increased deformation was evident in all experiments. Results from radial deformation testing reveal that radial deformation causes different permeation behaviors than biaxial or uniaxial deformation. In binary mixtures and the majority of ternary mixtures a decrease then increase in SSPR with increasing deformation was observed.

The experimental results contradict previous studies on uniaxial and biaxial deformation where deformation in the elastic region increased permeation and higher deformations decreased permeation. Initial observation would indicate that radial deformation is causing morphological changes in the material. CPC standard test methods would need to incorporate a radial means of deformation if indeed radial deformation simulates actual material use because permeation behaviors are different than uniaxial and biaxial. Interesting observations were made about the permeation chemicals. Xylene has elevated SSPRs in all experiments and chemical combinations. Chemical reactions between solvent and material are causing higher permeation rates. In single component experiments, toluene has the highest SSPR and shortest BT with the exception of xylene as a result of the similarity of solubility parameters. With toluene a decrease in SSPR was observed at 40% deformation and this behavior was expelled by confirmation experiments in increments of 5% deformation that showed a continual increase in SSPR at 40% deformation. Acetone has the same behavior as toluene in single component experiments and in binary experiments acetone transport was facilitated by toluene as it was the higher permeating component.

Potential improvements to current experimental methods as well as possible future experiments are explained in the next chapter.

Chapter 5: Future Work

The ASTM F-739 test method along with a novel radial deformation apparatus have been used to test the permeation of organic chemicals through neoprene. The uniqueness in this experimental setup is that uniform radial deformation is applied while the permeation test is conducted. Many organizations use a preconditioning protocol to represent real use conditions before the material is evaluated but not during evaluation. The previously mentioned test methods require the material to be tested as a flat swatch of material. In actuality the material is being stretched when it encounters a chemical. A better representation of protective ability is evaluation under mechanical deformation. Standard test methods are continually evolving to more accurately represent the true conditions of use. New test methods will need to be developed in order to optimize the evaluation of CPCs.

5.1 Future Experiments

Further experimentation is necessary to substantiate the results found in the present study. Preliminary testing was conducted to determine the repeatability of the deformation device in inducing the desired deformation and the functionality of the permeation equipment. Confirmation runs were conducted on toluene to verify a trend visible in the original results. In the present case a full factorial was conducted on the experimental levels in order to observe all behaviors. Future testing should incorporate more repeats to verify permeation behaviors observed.

The behavior visible in the permeation experiments due to the radial deformation is different than that observed with uniaxial and biaxial deformation studies. The exact

effect of radial deformation on the material's permeation properties needs to be further analyzed to determine how the morphology of the material has changed. In biaxial and uniaxial studies the deformation in the elastic/inelastic region were believed to cause decreased and increased barrier properties respectively in materials; i.e. higher SSPRs and lower SSPRs.

The swelling behavior of neoprene by binary and ternary mixtures of acetone, toluene, and xylene needs to be studied further. The results seen in binary mixture permeation are varied over the deformation levels studied. Knowing the swelling behaviors would help to elucidate mixture behavior in permeation.

References

[1] Aminabhavi TM, Phayde HTS. 1995 "Molecular-Transport Characteristics Of Santoprene Thermoplastic Rubber In The Presence Of Aliphatic Alkanes Over The Temperature Interval Of 25-Degrees-C To 70-Degrees-C" *Polymer* **36** 1023-1033.

[2] Aminabhavi TM, Aithal US, Shukla SS. 1989 "Molecular-Transport Of Organic Liquids Through Polymer-Films" *Journal Of Macromolecular Science-Reviews In Macromolecular Chemistry And Physics* **C29** 319-363.

[3] Aminabhavi TM, Aithal US, Shukla SS. 1988 "An Overview Of The Theoretical-Models Used To Predict Transport Of Small Molecules Through Polymer Membranes" *Journal Of Macromolecular Science-Reviews In Macromolecular Chemistry And Physics* **C28** 421-474 95.

[4] Aminabhavi TM, Naik GH. 1999 Sorption/desorption, diffusion, permeation and swelling of high density polyethylene geomembrane in the presence of hazardous organic liquids *Journal of Hazardous Materials* **64** 251-262.

[5] Aminabhavi TM, Harlapur SF, Aralaguppi MI. 1997 "A study on molecular transport of organic esters and aromatics into Viton fluoropolymers" *Journal Of Applied Polymer Science* 66 717-723.

[6] Anderson, Mark J., and Patrick J. Whitcomb. DOE Simplified. Portland, OR: Productivity, Inc., 2000.

[7] Anna DH, Zellers ET, Sulewski R. 1998 "ASTM F739 method for testing the permeation resistance of protective clothing materials: Critical analysis with proposed changes in procedure and test cell design" *American Industrial Hygiene Association Journal* **59** 547-556.

[8] ASTM F 739. "Resistance of Protective Clothing Materials to Permeation by Liquids or Gases Under Conditions of Continuous Contact." PA: ASTM, 1999.

[9] ASTM F739-99a. "Standard Test Method for Resistance of Protective Clothing Materials to Permeation by Liquids or Gases Under Conditions of Continuous Contact" 1999.

[10] August H, Tatzky R. "Permeabilities of commercially available polymeric liners for hazardous landfill leachate organic constituents." In: Int. Conf. Geomembr. 1984. 163.

[11] Blayney, Michael. 2001. "The Need for Empirically Derived Permeation Data for Personal Protective Equipment: The Death of Dr. Karen E. Wetterhahn." *Applied Occupational and Environmental Hygiene* **16** 233-236.

[12] Brandrup, J. et al. Polymer Handbook 4th ed. New York: Wiley, 2005.

[13] Britton LN, Ashman RB, Aminabhavi TM, Cassidy PE. 1989 "Permeation And Diffusion Of Environmental-Pollutants Through Flexible Polymers Journal Of Applied Polymer Science" 38 227-236.

[14] Chao, Keh-Ping, et al. 2003 "Organic Solvents Permeation Through Protective Nitrile Gloves." *Journal of Hazardous Materials* **99** 191-201.

[15] Cohen DS. 1984 "Diffusive Fronts Of Penetrants In Glassy-Polymers" *Physica D* **12** 369-374.

[16] Cohen DS, Goodhart C. 1987 "Sorption Of A Finite Amount Of Swelling Solvent In A Glassy Polymer" *Journal Of Polymer Science Part B-Polymer Physics* **25** 611-617.

[17] Cornell, John. Experiments with Mixtures. 3rd ed. New York: Wiley, 2002.

[18] Crank J, Park GS, Editors. Diffusion in Polymers. New York: Academic Press; 1968.

[19] De Kee D, Fong C, Pintauro P, Hinestroza J, Yuan C, Burczyk A. 2000 "Effect of temperature and elongation on the liquid diffusion and permeation characteristics of natural rubber, nitrile rubber, and bromobutyl rubber." *Journal Of Applied Polymer Science* **78** 1250-1255.

[20] "Deformation and flow." The New Encyclopedia Britannica. Chicago: Encylcopedia Britannica, 2002.

[21] Dhoot, S. et al. 2004 "Sorption and Transport of Linear and Branched Ketones in Biaxially Oriented Polyethylene Terephthalate." *Polymer* **45**: 5619-5628.

[22] Dhoot, S., and Benny D. Freeman. 2004 "Sorption and Transport of Linear Esters and Branched Alkanes in Biaxially Oriented Polyethylene Terephthalate." *Ind. Eng. Chem. Res.* **43**: 2966-2976.

[23] Dixon-Garrett SV, Nagai K, Freeman BD. 2000 "Sorption, diffusion, and permeation of ethylbenzene in poly(1-trimethylsilyl-1-propyne)" *Journal Of Polymer Science Part BPolymer Physics* **38** 1078-1089.

[24] Doumenc, F., B. Guerrier, and C. Allain. 2005 "Coupling between mass diffusion and film temperature evolution in gravimetric experiments." *Polymer* **46**: 3708-3719.

[25] Dowling, Norman E. Mechanical Behavior of Materials: Engineering Methods for Deformation, Fracture, and Fatigue. NJ: Prentice Hall, 1999.

[26] Durning CJ, Russel WB. 1985 "A Mathematical-Model For Diffusion With Induced Crystallization.1" *Polymer* **26** 119-130.

[27] Durning CJ, Russel WB. 1985 "A Mathematical-Model For Diffusion With Induced Crystallization.2 "*Polymer* **26** 131-140.

[28] Ehnthold D.J. et al. 1988 "Test method development and evaluation of protective clothing items used in agricultural pesticide operations." *ASTM Spec. Tech. Publ.* **989** 727.

[29] Fong C, Moresoli C, Xiao S, Li Y, Bovenkamp J, De Kee D. 1998 "Modeling diffusion through geomembranes" *Journal Of Applied Polymer Science* 67 1885-1889.

[30] Forsberg, K. Quick selection guide to chemical protective clothing. New York: J. Wiley, 2002.

[31] Fung, Y. C. and Pin Tong. Classical and Computational Solid Mechanics. NJ: World Scientific Publishing, 2001.

[32] Gao, Pengfei et al. 2005 "Change in Permeation Parameters and the Decontamination Efficacy of Three Chemical Protective Gloves After Repeated Exposures to Solvents and Thermal Decontaminations." *American Journal of Industrial Medicine* **47**: 131-143.

[33] Georgoulis, LB et al. 2004 "Swelling of Polymeric Glove Materials during Permeation by Solvent Mixtures." *Journal of Applied Polymer Science* **97** 775-783.

[34] Hansen CM. 2004 "Aspects of solubility, surfaces and diffusion in polymers" *Progress In Organic Coatings* **51** 55-66.

[35] Hansen, Charles M. Hansen solubility parameters: a user's handbook. Boca Raton, FL: CRC Press, 2000.

[36] Haxo HE, Jr. 1990 "Determining the transport through geomembranes of various permeants in different applications" ASTM Spec. Tech. Publ. 1081 75.

[37] Hedlund J, Jareman F, Andersson C. Factors affecting the performance of MFI membranes. In: Recent Advances In The Science And Technology Of Zeolites And Related Materials, Pts A - C. Amsterdam: Elsevier Science Bv; 2004. p. 640-646.

[38] Hinestroza, Juan, et al. 2001 "Apparatus for Studying the Effect of Mechanical Deformation on the Permeation of Organics through Polymeric Films." *Industrial Engineering & Chem. Res.* **40** 2183 – 2187.

[39] Hinestroza J, De Kee D. 2004 "Permeation of organics through linear low density polyethylene geomembranes under mechanical deformation." *Journal Of Environmental Engineering-Asce* **130** 1468-1474.

[40] Islam MA, Buschatz H. 2005 "Assessment of thickness-dependent gas permeability of polymer membranes" *Indian Journal Of Chemical Technology* **12** 88-92.

[41] Kulkami, Sangeeta B. et al. 2003 "Sorption, Diffusion, and Permeation of Esters, Aldehydes, Ketones, and Aromatic Liquids into Tetrafluoroethylene/Propylene at 30, 40, and 50C." *Journal of Applied Polymer Science* **89**: 3201-3209.

[42] Lee BL, Yang TW, Hassler KD, Wilusz E 1996 "Effects of Biaxial Tensile Strain on Hydrocarbon Permeability of Butyl Rubber Composite Barriers" ASTM Spec. Tech. Publ. 1237 157-174.

[43] Li Y, De Kee D, Fong C, Pintauro P, Burczyk A. 1999 "Influence of external stress on the barrier properties of rubbers." *Journal Of Applied Polymer Science* **74** 1584-1595.

[44] Liu CPA, Nguyen DC, Neogi P. 1990 "Effects Of Constrained Chain Conformations On Polymer-Solute Interactions In Semicrystalline Polymers" *Journal Of Macromolecular Science-Physics* **B29** 203-220.

[45] Liu, Chien-Kuo et al. 2005 "Effect of Compression and Thickness on Acetone Transport in Polycarbonate." *Polymer and Engineering Science* 687-693.

[46] Long FA, Richman D. 1960 "Concentration Gradients For Diffusion Of Vapors In Glassy Polymers And Their Relation To Time Dependent Diffusion Phenomena" *Journal Of The American Chemical Society* 82 513-519.

[47] Mores M, Cassidy PE, Kerwick DJ, Koeck DC. 1990 "A review of polymer test methods applicable to geosynthetics for waste containment" ASTM Spec. Tech. Publ. 1081 12.

[48] Nelson, C. N., and N. W. Henry. Performance of Protective Clothing: Issues and Priorities for the 21st Century: Seventh Volume. West Conshohocken, PA: ASTM, 2000; 583: 365-374.

[49] Nelson GO, Priante SJ, Strong M, Anderson D, Fallon-Carine J. 2000 "Permeation of substituted silanes and siloxanes through selected gloves and protective clothing" Aihaj 61 709-714.

[50] Neogi P. Diffusion in Polymers. New York, NY: Marcel Dekker, 1996: 173-209.

[51] O'Callaghan K, Fredericks PM, Bromwich D. 2001 "Evaluation of chemical protective clothing by FT-IR/ATR spectroscopy" *Applied Spectroscopy* 55 555-562.

[52] Park JK, Sakti JP, Hoopes JA. 1996 "Determination of volatile organic compound permeation through geomembranes" ASTM Spec. Tech. Publ. 1261 245.

[53] Perkins JL. AIHA Chemical Protective Clothing Series. VA: AIHA, 2003.

[54] "Permeability." The New Encyclopedia Britannica. Chicago: Encyclopedia Britannica, 2002.

[55] Perron, Gerald et al. 2002 "Permeation of Mixtures of Organic Liquids through Polymeric Membranes: Role of Liquid-Liquid Interactions" *Journal of Applied Polymer Science* **86** 195-215.

[56] Perron G, Banh TN, Pelletier L, Desnoyers JE, Lara J. 2000 "Volumetric and swelling techniques for studying the permeation of protective gloves to solvents" ASTM Spec. Tech. Publ. 1386.

[57] Petropoulos JH, Sanopoulous M, Papadokostaki KG. 1999 "Fundamentals of transport phenomena in polymer solution-diffusion membranes" *Surfactant Sci. Ser.* **79** 167.

[58] Petropoulos JH, Roussis PP. 1978 "Influence Of Transverse Differential Swelling Stresses On Kinetics Of Sorption Of Penetrants By Polymer Membranes" *Journal Of Membrane Science* 3 343-356.

[59] Pinette MFS et al. 1992 "A preliminary study of an intermittent collection procedure as an alternative permeation method for non-volatile, water insoluble chemicals." *ASTM Spec. Tech. Publ.* **1133** 339.

[60] Prasad TV, Brown KW, Thomas JC. 1994 "Diffusion-Coefficients Of Organics In High-Density Polyethylene (Hdpe)" *Waste Management & Research* 12 61-71

[61] Puri P, Hinestroza J, De Kee D. 2005 "Transport of small molecules through mechanically elongated polymeric membranes." *Journal Of Applied Polymer Science* **96** 1200-1203.

[62] Que Hee SS. 1996 "Simple glove permeation models" *Appl. Occup. Environ. Hyg.* 11 117.

[63] Richman D, Long FA. 1960 "Measurement Of Concentration Gradients For Diffusion Of Vapors In Polymers" *Journal Of The American Chemical Society* 82 509-513.

[64] Ridge MC, PJ. 1989 "Permeation of solvent mixtures through protective clothing elastomers" *ASTM Spec. Tech. Publ.* **1037** 113.

[65] Riley, Beck and Lauren Sternsen-Newman. "On the Front Lines: Health Hazards Posed to Pesticide Applicators." Restoring Healthy School Landscapes. January 2003. <http://www.pesticide.org/RHSLApplicatorExposure.pdf>.

[66] Rodriguez, Axel and Donald Rivin. "Liquid Permeation of Elastomers with a Fully Flooded Cell Test Method." *ANTEC 2004 Plastics: Annual Technical Conference, Volume 2: Materials* 2410-2412.

[67] Sanopoulou M, Stamatialis DF, Petropoulos JH. 2002 "Investigation of case II diffusion behavior. 1. Theoretical studies based on the relaxation dependent solubility model" *Macromolecules* **35** 1012-1020.

[68] Schwope A.D., Klein J, Sidman KR, and Reid R.C. 1986 "Sorption Desorption Phenomena Of Chemicals From Polymer (Paint) Films." *Journal Of Hazardous Materials* **13** 353-367.

[69] Strong, Clyde B., et al. Emergency Response and Hazardous Chemical Management. Florida: St. Lucie Press, 1996.

[70] Thomas NL, Windle AH. 1980 "A Deformation Model For Case-II Diffusion" *Polymer* 21 613-619.

[71] Thomas N, Windle AH. 1978 "Transport Of Methanol In Poly(Methyl Methacrylate)" *Polymer* 19 255-265.

[72] Treloar LRG. 1950 "The Swelling Of Cross-Linked Amorphous Polymers Under Strain." *Transactions Of The Faraday Society* **46** 783-789.

[73] Vahdat, Nader, and Victor D. Sullivan. 2000 "Estimation of Permeation Rate of Chemicals Through Elastomeric Materials." *Journal of Applied Polymer Science* **79**: 1265-1272.

[74] Valente AJM, Polishchuk AY, Burrows HD, Lobo VMM. 2005 "Permeation of water as a tool for characterizing the effect of solvent, film thickness and water solubility in cellulose acetate membranes" *European Polymer Journal* **41** 275-281.

[75] Van der Bruggen B, Jansen JC, Figoli A, Geens J, Van Baelen D, Drioli E, et al. 2004 "Determination of parameters affecting transport in polymeric membranes: Parallels between pervaporation and nanofiltration" *Journal Of Physical Chemistry B* **108** 13273-13279.

[76] Vrentas JS, Vrentas CM, Huang WJ. 1997 "Anticipation of anomalous effects in differential sorption experiments" *Journal Of Applied Polymer Science* **64** 2007-2013.

[77] Vrentas JS, Vrentas CM. 1993 "Evaluation Of Free-Volume Theories For Solvent Self-Diffusion In Polymer Solvent Systems" *Journal Of Polymer Science Part B-Polymer Physics* **31** 69-76.

[78] Vrentas JS, Vrentas CM. 1998 "Temperature dependence of partition coefficients for polymer-solvent systems" *Macromolecules* **31** 5539-5541.

[79] Vrentas JS, Duda JL, Hsieh ST. 1983 "Thermodynamic Properties Of Some Amorphous Polymer Solvent Systems" *Industrial & Engineering Chemistry Product Research And Development* 22 326-330.

[80] Wilusz E, Hassler KD. 1992 "Chemical resistance properties of advanced glove materials" ASTM Spec. Tech. Publ. 1133 114.

[81] Wilusz E, Brennick JR, Gulliani DK, Hassler KD. 1991 "Novel barrier materials based on butyl rubber" *Polym. Prepr. (Am. Chem. Soc., Div. Polym. Chem.)* 32 296.

[82] Wolf CJ, Fu H. 1996 "Stress-enhanced transport of toluene in poly aryl ether ether ketone (PEEK)" *Journal Of Polymer Science Part B-Polymer Physics* **34** 75-82.

[83] Xiao S, Moresoli C, Bovenkamp J, DeKee D. 1997 "Sorption and permeation of organic contaminants through high-density polyethylene geomembranes." *Journal Of Applied Polymer Science* **65** 1833-1836.

[84] Xiao S, Moresoli C, Burczyk A, Pintauro P, De Kee D. 1999 "Transport of organic contaminants in geomembranes under stress." *Journal Of Environmental Engineering Asce* **125** 647-652.

[85] Ybarra RM, Neogi P, MacElroy JMD 1998 Osmotic stresses and wetting by polymer solutions *Industrial & Engineering Chemistry Research* **37** 427-434.

[86] Zhen, Hanfei, Steven Jang, and W.K.Teo. 2003 "Sorption Studies of Volatile Organic Compounds in a Divinyl-Terminated Polydimethylsiloxane-Oligo Polymer." *Journal of Applied Polymer Science* **92**: 920-927.

Appendices

Appendix A: Randomized run order of experiments

Table 7: Randomized run order of experimental combinations

Run Order	Deformation Level	Xylene % by Vol.	Acetone % by Vol.	Toluene % by Vol.
31	0	0.8	0	0.2
12	0	0.6	0.4	0
75	0	0.4	0	0.6
28	0	0.2	0.6	0.2
7	0	0	1	0
63	0	1	0	0
81	0	0	0	1
51	0	0.6	0.2	0.2
62	0	0	0.8	0.2
30	0	0.2	0.8	0
82	0	0.8	0.2	0
76	0	0.4	0.2	0.4
56	0	0	0.6	0.4
38	0	0	0.2	0.8
14	0	0	0.4	0.6
26	0	0.2	0	0.8
24	0	0.4	0.6	0
16	0	0.4	0.4	0.2
27	0	0.2	0.2	0.6
3	0	0.2	0.4	0.4
47	0	0.6	0	0.4
39	20	0.8	0	0.2
23	20	0.6	0.4	0
29	20	0.4	0	0.6
20	20	0.2	0.6	0.2
11	20	0	1	0
49	20	1	0	0
61	20	0	0	1
45	20	0.6	0.2	0.2
48	20	0	0.8	0.2
40	20	0.2	0.8	0
53	20	0.8	0.2	0
32	20	0.4	0.2	0.4
19	20	0	0.6	0.4
55	20	0	0.2	0.8
68	20	0	0.4	0.6
42	20	0.2	0	0.8
77	20	0.4	0.6	0
60	20	0.4	0.4	0.2

Table 7 (continued)

Run Order	Deformation Level	Xylene % by Vol.	Acetone % by Vol.	Toluene % by Vol.
44	20	0.2	0.2	0.6
22	20	0.2	0.4	0.4
13	20	0.6	0	0.4
71	30	0.8	0	0.2
33	30	0.6	0.4	0
41	30	0.4	0	0.6
18	30	0.2	0.6	0.2
46	30	0	1	0
43	30	1	0	0
57	30	0	0	1
58	30	0.6	0.2	0.2
25	30	0	0.8	0.2
79	30	0.2	0.8	0
52	30	0.8	0.2	0
6	30	0.4	0.2	0.4
1	30	0	0.6	0.4
70	30	0	0.2	0.8
73	30	0	0.4	0.6
80	30	0.2	0	0.8
17	30	0.4	0.6	0
66	30	0.4	0.4	0.2
69	30	0.2	0.2	0.6
84	30	0.2	0.4	0.4
34	30	0.6	0	0.4
83	40	0.8	0	0.2
72	40	0.6	0.4	0
9	40	0.4	0	0.6
4	40	0.2	0.6	0.2
50	40	0	1	0
37	40	1	0	0
36	40	0	0	1
67	40	0.6	0.2	0.2
21	40	0	0.8	0.2
54	40	0.2	0.8	0
64	40	0.8	0.2	0
78	40	0.4	0.2	0.4
59	40	0	0.6	0.4
74	40	0	0.2	0.8
8	40	0	0.4	0.6
2	40	0.2	0	0.8
15	40	0.4	0.6	0
65	40	0.4	0.4	0.2

Table 7 (continued)

Run Order	Deformation Level	Xylene % by Vol.	Acetone % by Vol.	Toluene % by Vol.
5	40	0.2	0.2	0.6
10	40	0.2	0.4	0.4
35	40	0.6	0	0.4

Appendix B: FTIR peak area conversion to concentration

Table 8: Concentration calculations

Toluene							
Concentration (µg/cm^3)	2.41	6.93	21.14	23.25	48.00		Factor
Mixture Percent	14.30	28.60	42.90	57.10	100.00		
Chemical Flowrate (L/min)	0.10	0.20	0.30	0.40	0.70		
Area	1.44	4.14	12.62	13.88	28.66		1.67
Area = -3.4496 + 0.3211 * Mixture Percent							
Concentration = -0.0011 + 1.6749 * Area							
Xylene							
Concentration (µg/cm^3)	0.61	14.07	35.64	69.66	133.00		
Mixture Percent	14.30	28.60	42.90	57.10	100.00		
Chemical Flowrate (L/min)	0.10	0.20	0.30	0.40	0.70		
Area	0.12	2.78	7.04	13.76	26.27		5.06
Area = -5.3821 + 0.3165 * Mixture Percent							
Concentration = -0.0017 + 5.0628 * Area							
Acetone							
Concentration (µg/cm^3)	7.90	18.35	29.04	33.73	34.09	682.00	
Mixture Percent	1.00	2.00	3.00	4.00	5.00	100.00	
Chemical Flowrate (L/min)	0.07	0.14	0.21	0.28	0.35	7.00	
Area	14.48	33.64	53.24	61.83	62.50	1250.17	0.54
Area = 7.869 + 12.423 * Mixture Percent							
Concentration = -0.0019 + 0.5455 * Area							

Appendix C: Flux versus time graphs for the 84 experimental combinations

Flux values are reported in μg/cm^2/min. Time is reported in minutes. In single component, binary and ternary mixtures where a component is designated as 0, the reported flux is not zero as there is interference. The graphs show zero flux for simplicity in reporting.

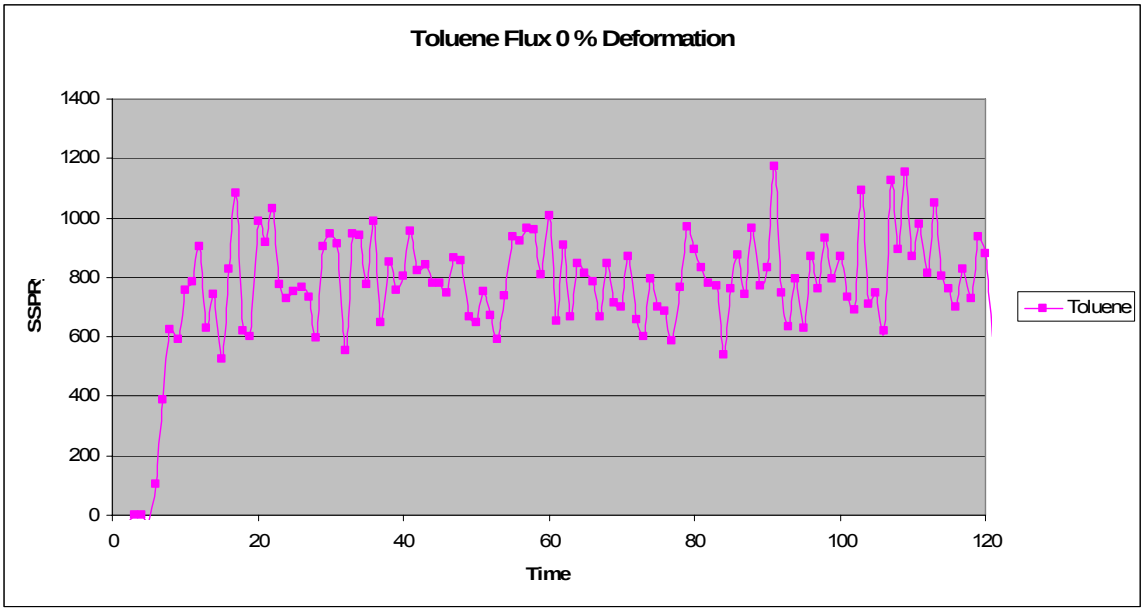

Figure 29: 100% Toluene flux 0% deformation

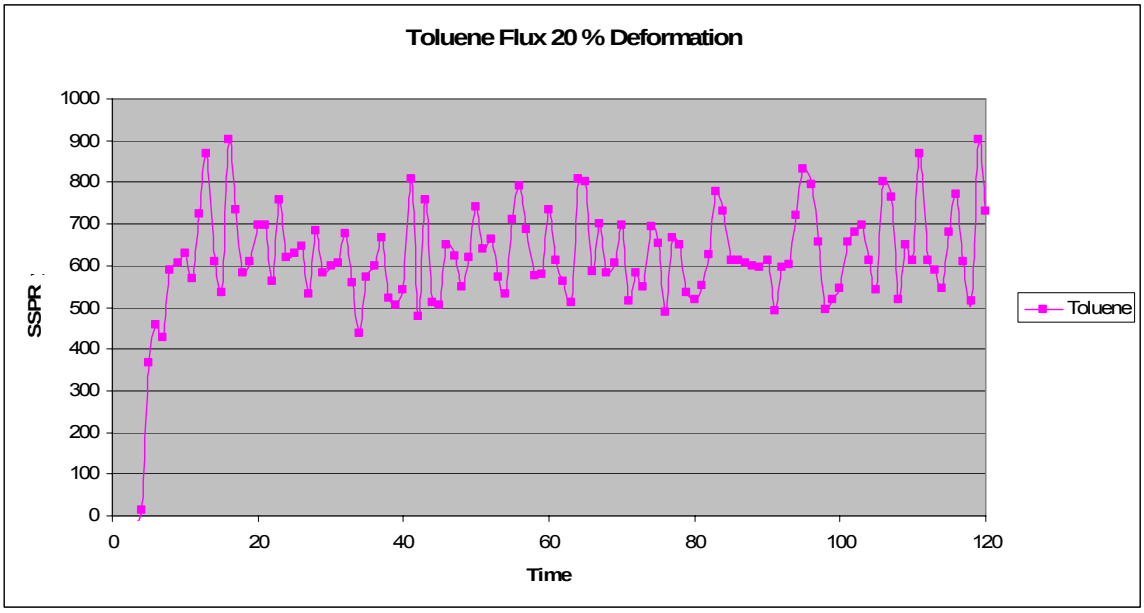

Figure 30: 100% Toluene flux 20% deformation

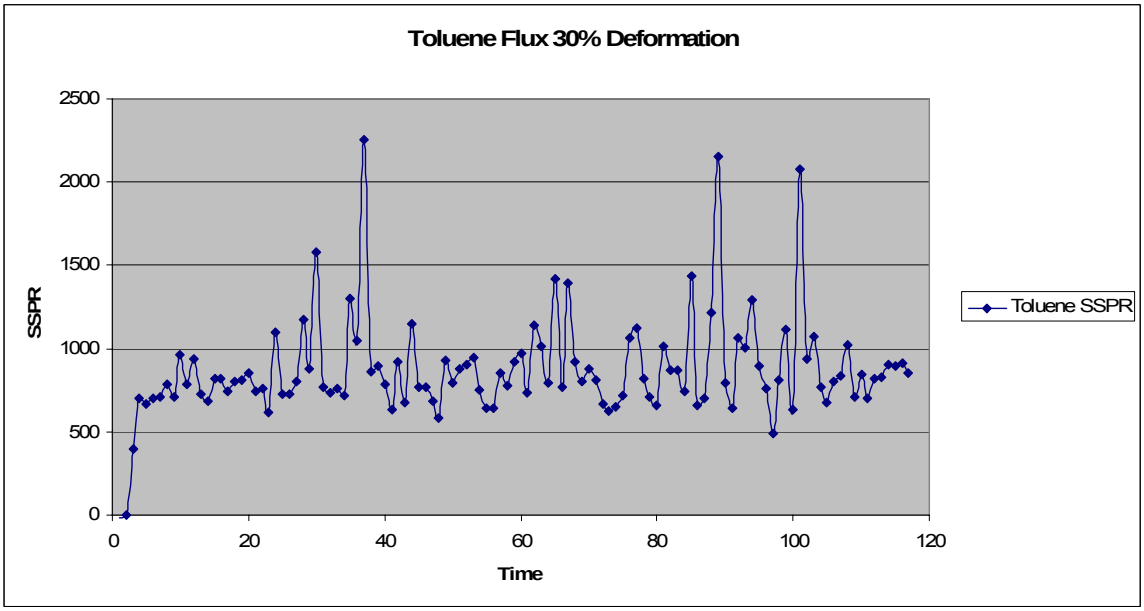

Figure 31: 100% Toluene flux 30% deformation

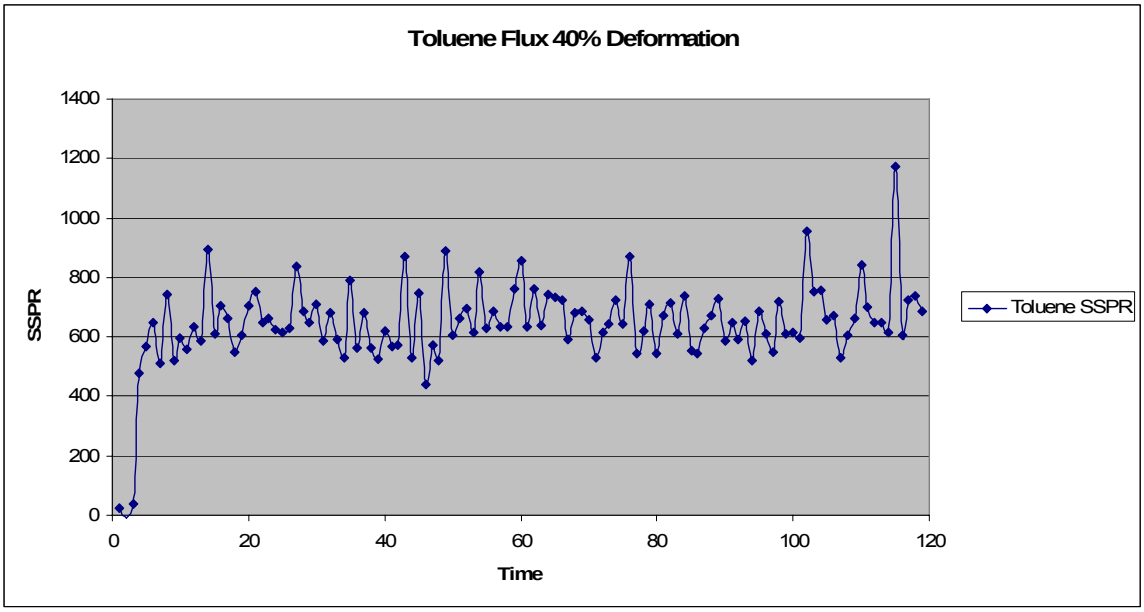

Figure 32: 100% Toluene flux 40% deformation

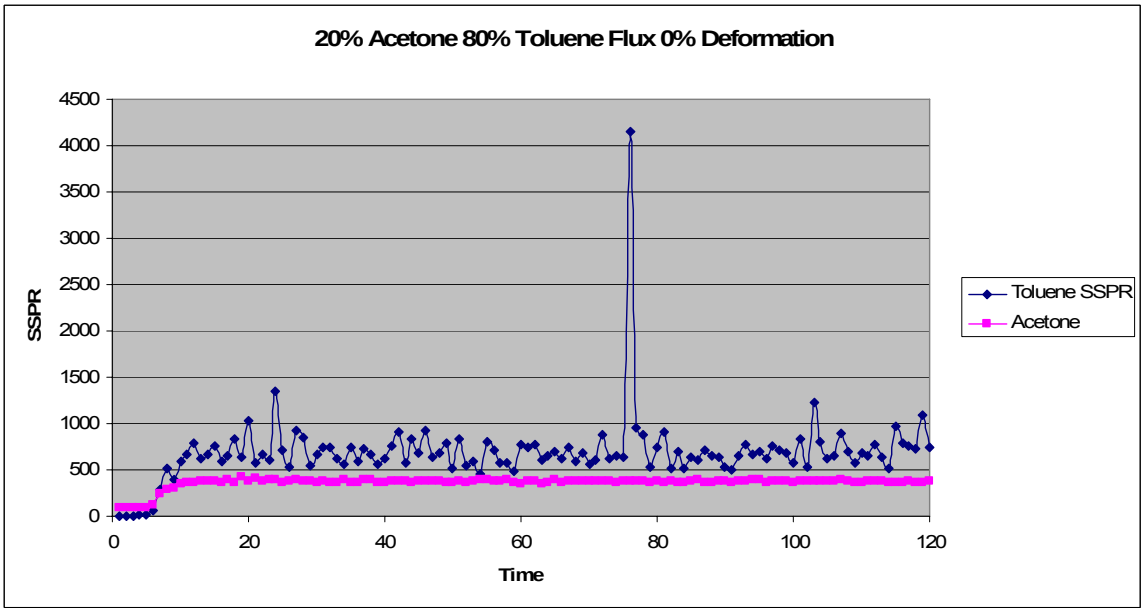

Figure 33: 20% acetone 80% toluene flux 0% deformation

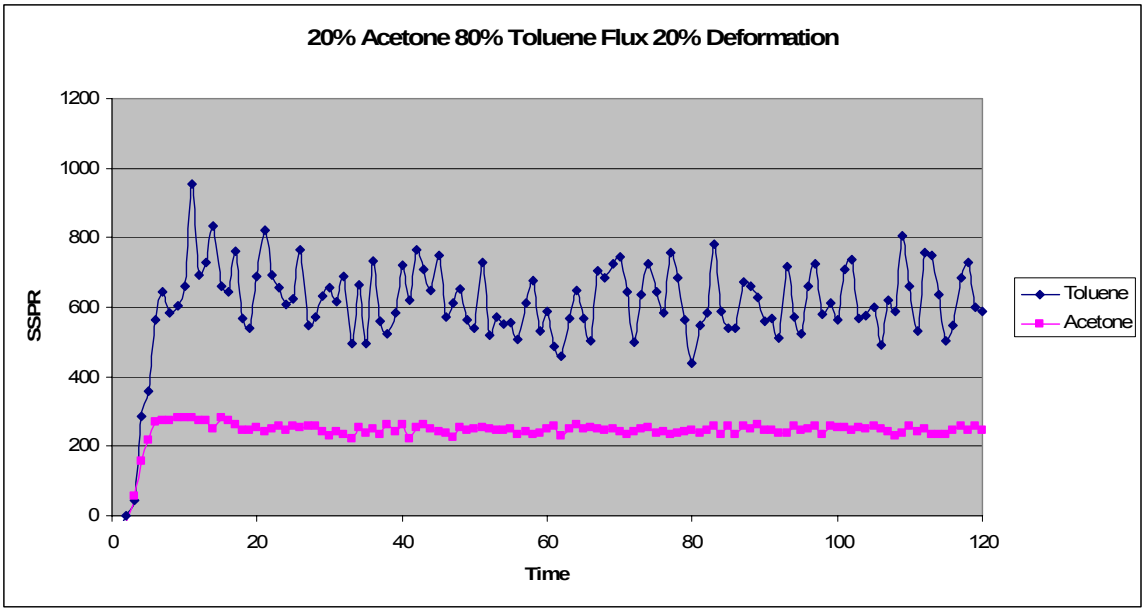

Figure 34: 20% acetone 80% toluene flux 20% deformation

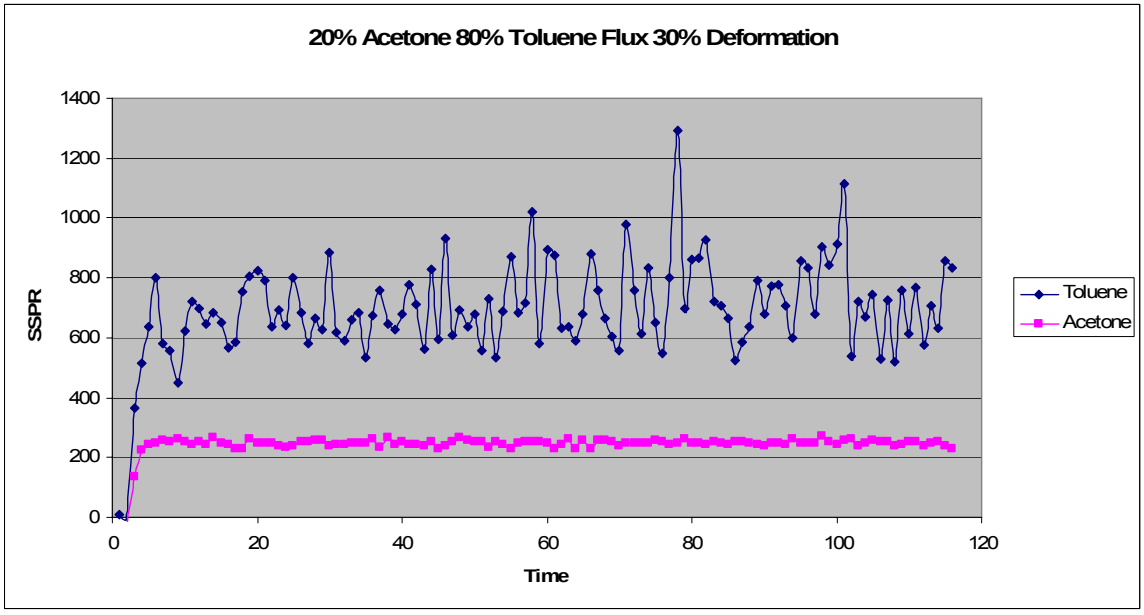

Figure 35: 20% acetone 80% toluene flux 30% deformation

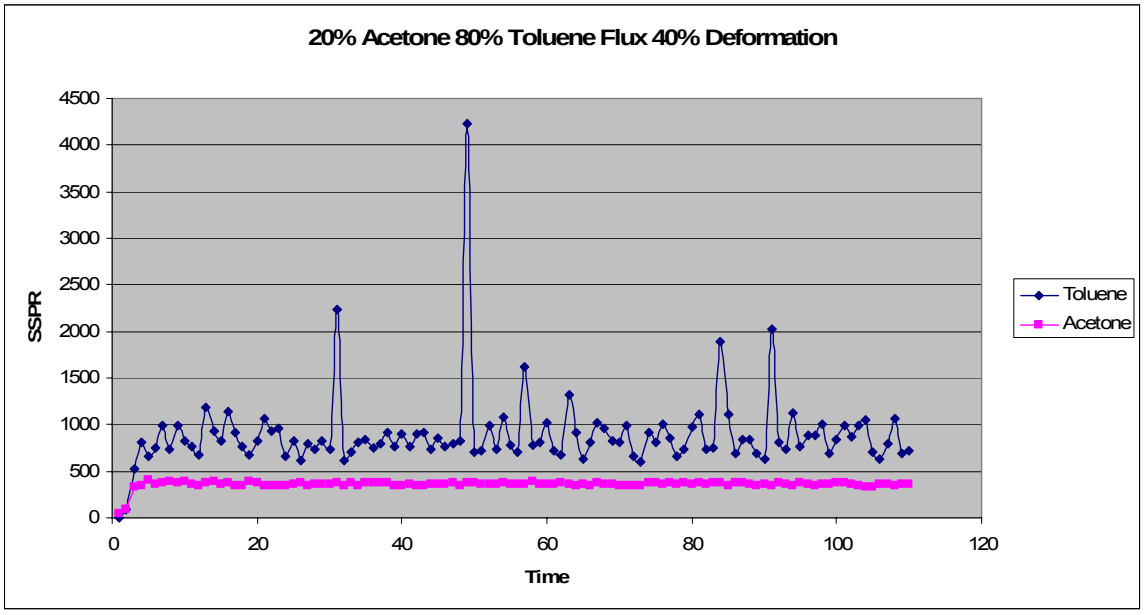

Figure 36: 20% acetone 80% toluene flux 40% deformation

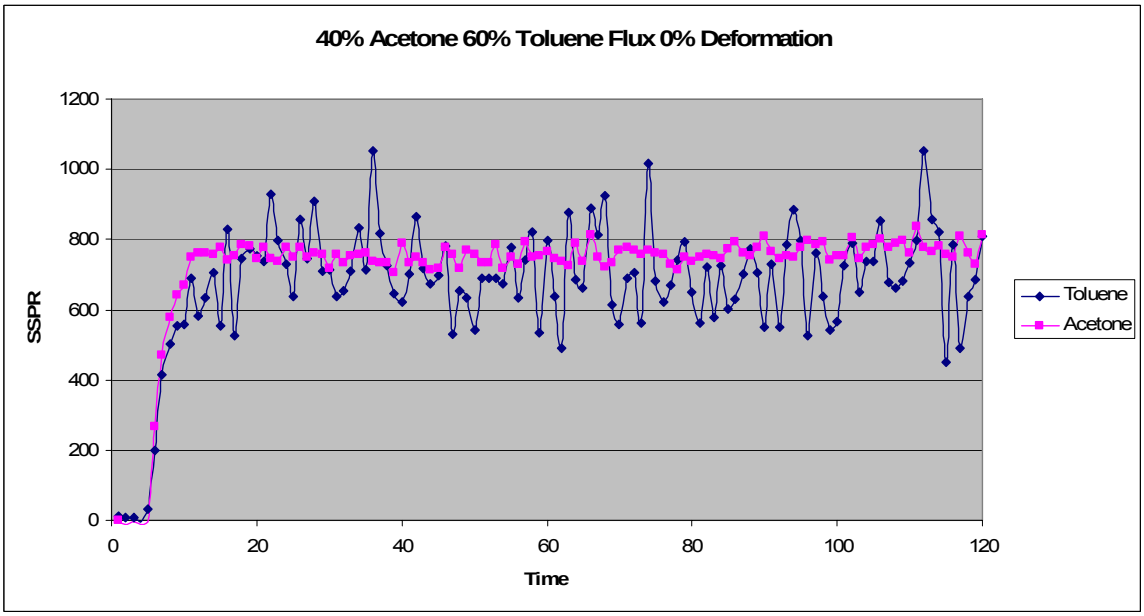

Figure 37: 40% acetone 60% toluene flux 0% deformation

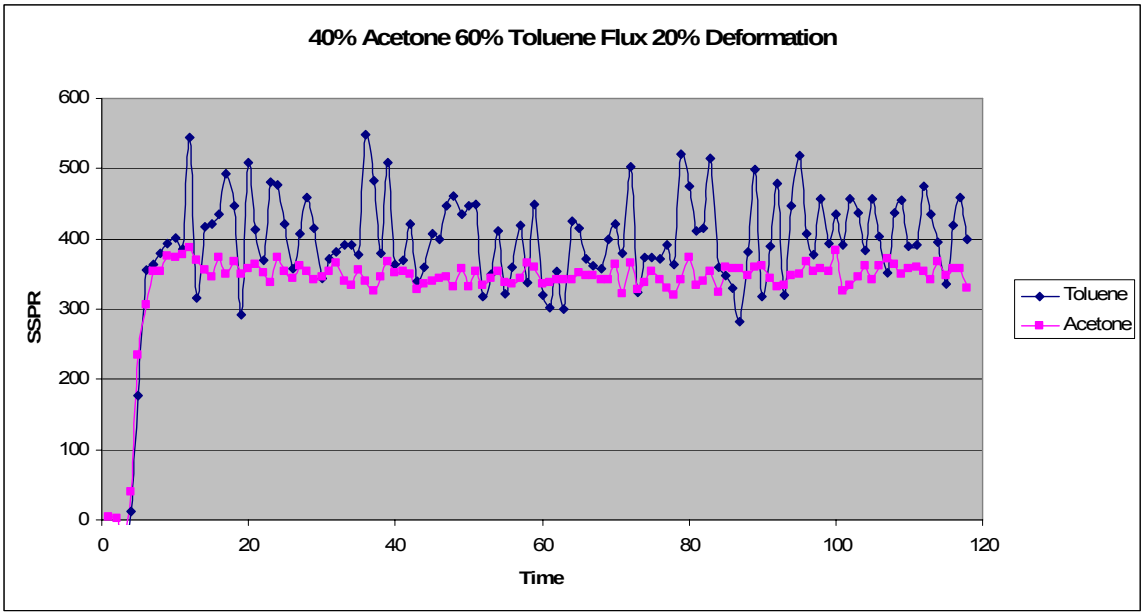

Figure 38: 40% acetone 60% toluene flux 20% deformation

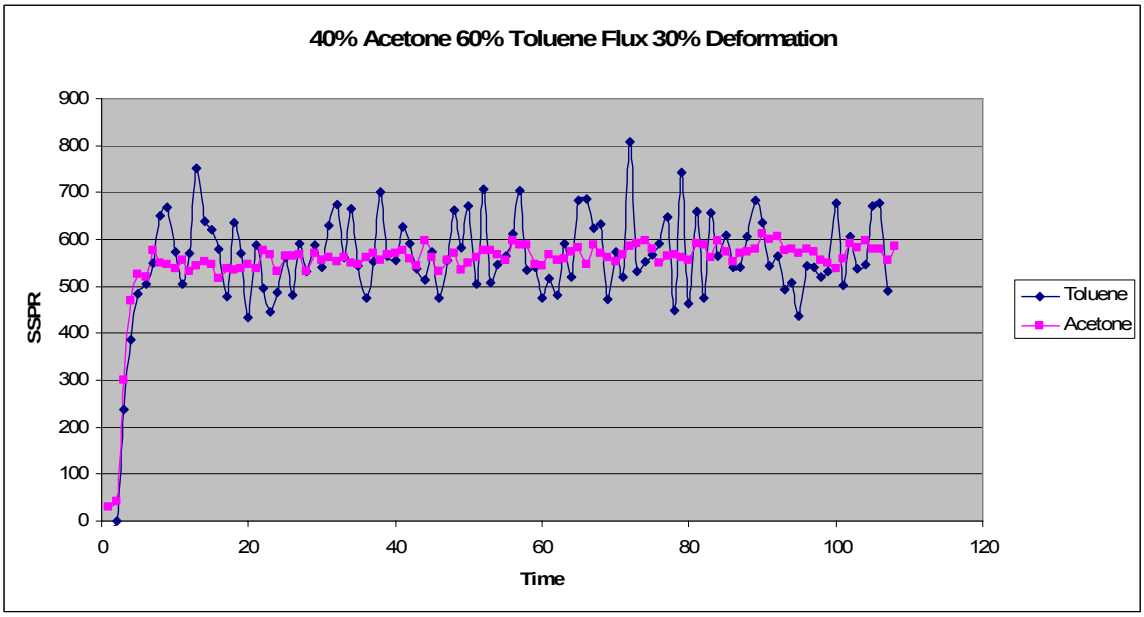

Figure 39: 40% acetone 60% toluene flux 30% deformation

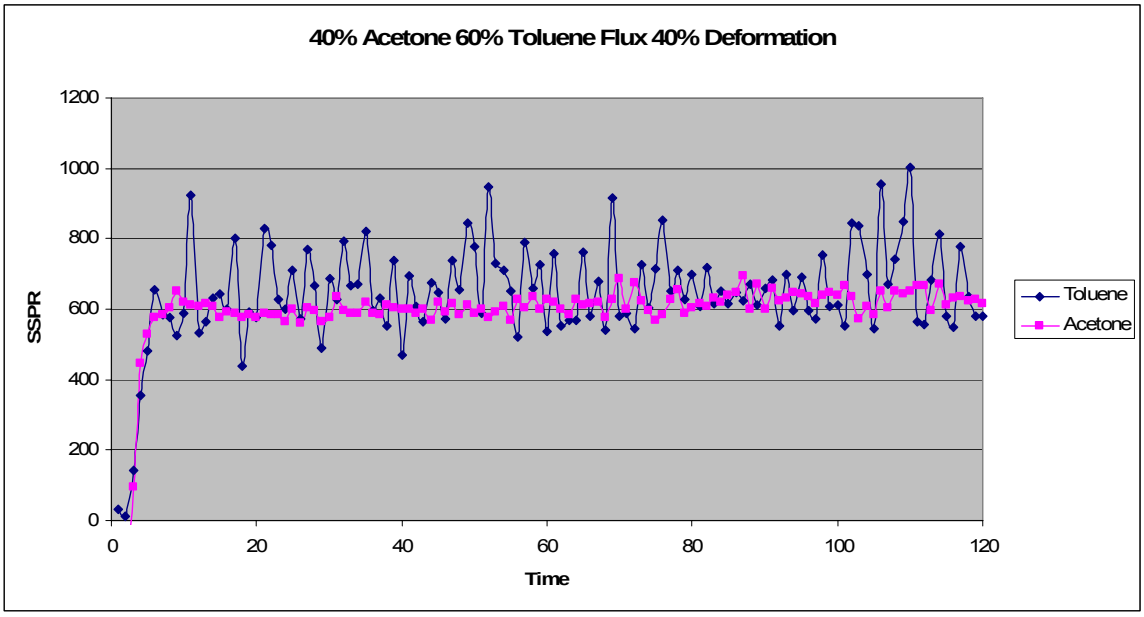

Figure 40: 40% acetone 60% toluene flux 40% deformation

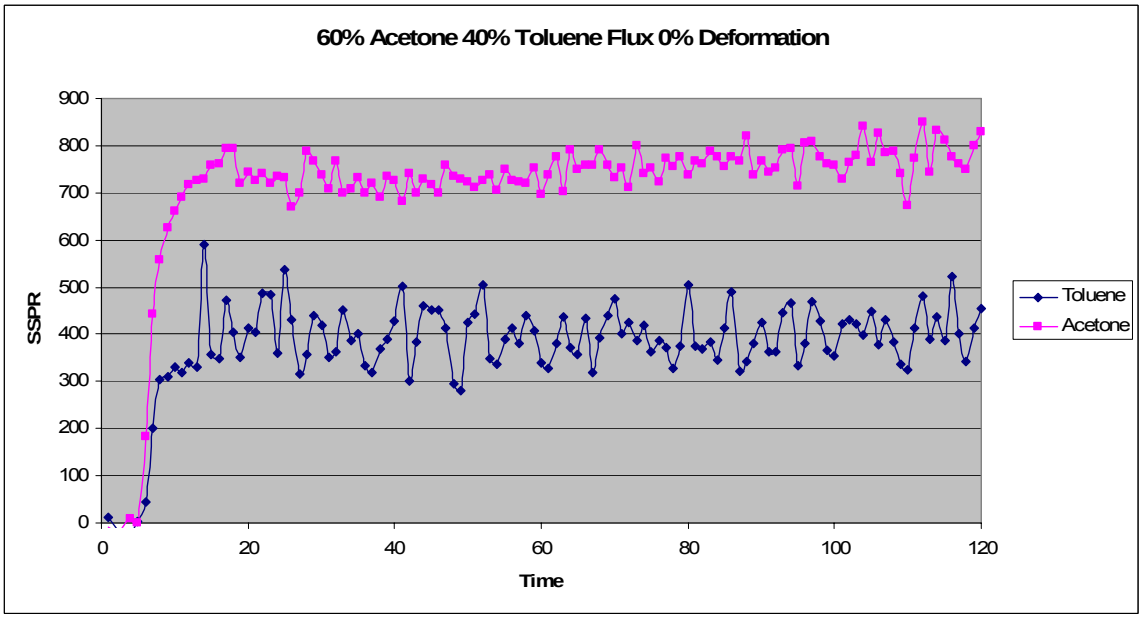

Figure 41: 60% acetone 40% toluene flux 0% deformation

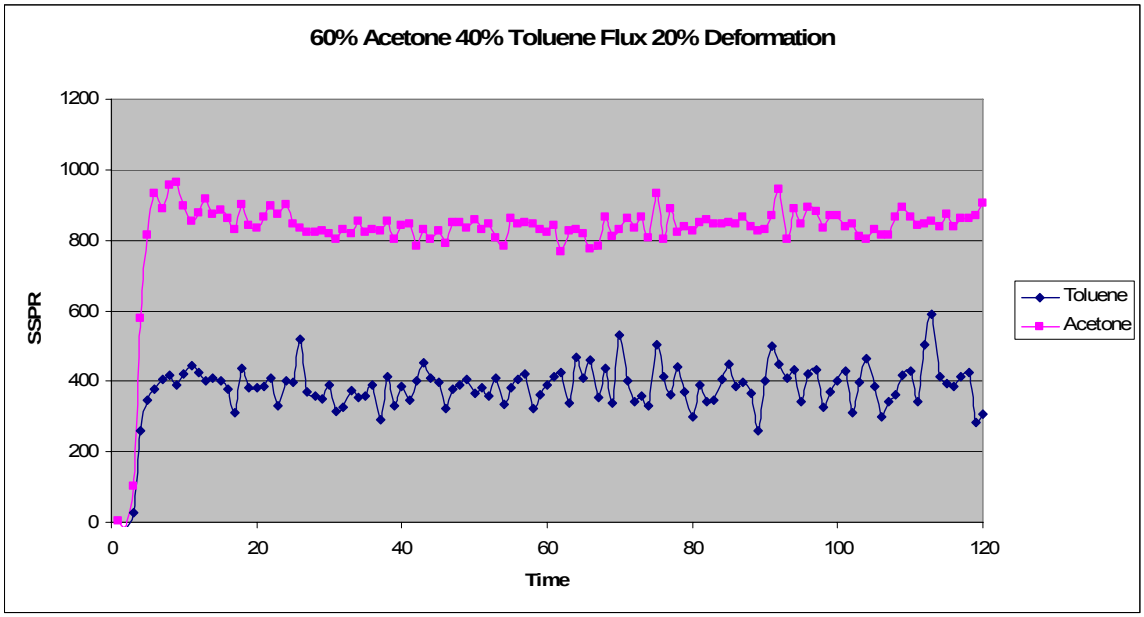

Figure 42: 60% acetone 40% toluene flux 20% deformation

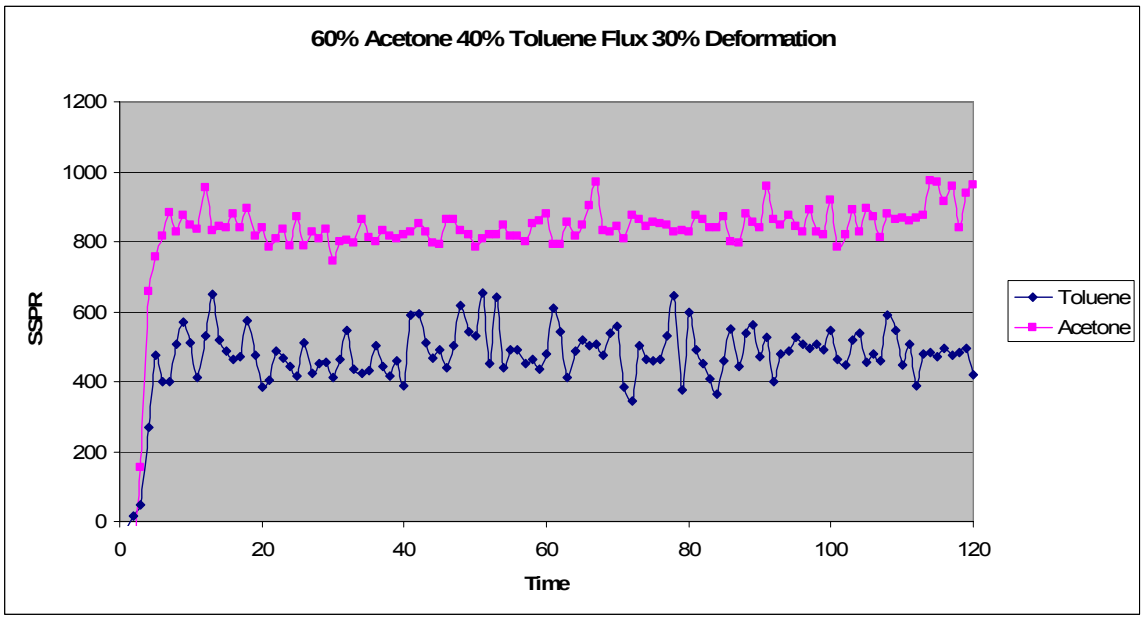

Figure 43: 60% acetone 40% toluene flux 30% deformation

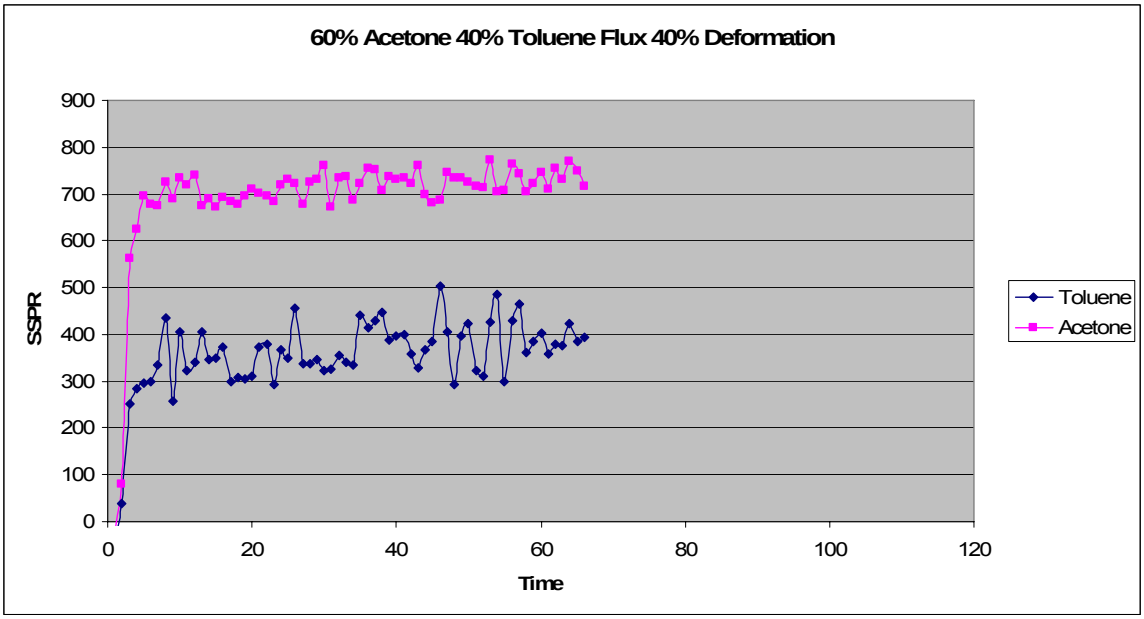

Figure 44: 60% acetone 40% toluene flux 40% deformation

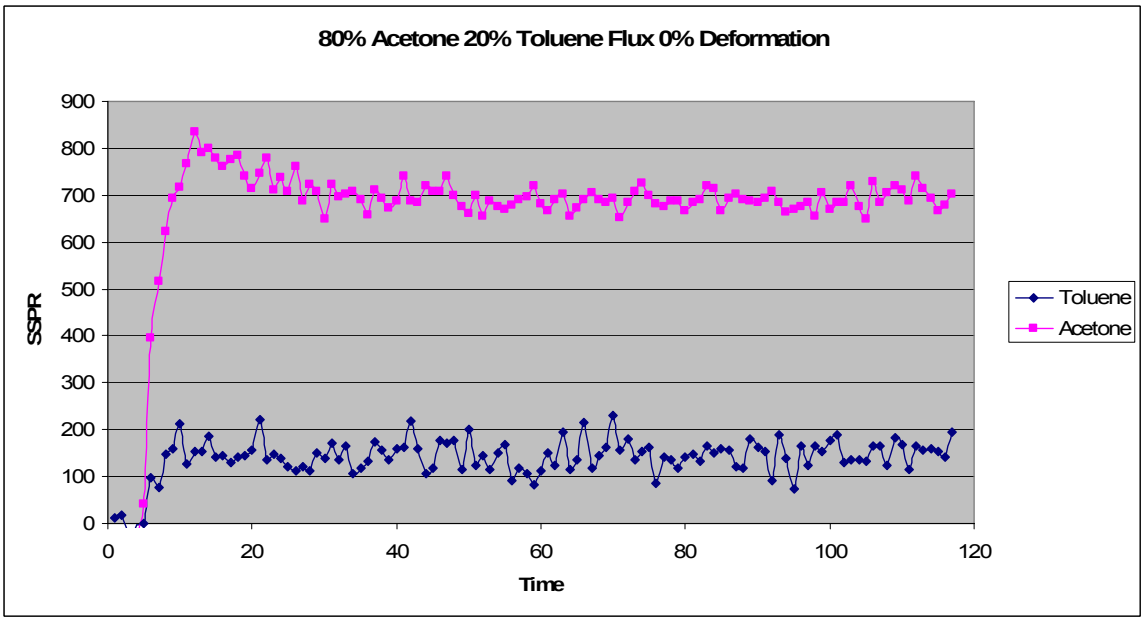

Figure 45: 80% acetone 20% toluene flux 0% deformation

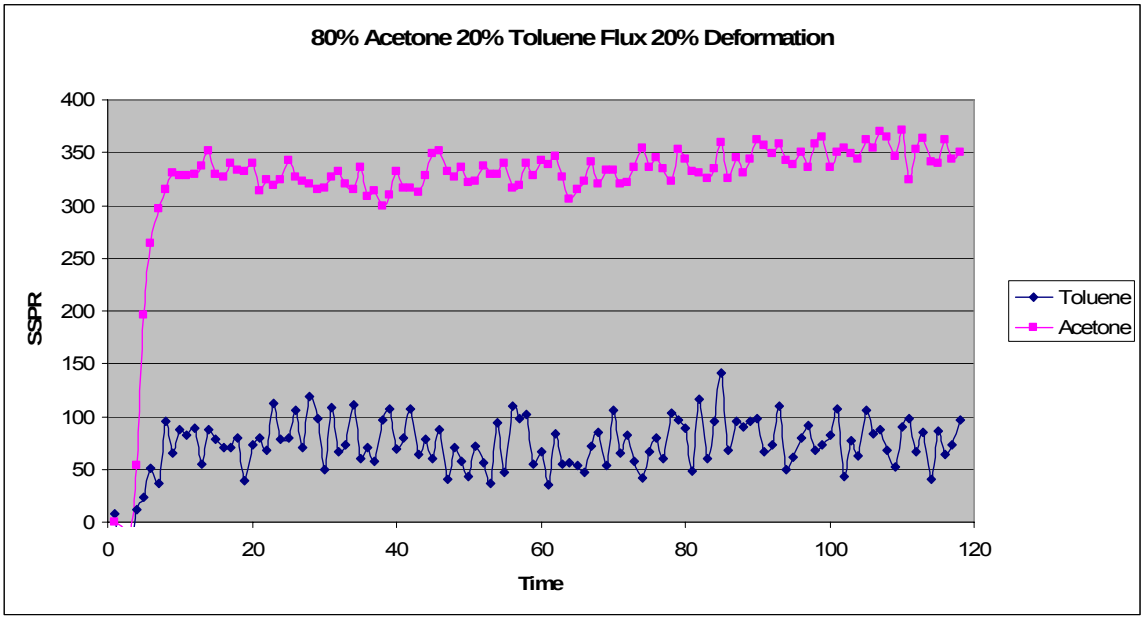

Figure 46: 80% acetone 20% toluene flux 20% deformation

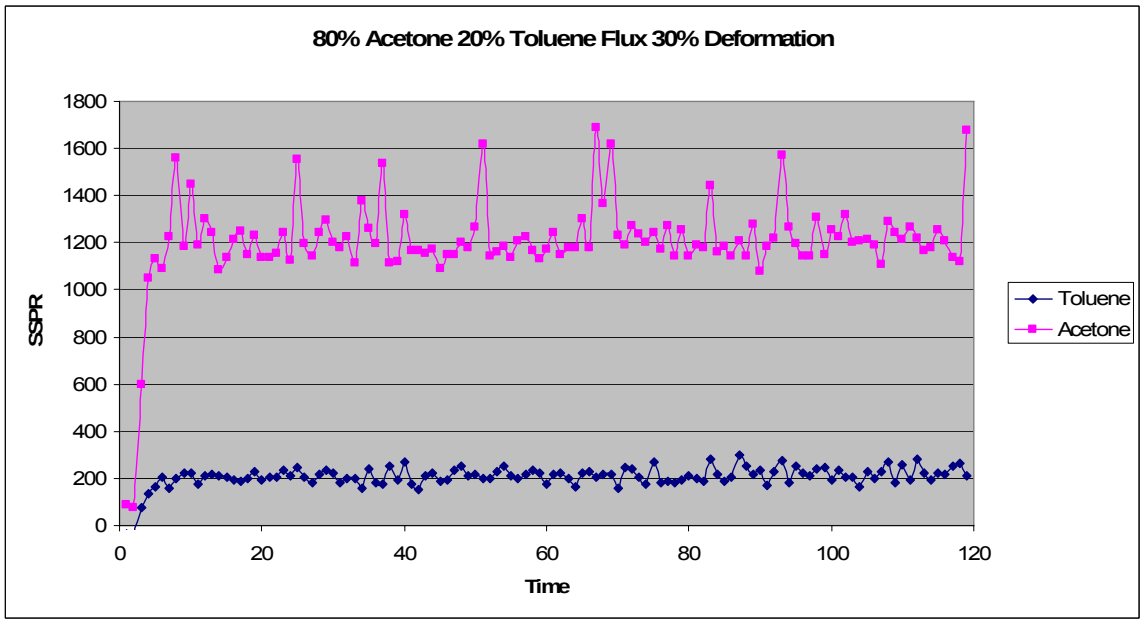

Figure 47: 80% acetone 20% toluene flux 30% deformation

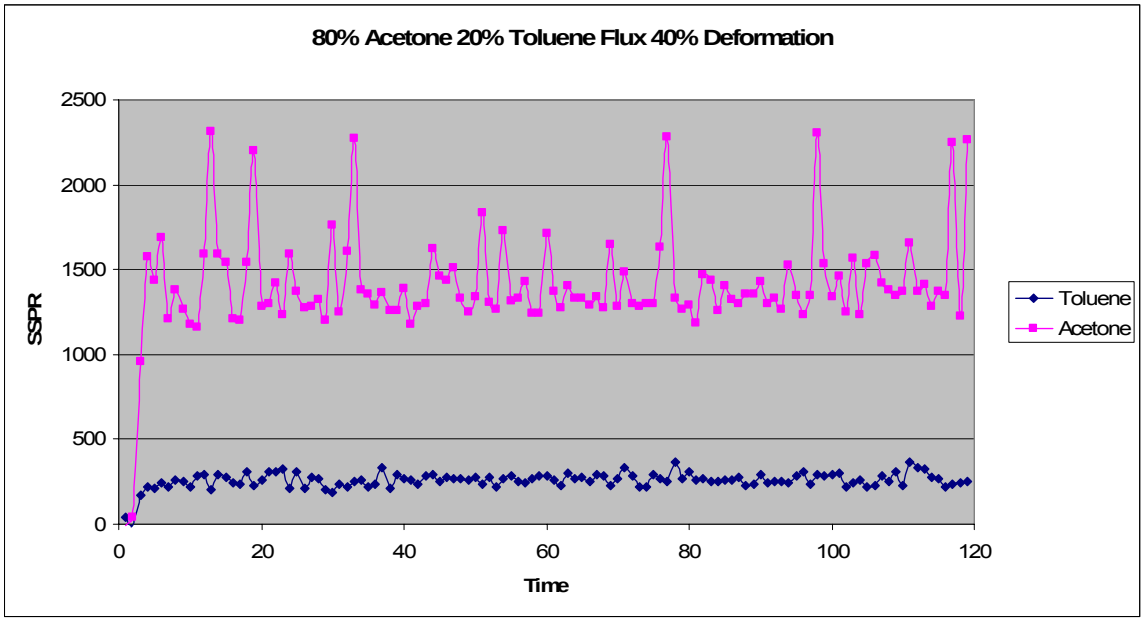

Figure 48: 80% acetone 20% toluene flux 40% deformation

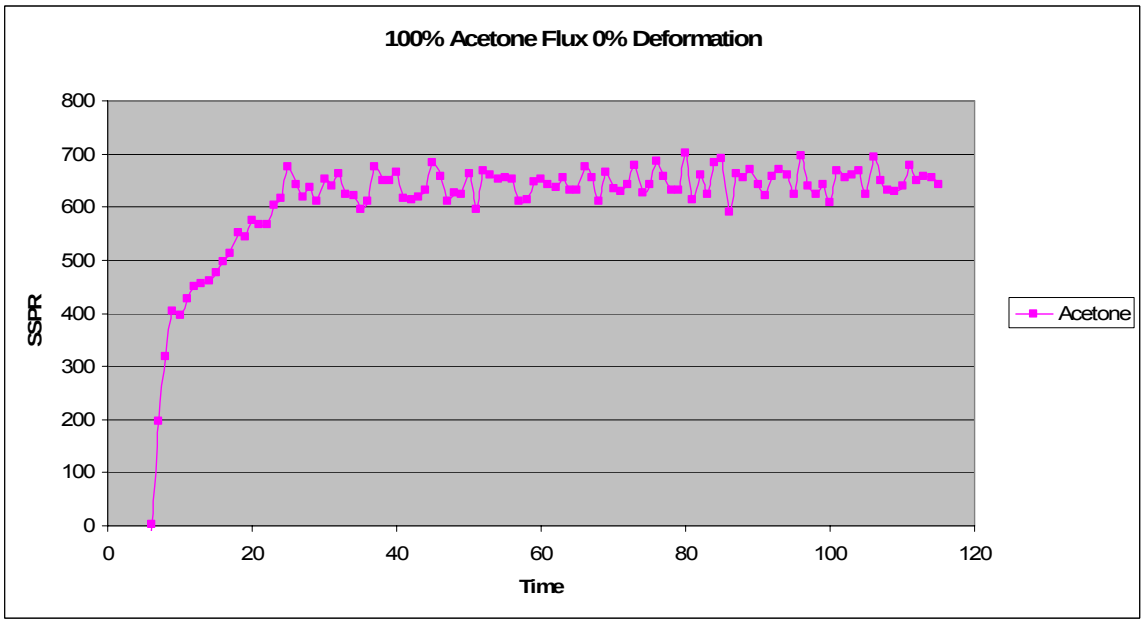

Figure 49: 100% acetone flux 0% deformation

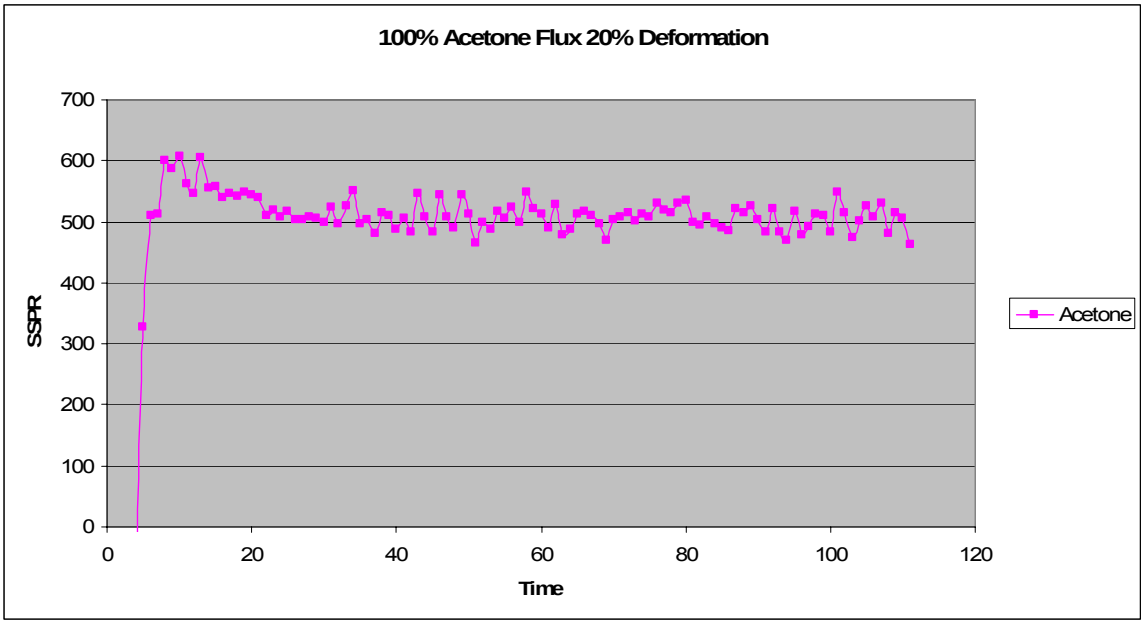

Figure 50: 100% acetone flux 20% deformation

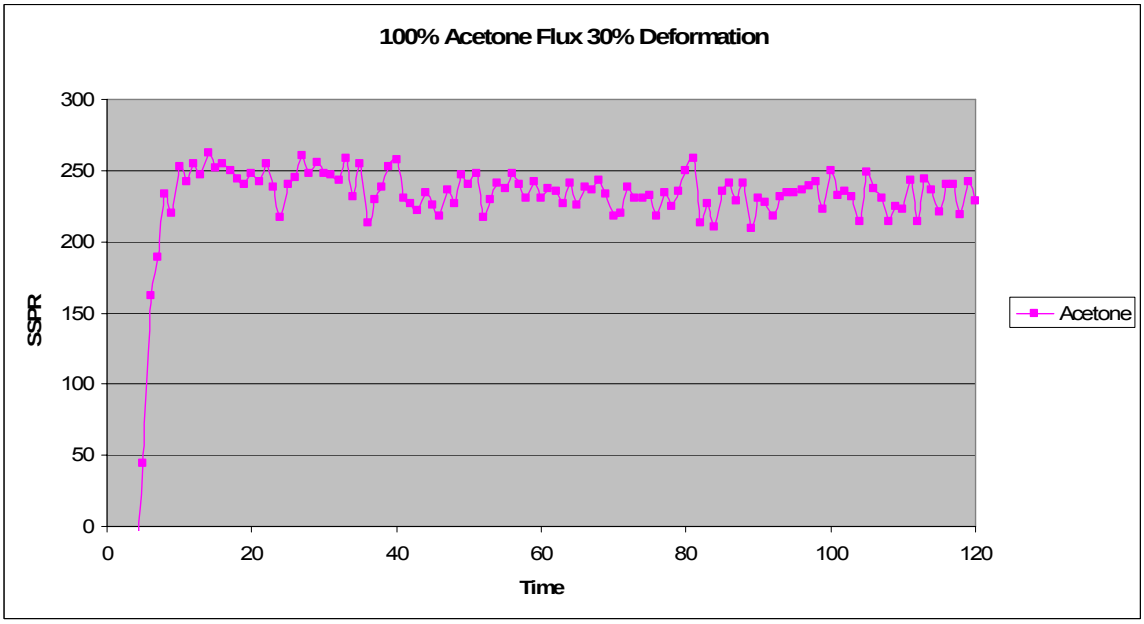

Figure 51: 100% acetone flux 30% deformation

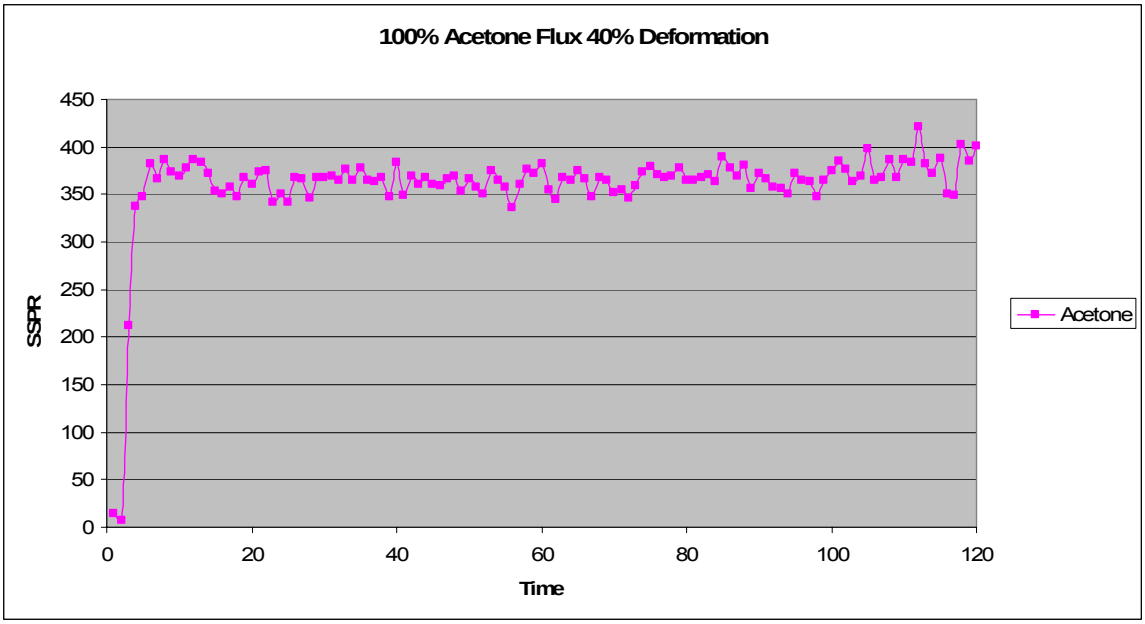

Figure 52: 100% acetone flux 40% deformation

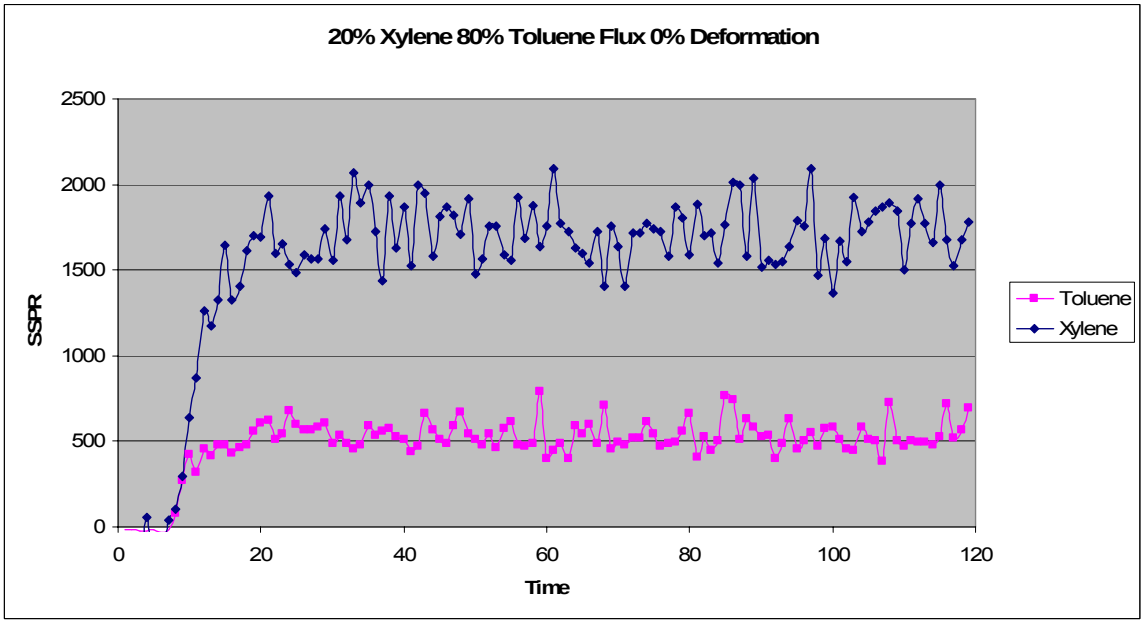

Figure 53: 20% xylene 80% toluene flux 0% deformation

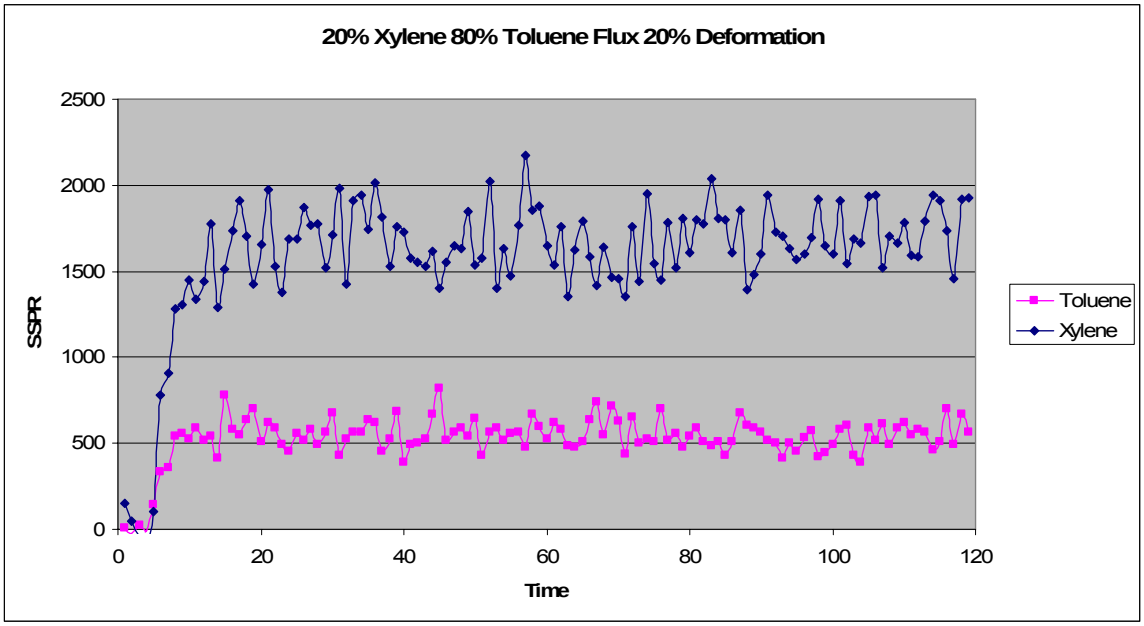

Figure 54: 20% xylene 80% toluene flux 20% deformation

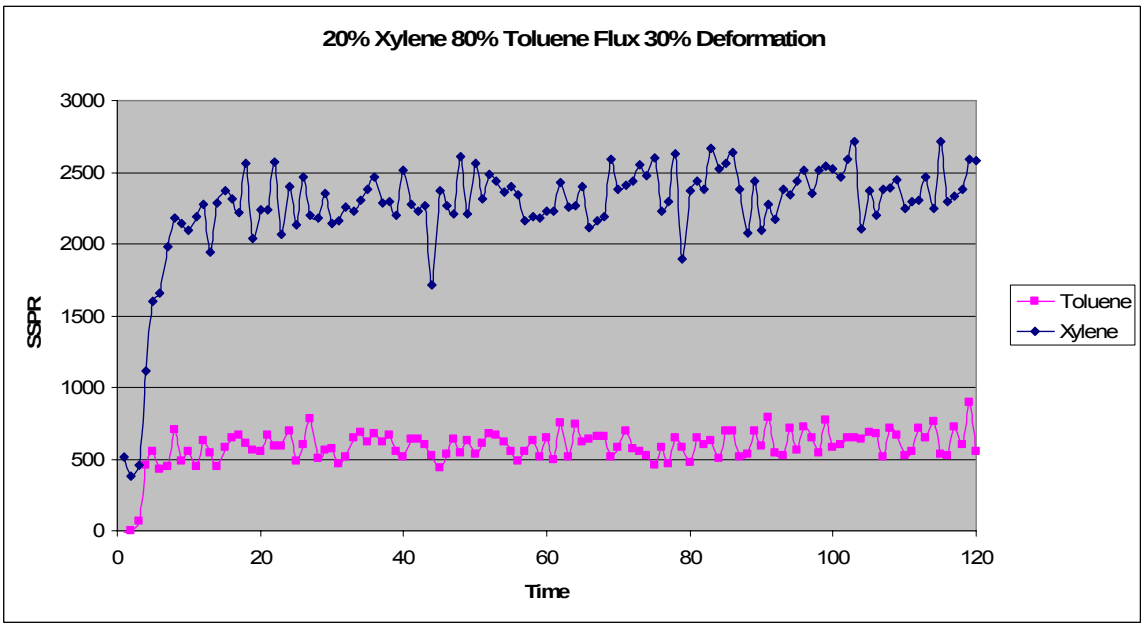

Figure 55: 20% xylene 80% toluene flux 30% deformation

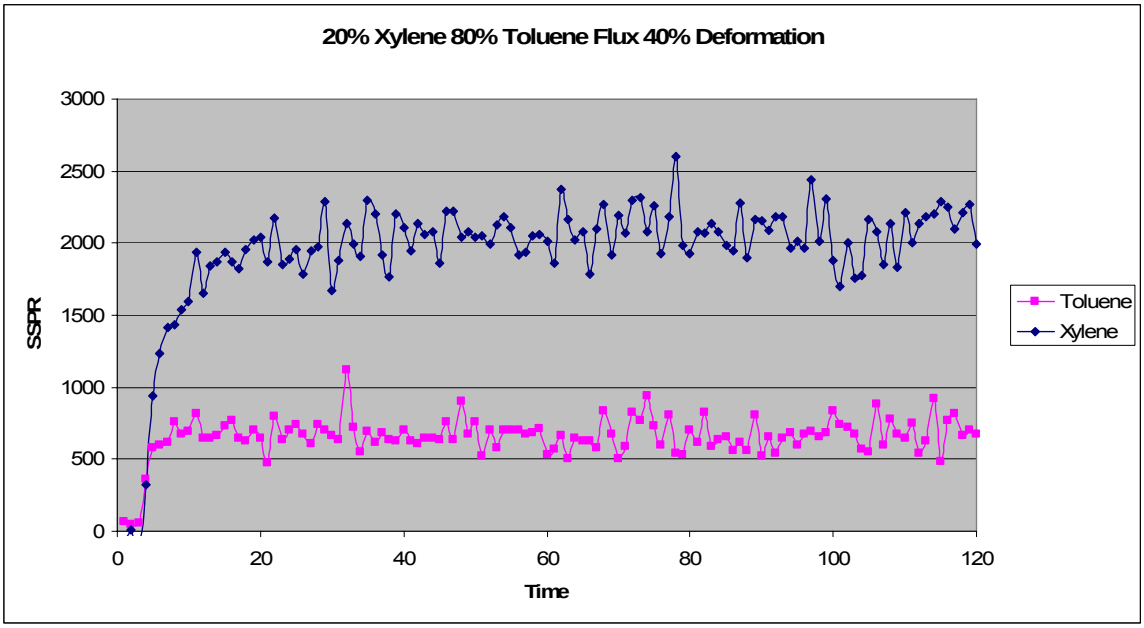

Figure 56: 20% xylene 80% toluene flux 40% deformation

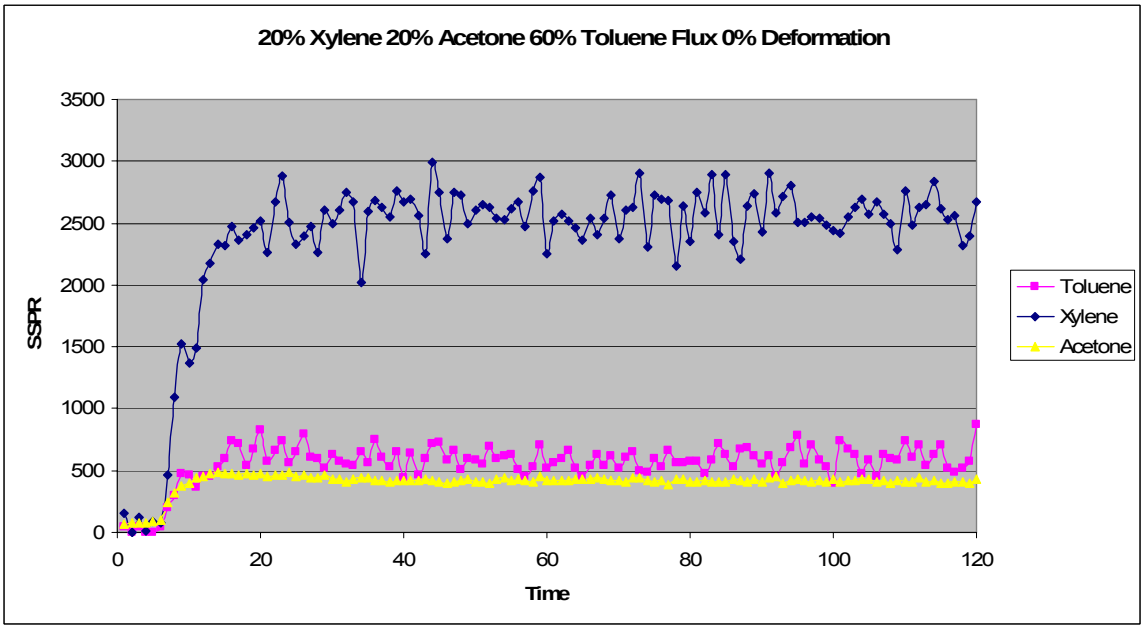

Figure 57: 20% xylene 20% acetone 60% toluene flux 0% deformation

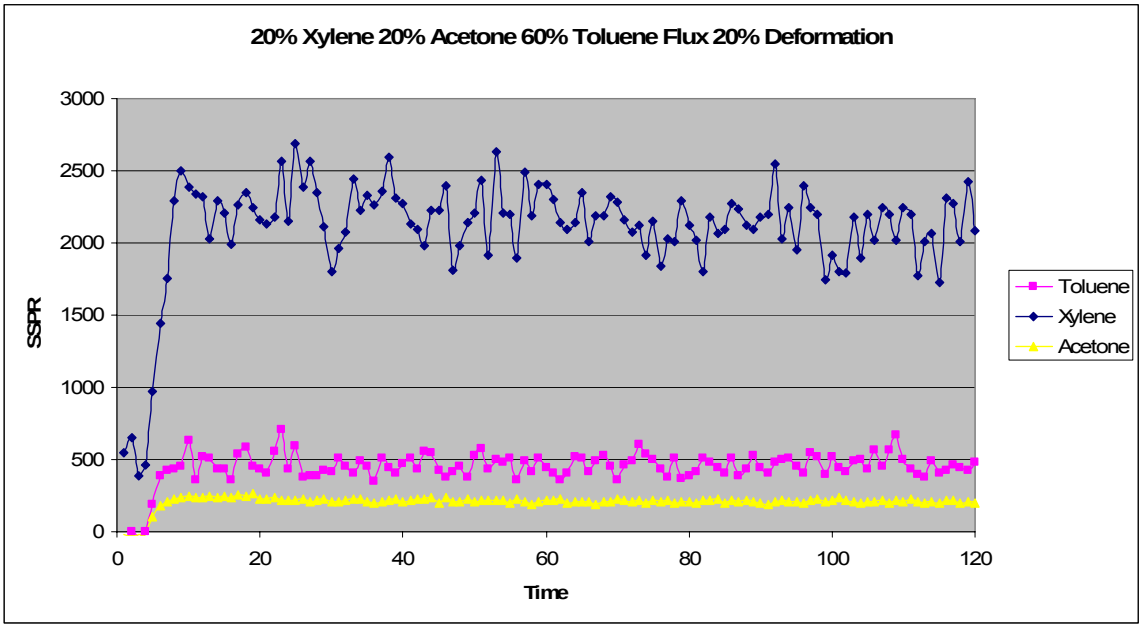

Figure 58: 20% xylene 20% acetone 60% toluene flux 20% deformation

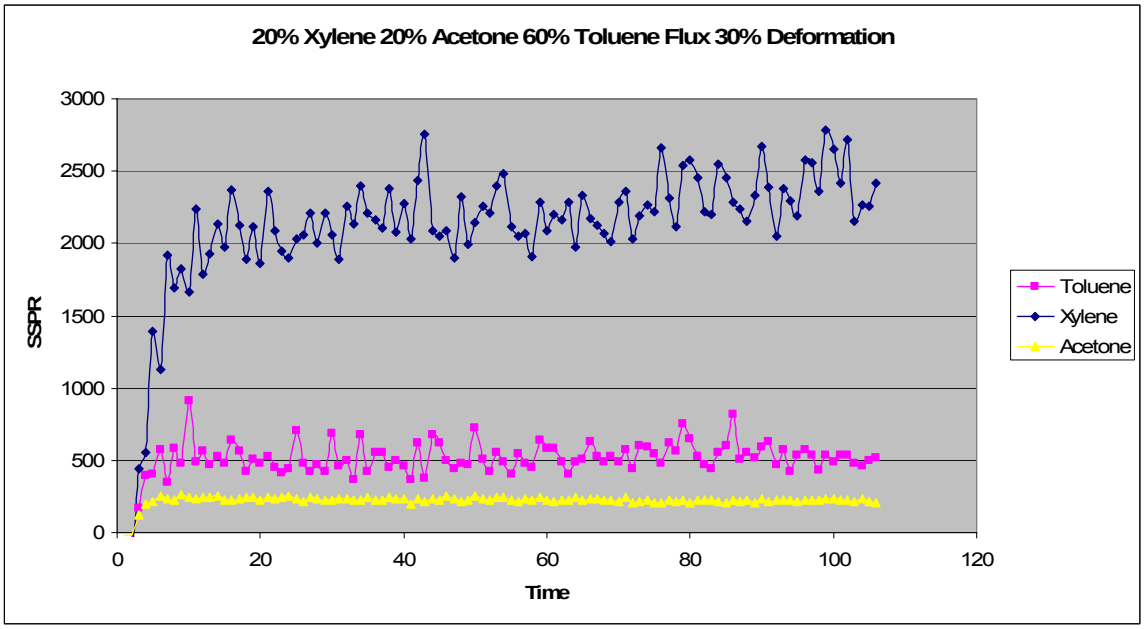

Figure 59: 20% xylene 20% acetone 60% toluene flux 30% deformation

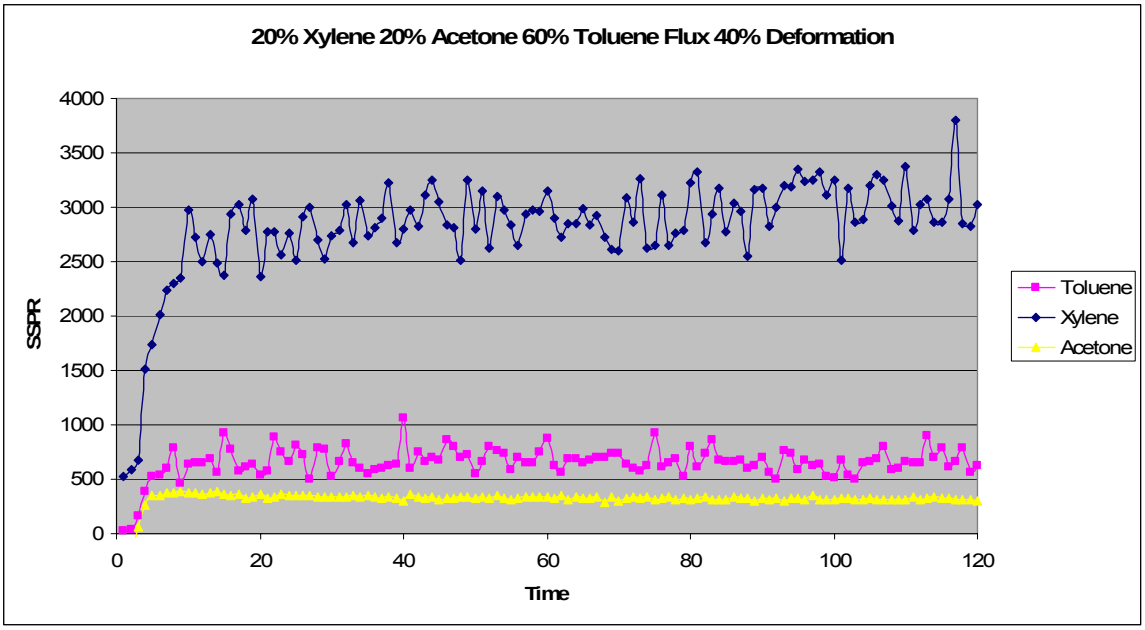

Figure 60: 20% xylene 20% acetone 60% toluene flux 40% deformation

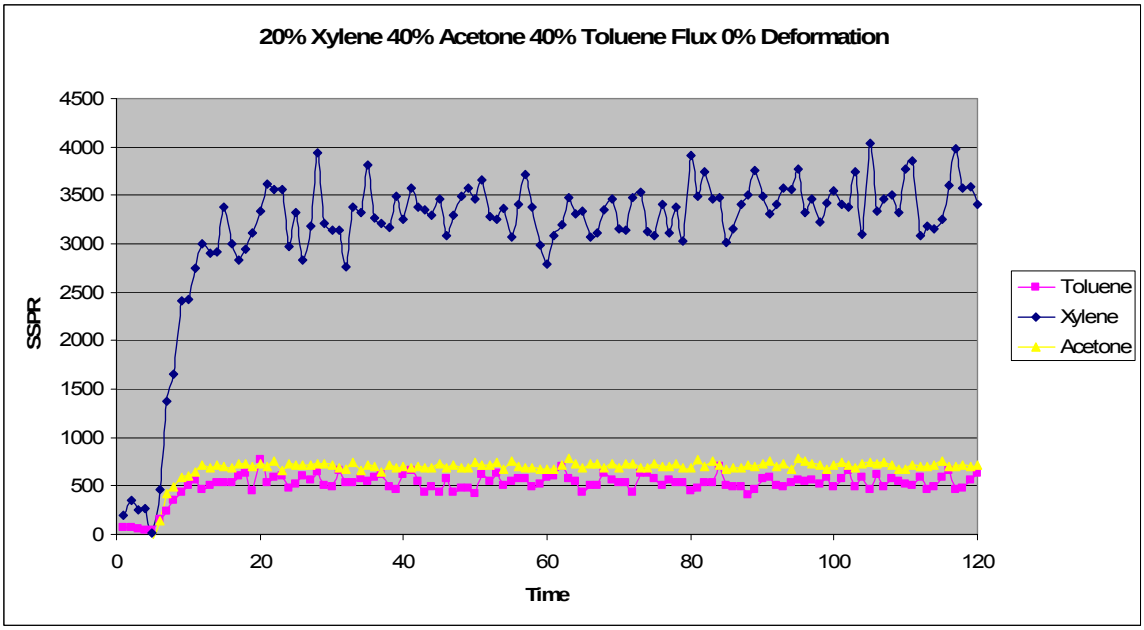

Figure 61: 20% xylene 40% acetone 40% toluene flux 0% deformation

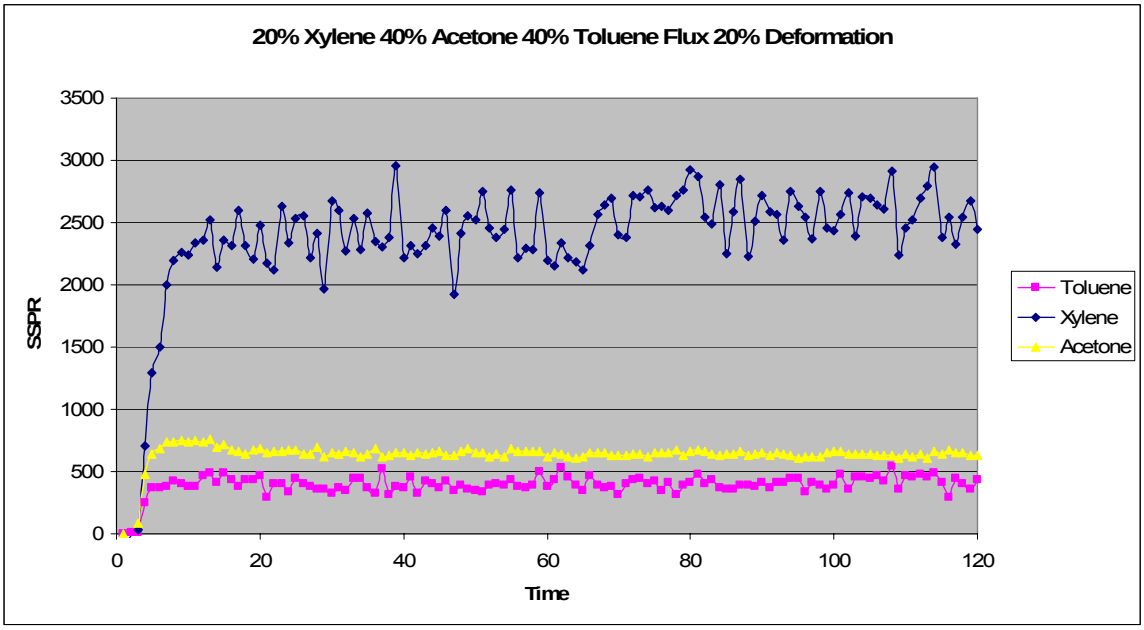

Figure 62: 20% xylene 40% acetone 40% toluene flux 20% deformation

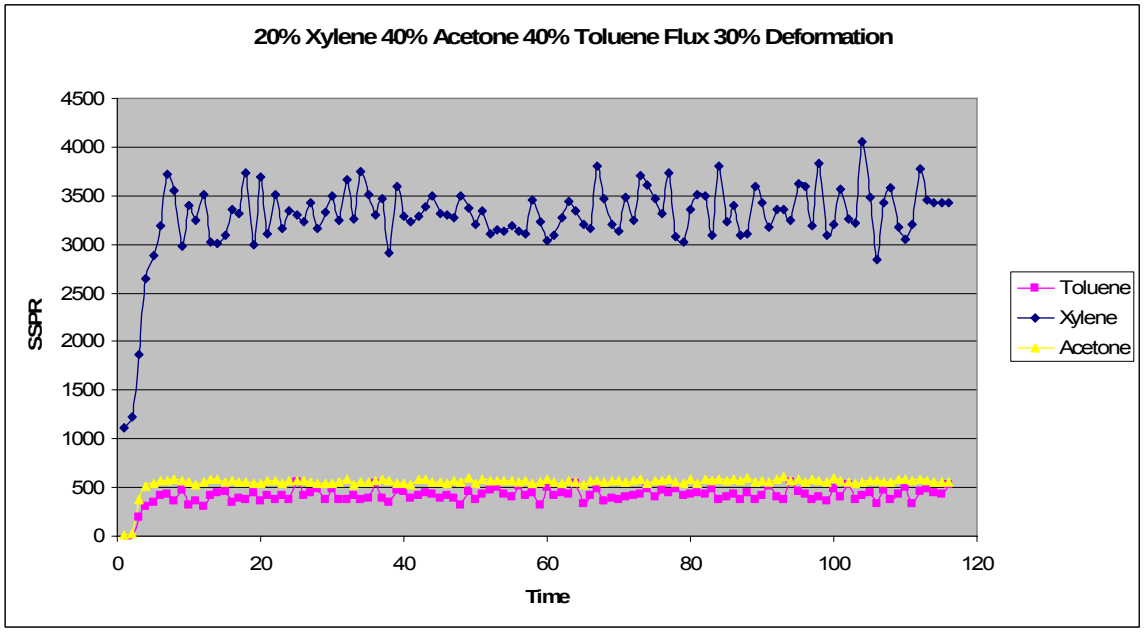

Figure 63: 20% xylene 40% acetone 40% toluene flux 30% deformation

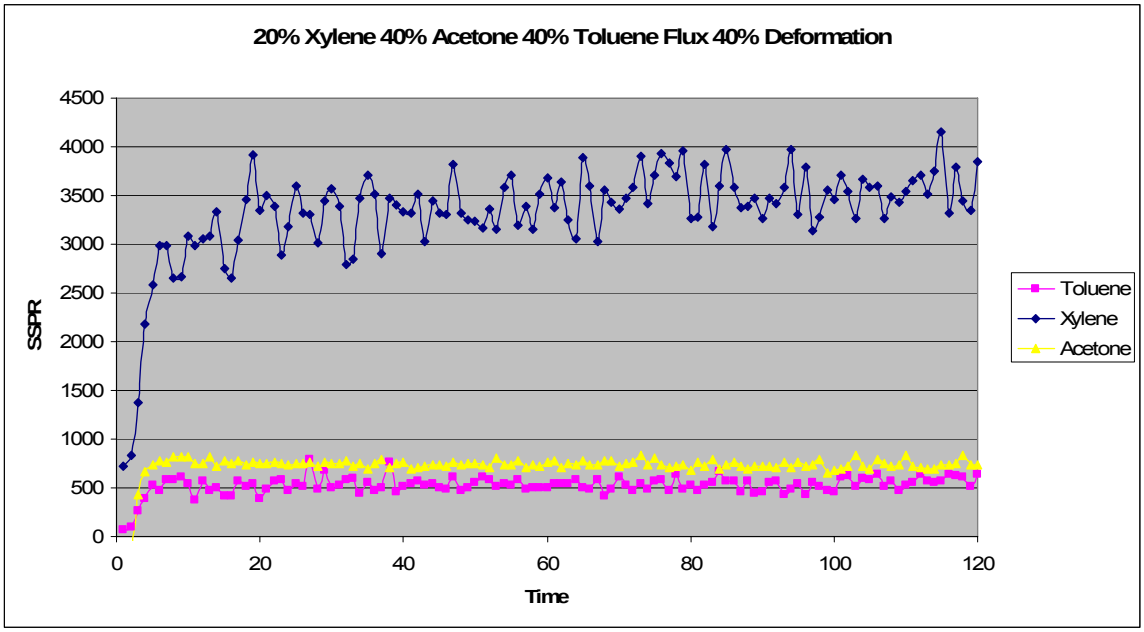

Figure 64: 20% xylene 40% acetone 40% toluene flux 40% deformation

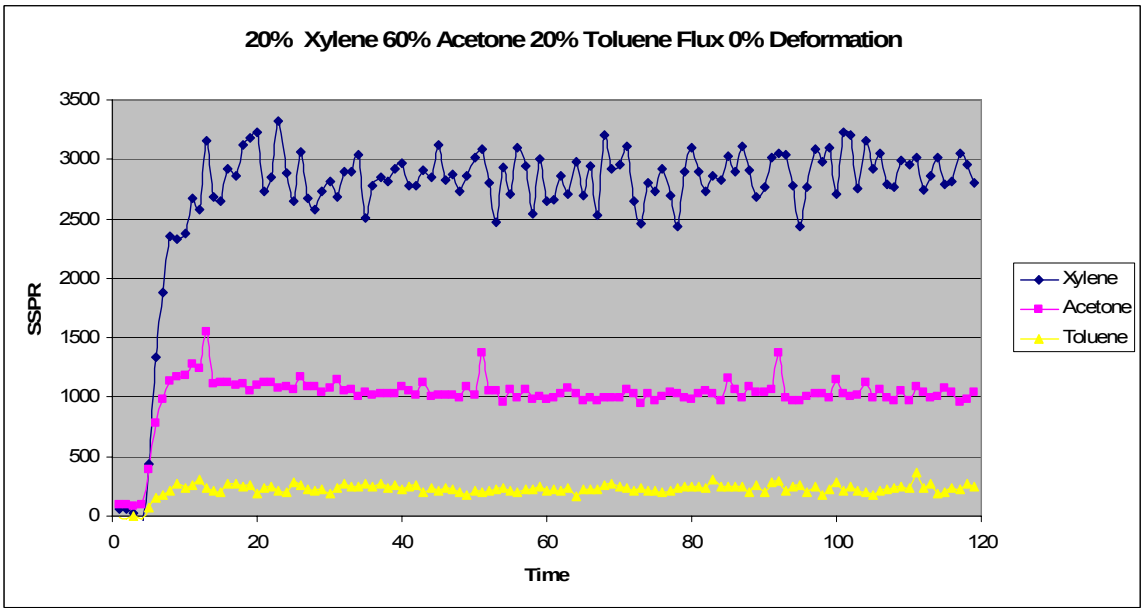

Figure 65: 20% xylene 60% acetone 20% toluene flux 0% deformation

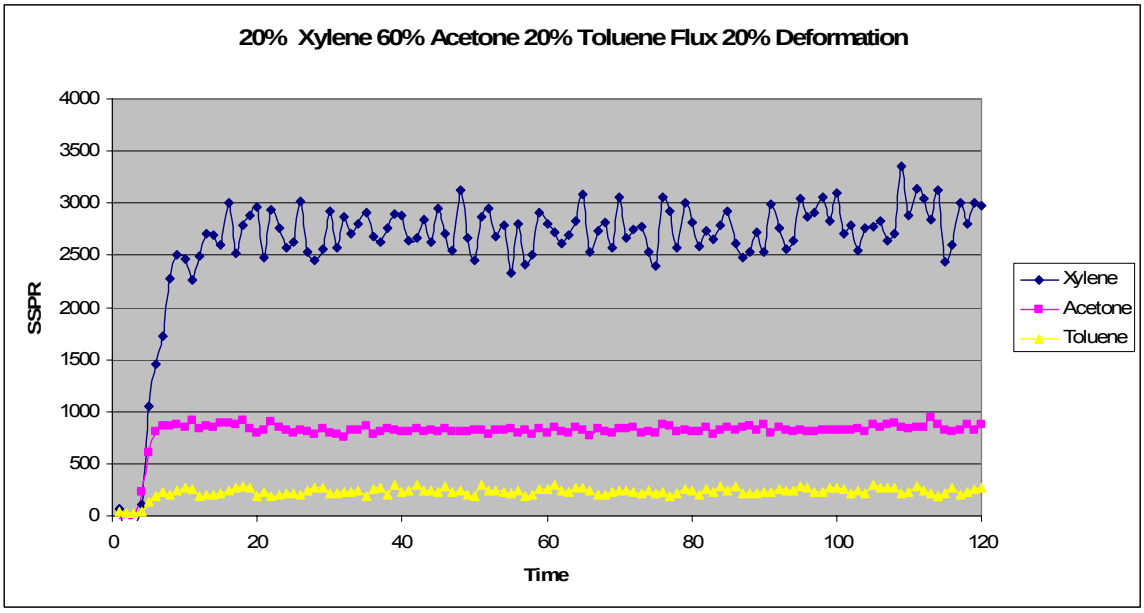

Figure 66: 20% xylene 60% acetone 20% toluene flux 20% deformation

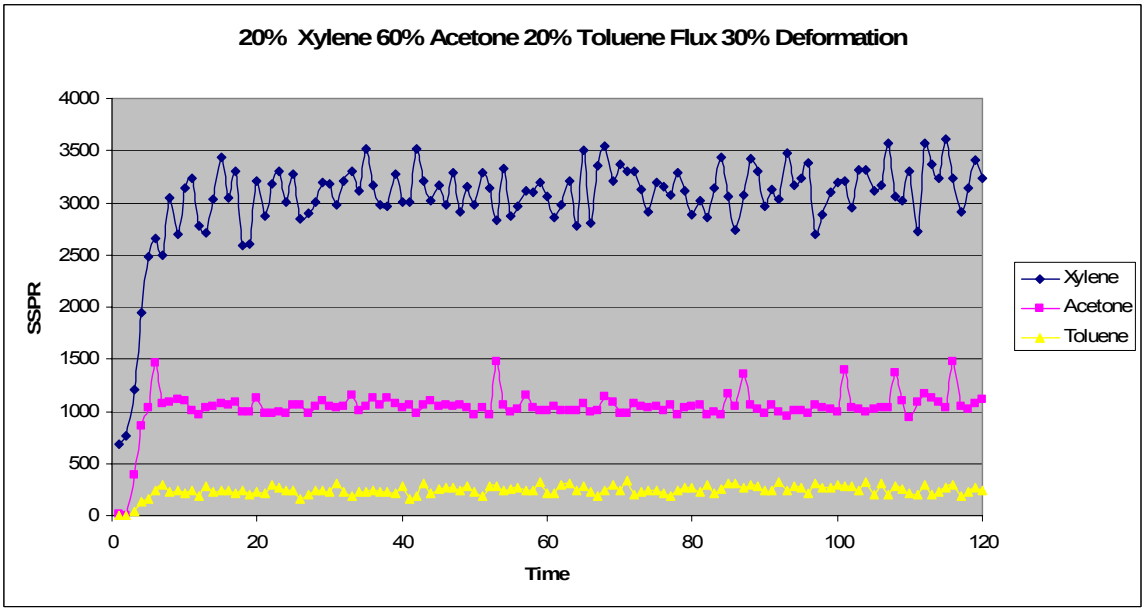

Figure 67: 20% xylene 60% acetone 20% toluene flux 30% deformation

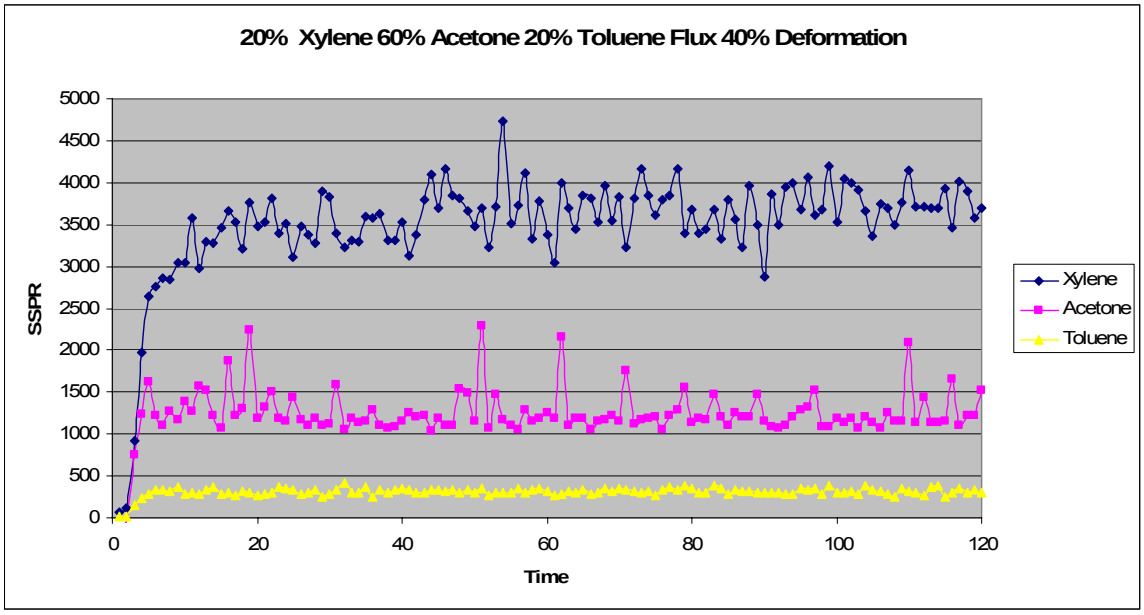

Figure 68: 20% xylene 60% acetone 20% toluene flux 40% deformation

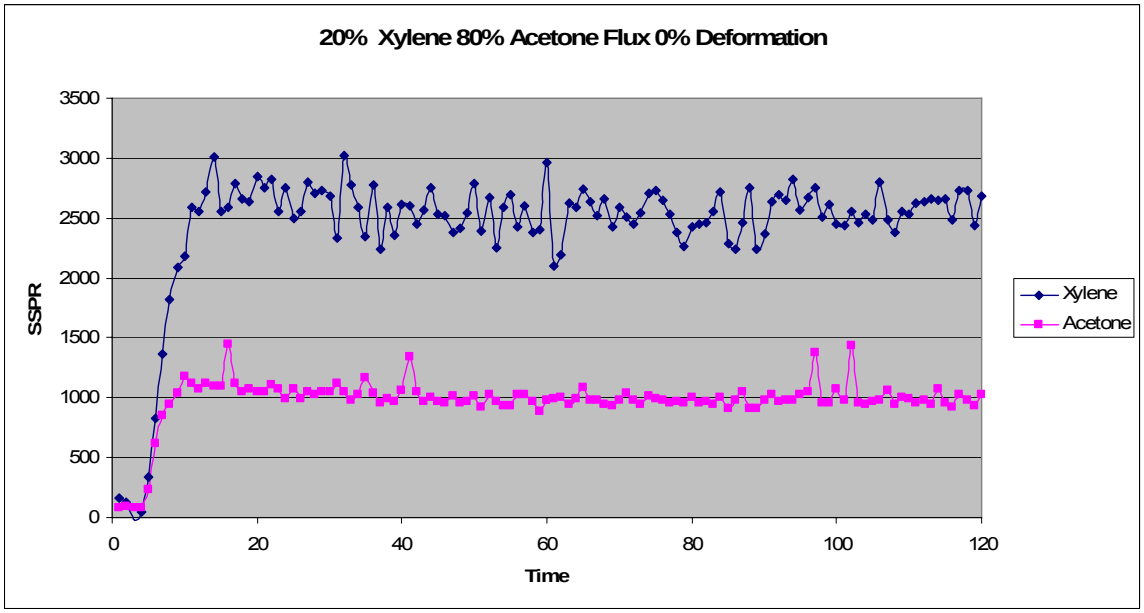

Figure 69: 20% xylene 80% acetone flux 0% deformation

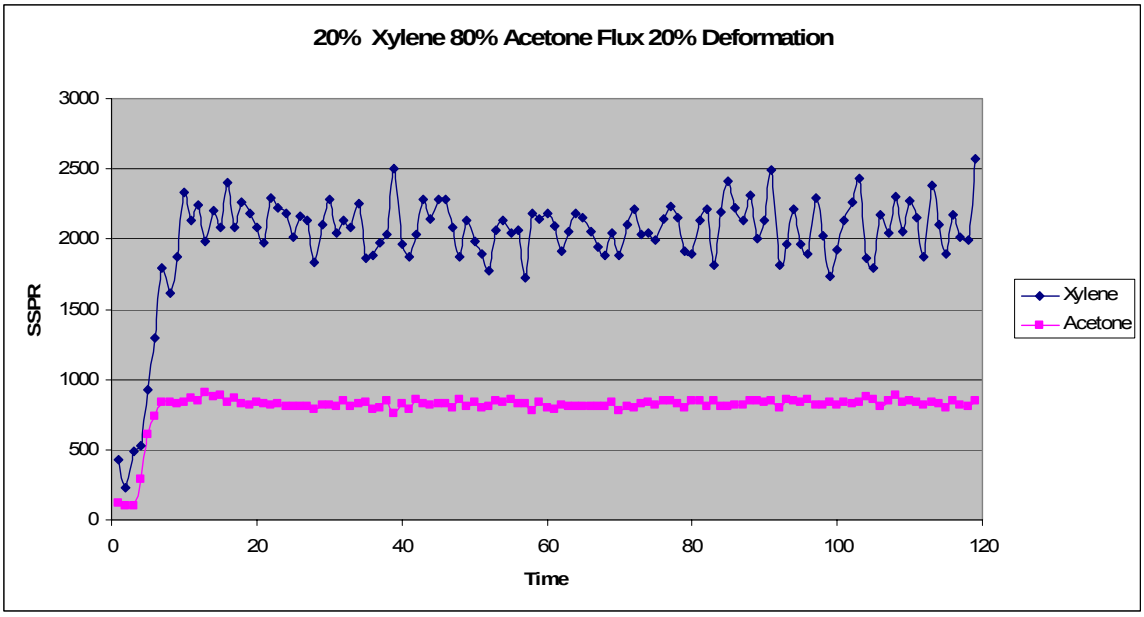

Figure 70: 20% xylene 80% acetone flux 20% deformation

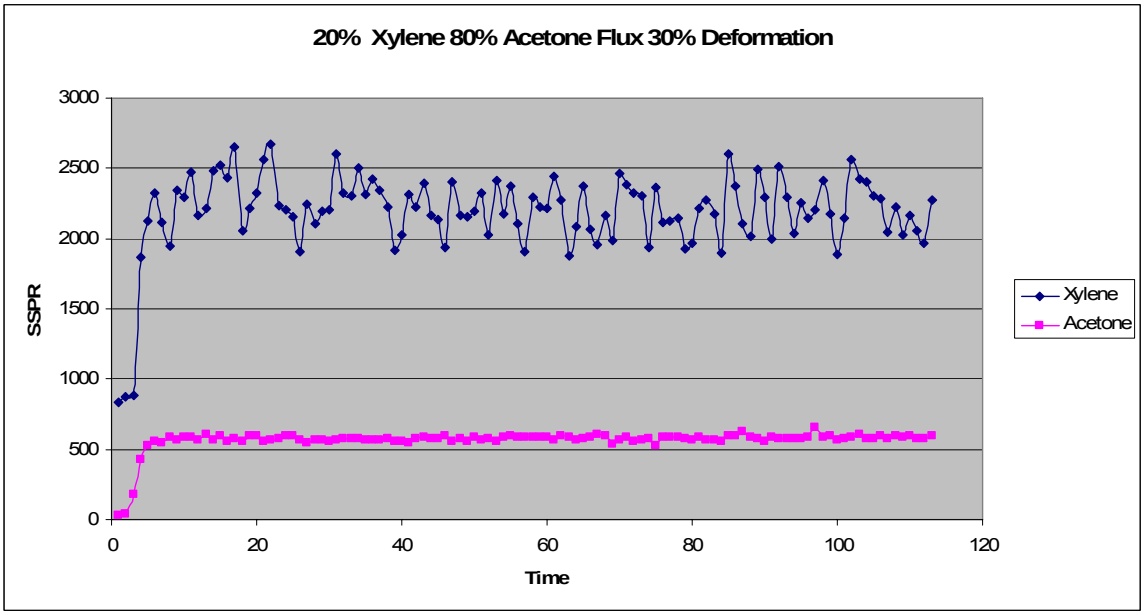

Figure 71: 20% xylene 80% acetone flux 30% deformation

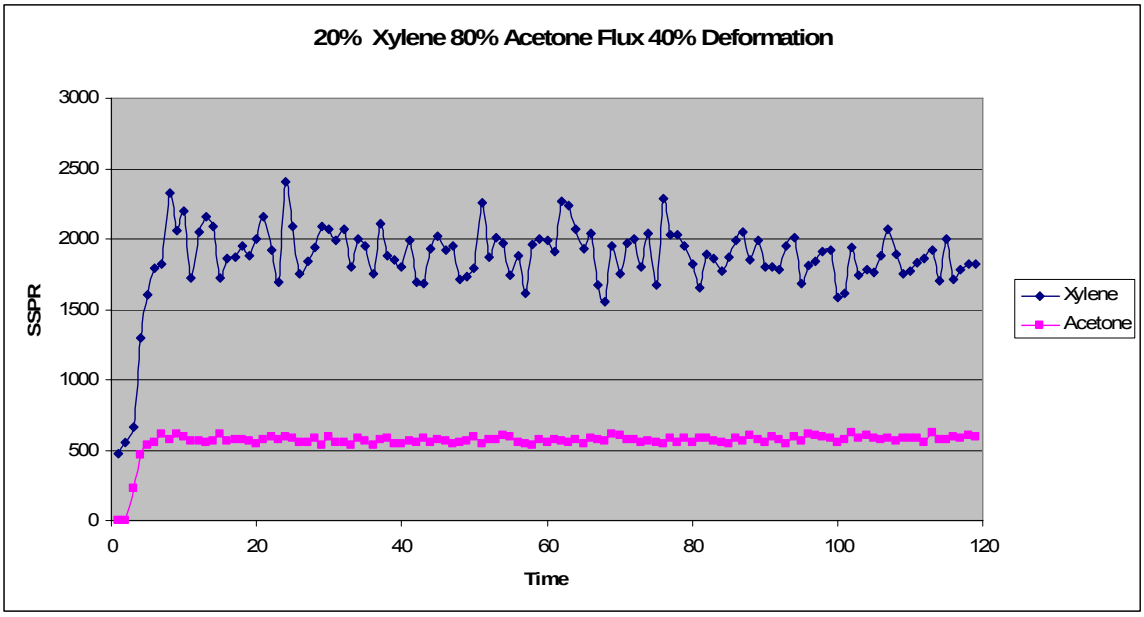

Figure 72: 20% xylene 80% acetone flux 40% deformation

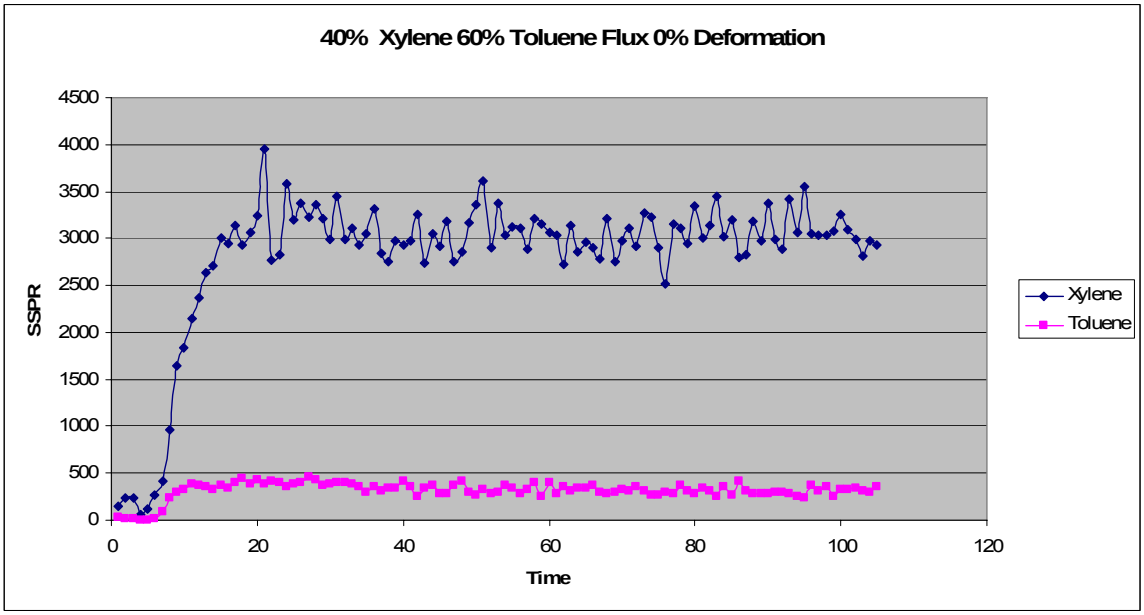

Figure 73: 40% xylene 60% toluene flux 0% deformation

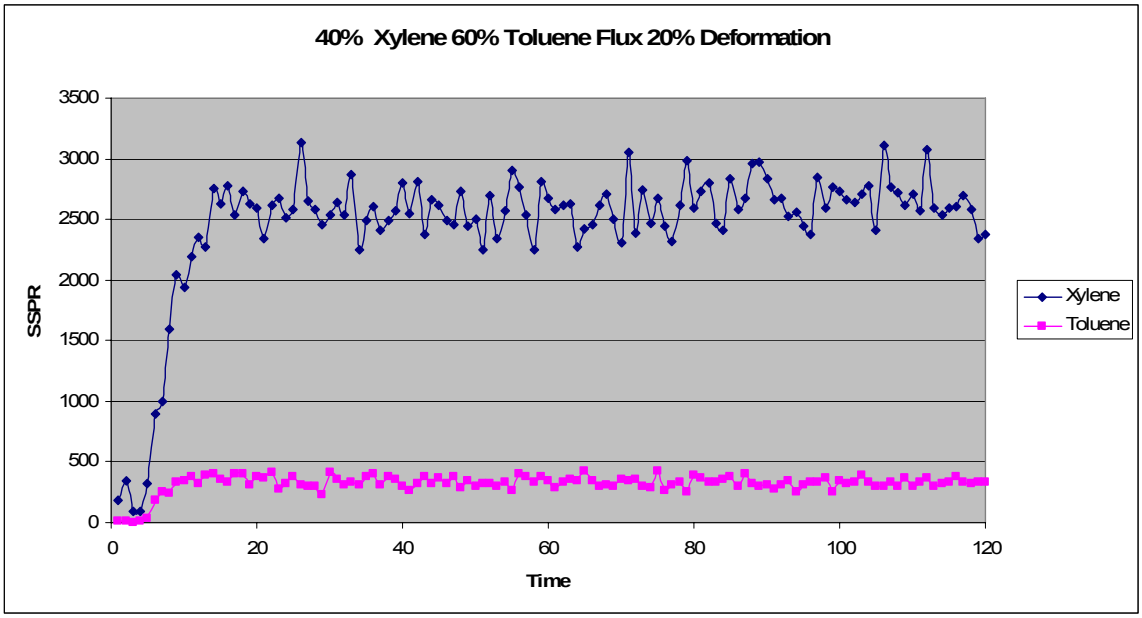

Figure 74: 40% xylene 60% toluene flux 20% deformation

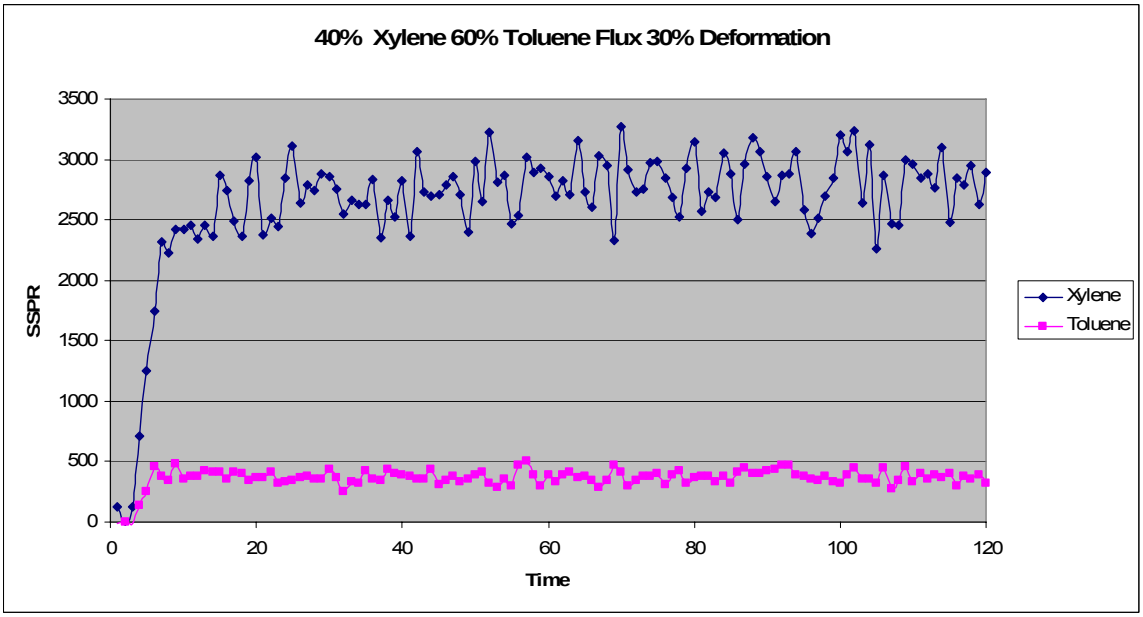

Figure 75: 40% xylene 60% toluene flux 30% deformation

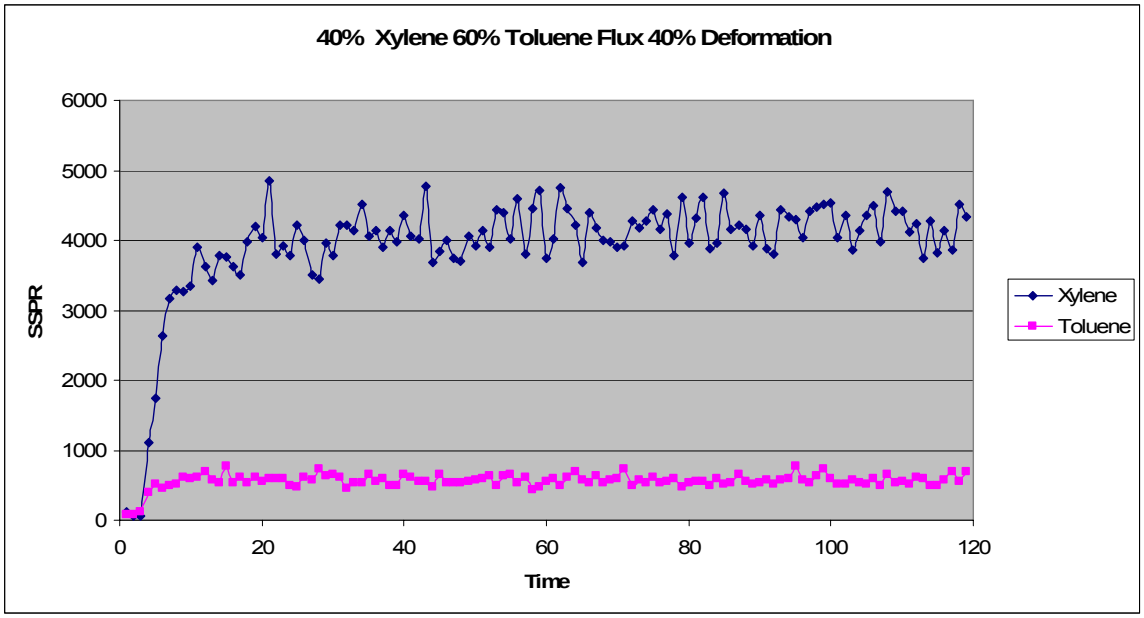

Figure 76: 40% xylene 60% toluene flux 40% deformation

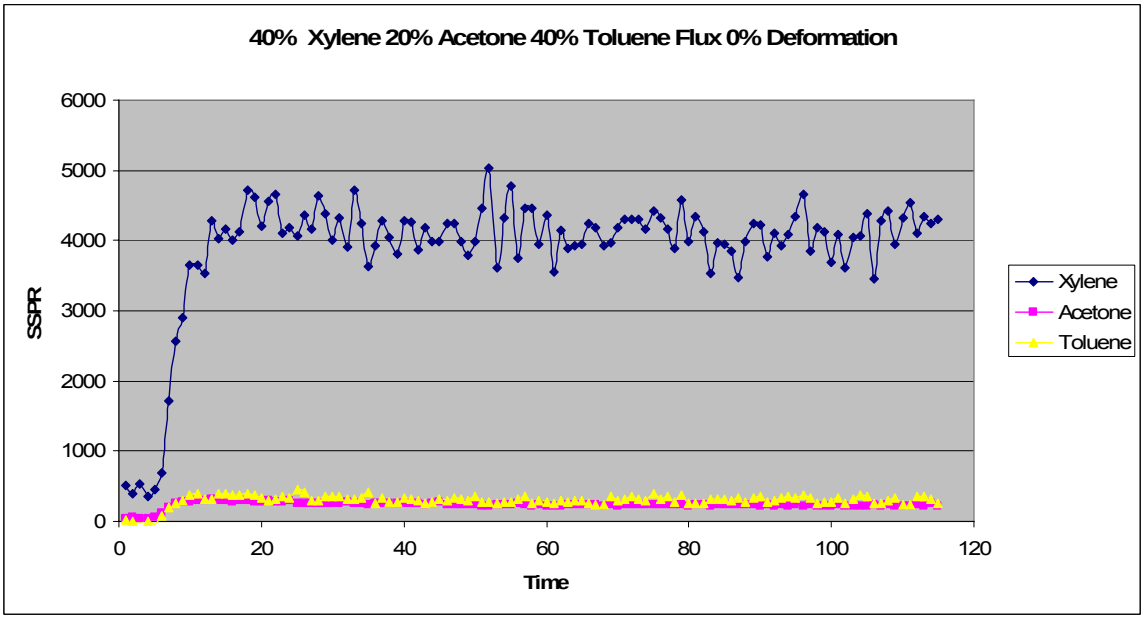

Figure 77: 40% xylene 20% acetone 40% toluene flux 0% deformation

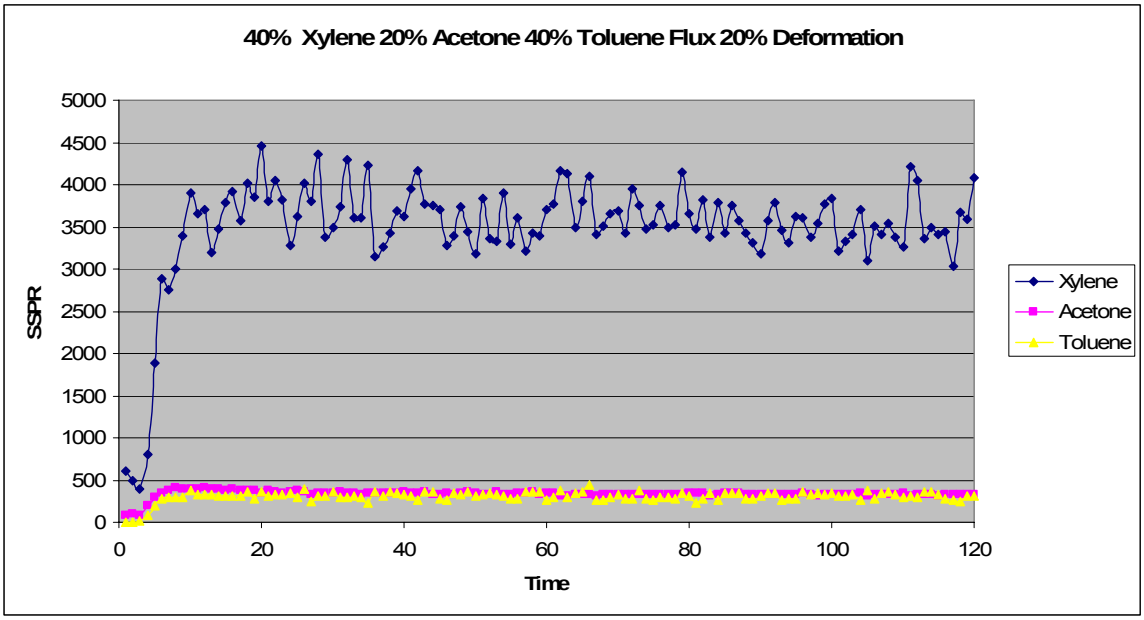

Figure 78: 40% xylene 20% acetone 40% toluene flux 20% deformation

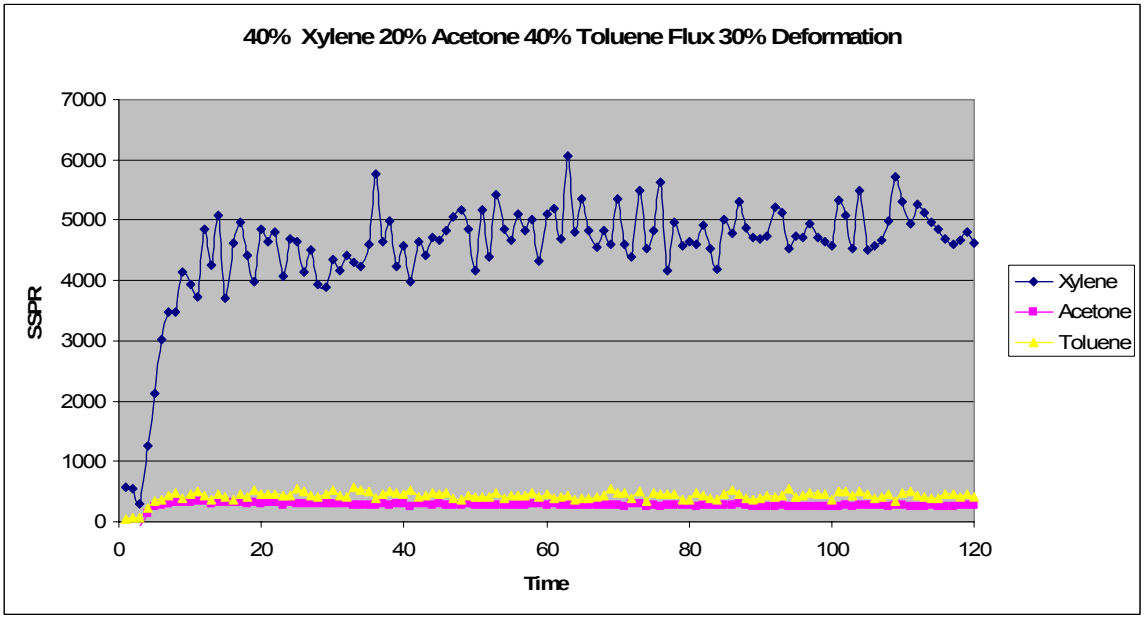

Figure 79: 40% xylene 20% acetone 40% toluene flux 30% deformation

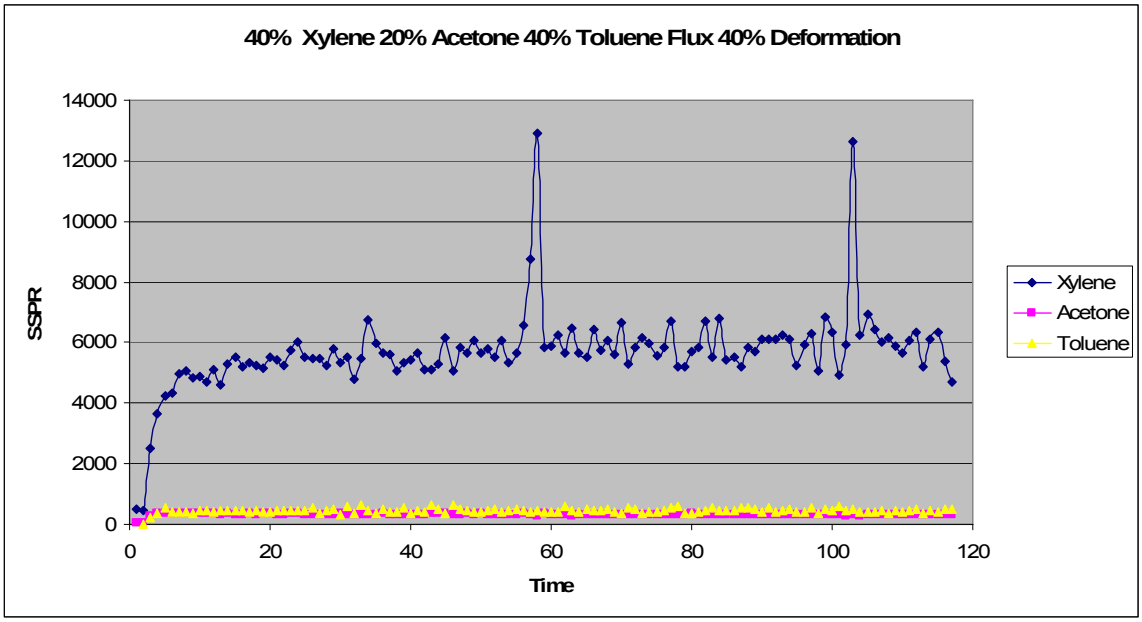

Figure 80: 40% xylene 20% acetone 40% toluene flux 40% deformation

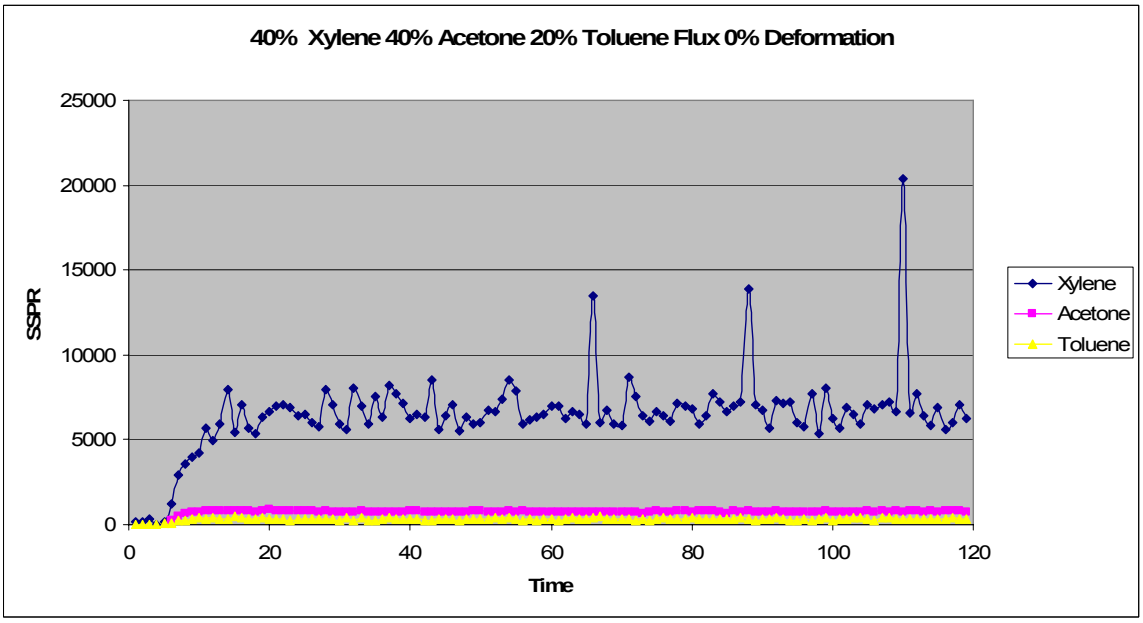

Figure 81: 40% xylene 40% acetone 20% toluene flux 0% deformation

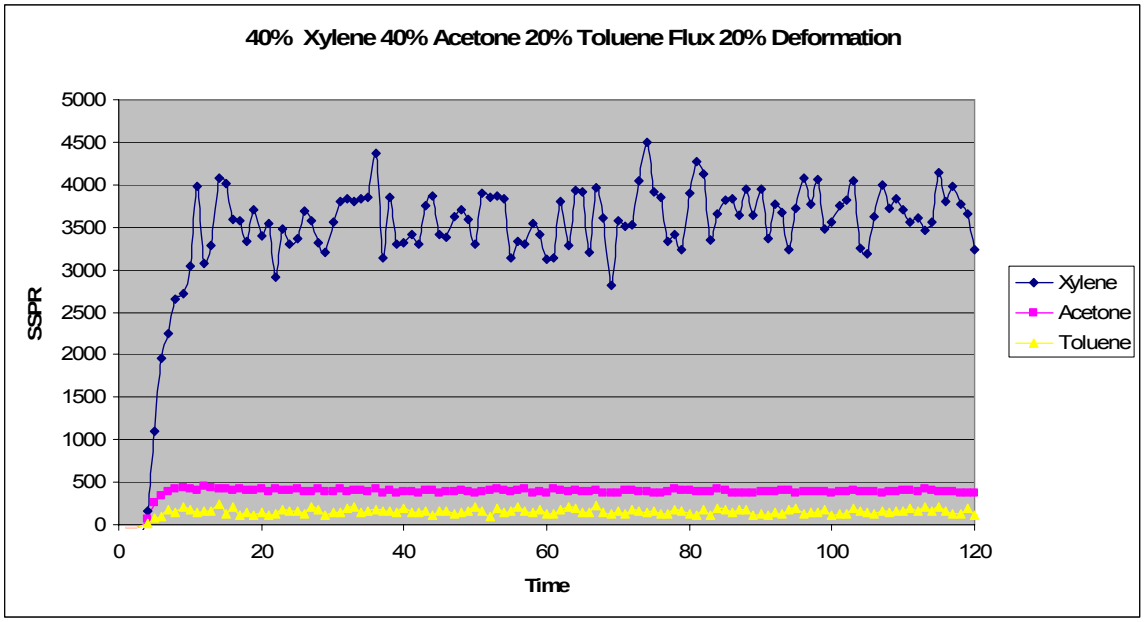

Figure 82: 40% xylene 40% acetone 20% toluene flux 20% deformation

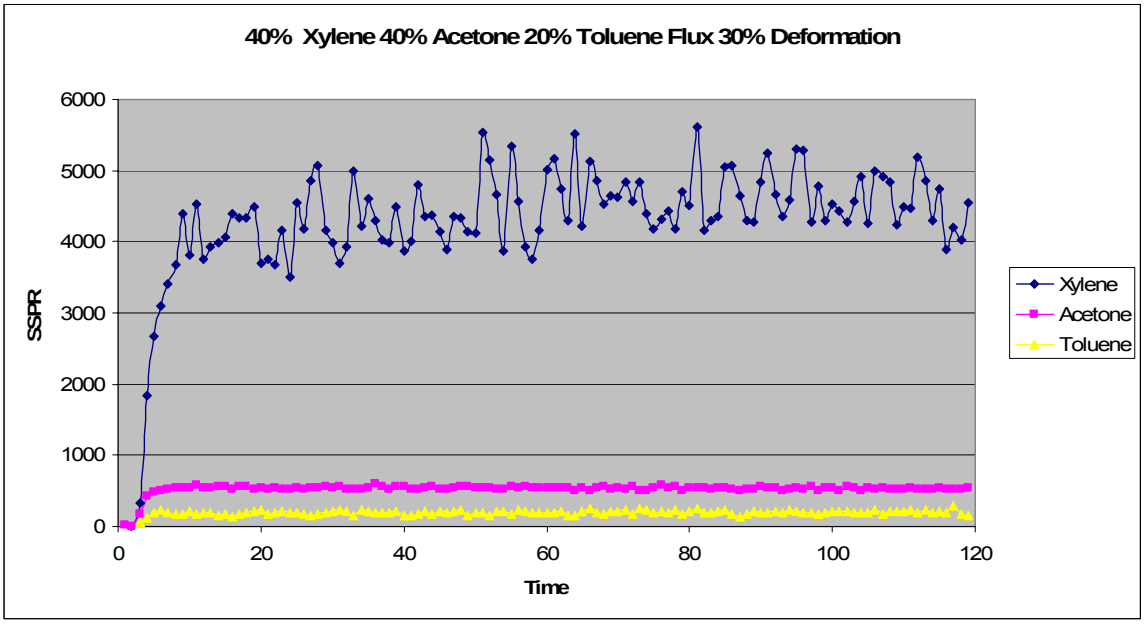

Figure 83: 40% xylene 40% acetone 20% toluene flux 30% deformation

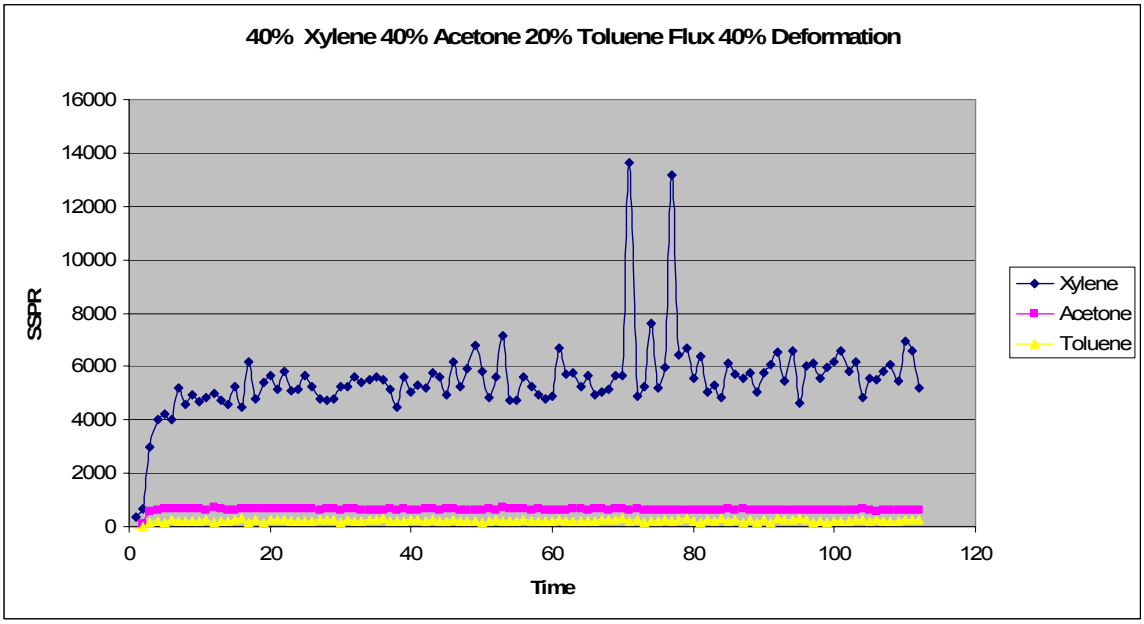

Figure 84: 40% xylene 40% acetone 20% toluene flux 40% deformation

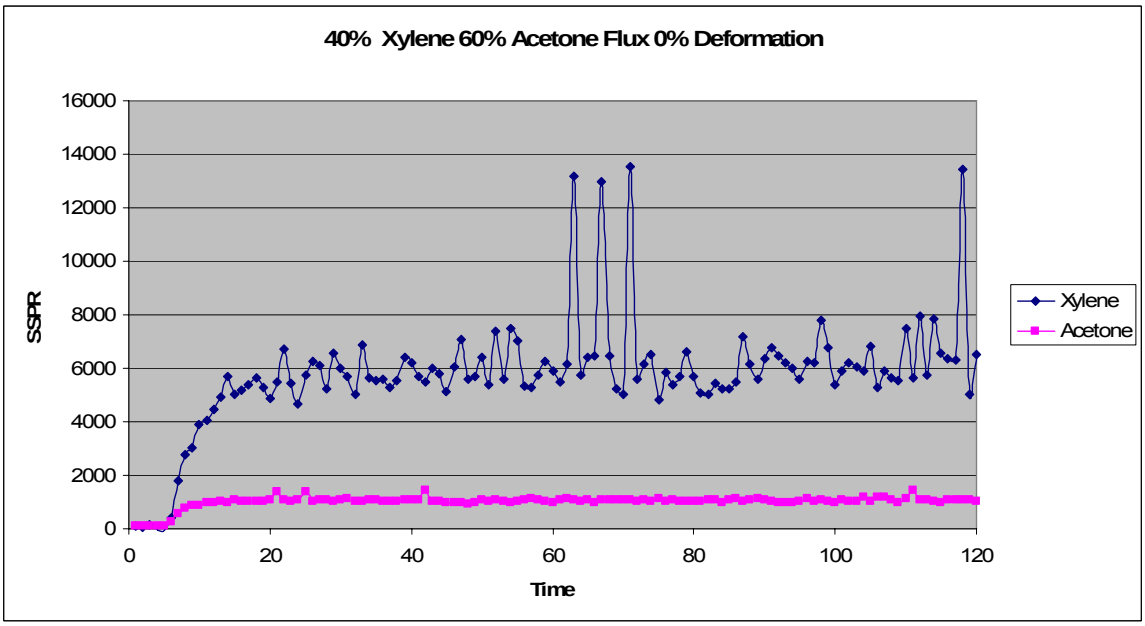

Figure 85: 40% xylene 60% acetone flux 0% deformation

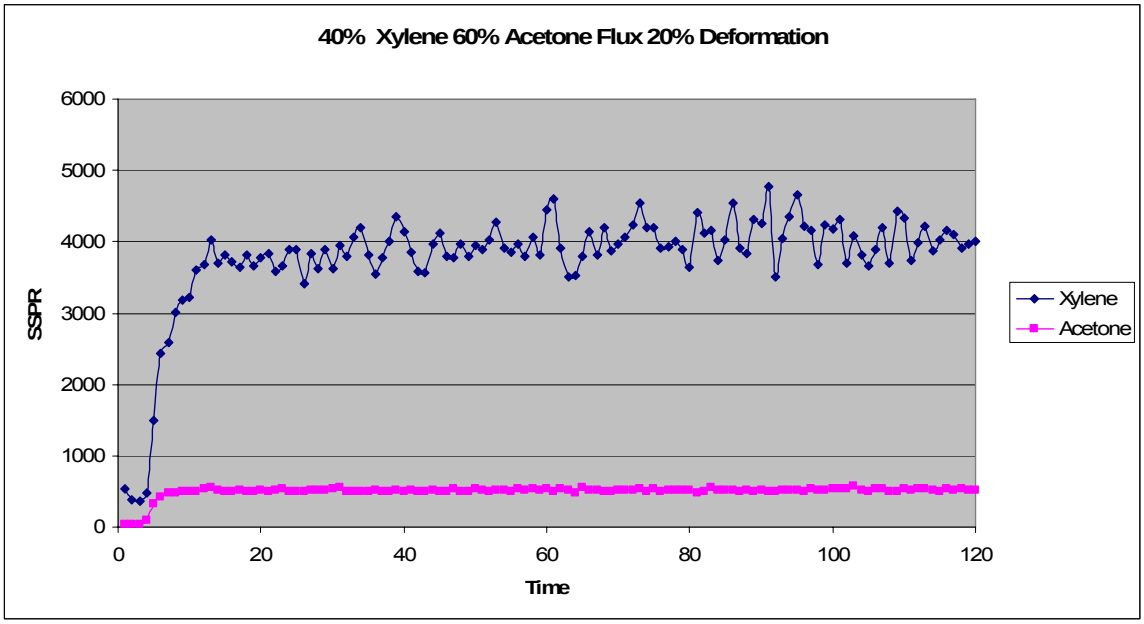

Figure 86: 40% xylene 60% acetone flux 20% deformation

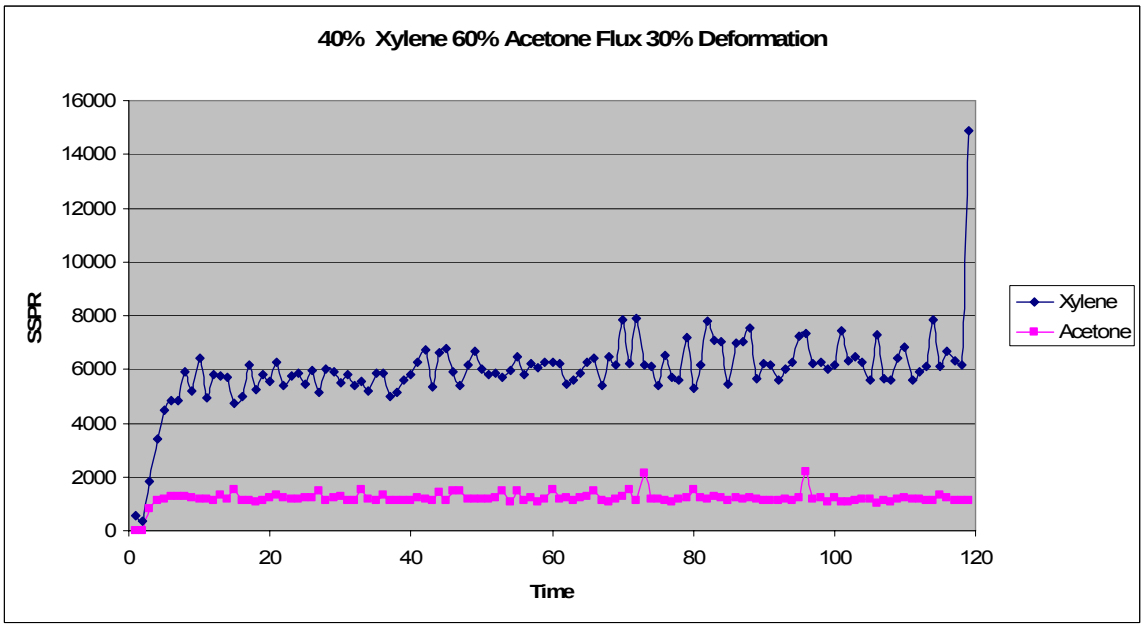

Figure 87: 40% xylene 60% acetone flux 30% deformation

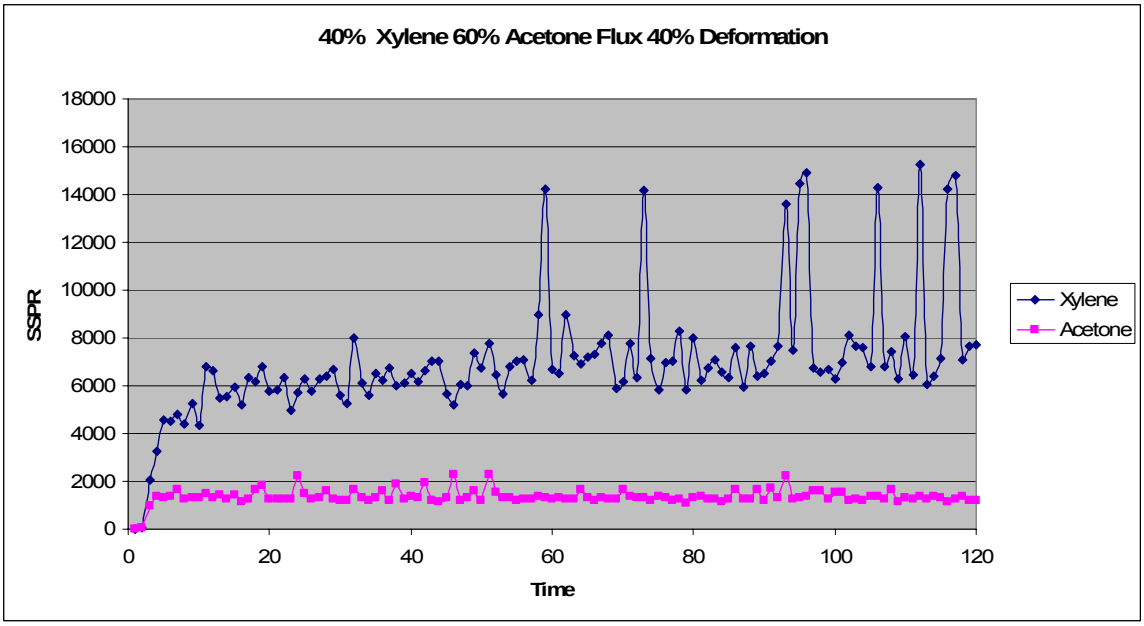

Figure 88: 40% xylene 60% acetone flux 40% deformation

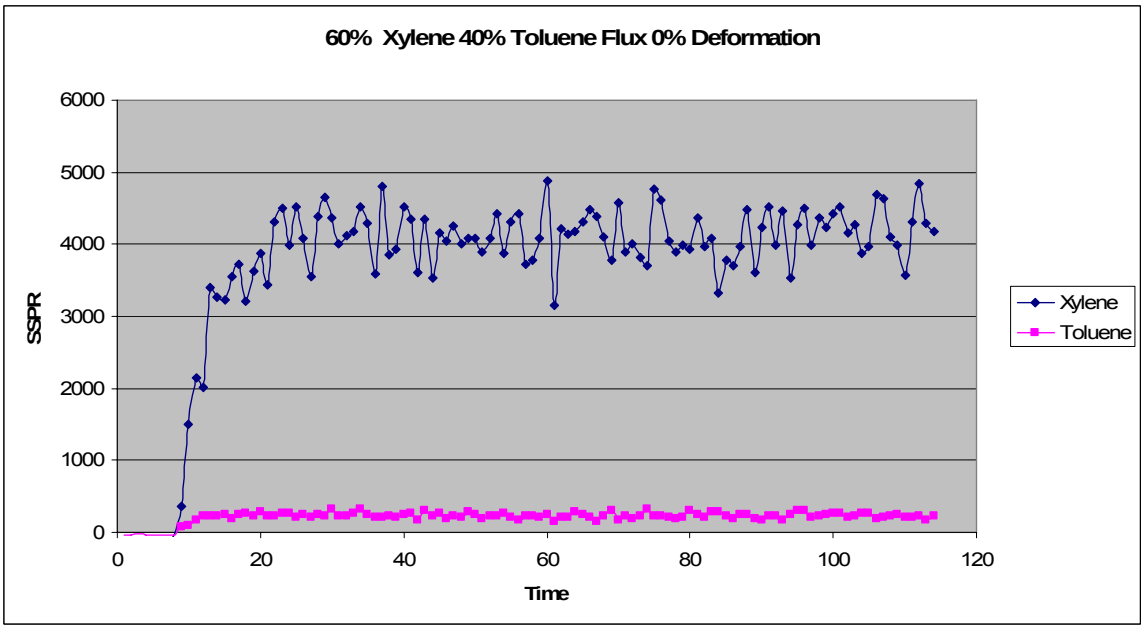

Figure 89: 60% xylene 40% toluene flux 0% deformation

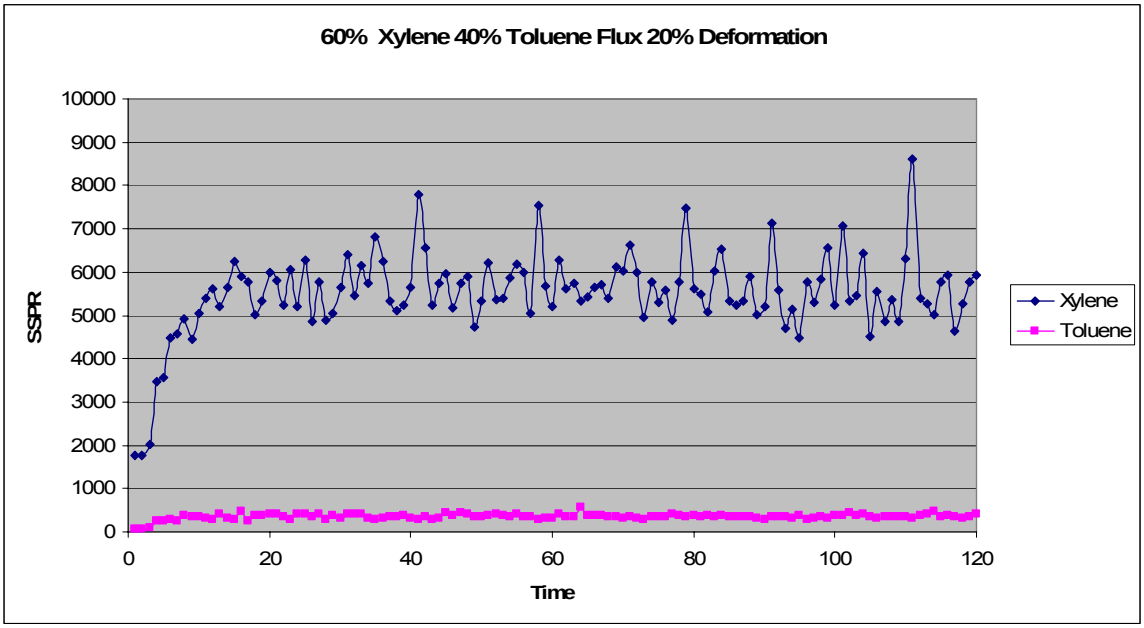

Figure 90: 60% xylene 40% acetone flux 20% deformation

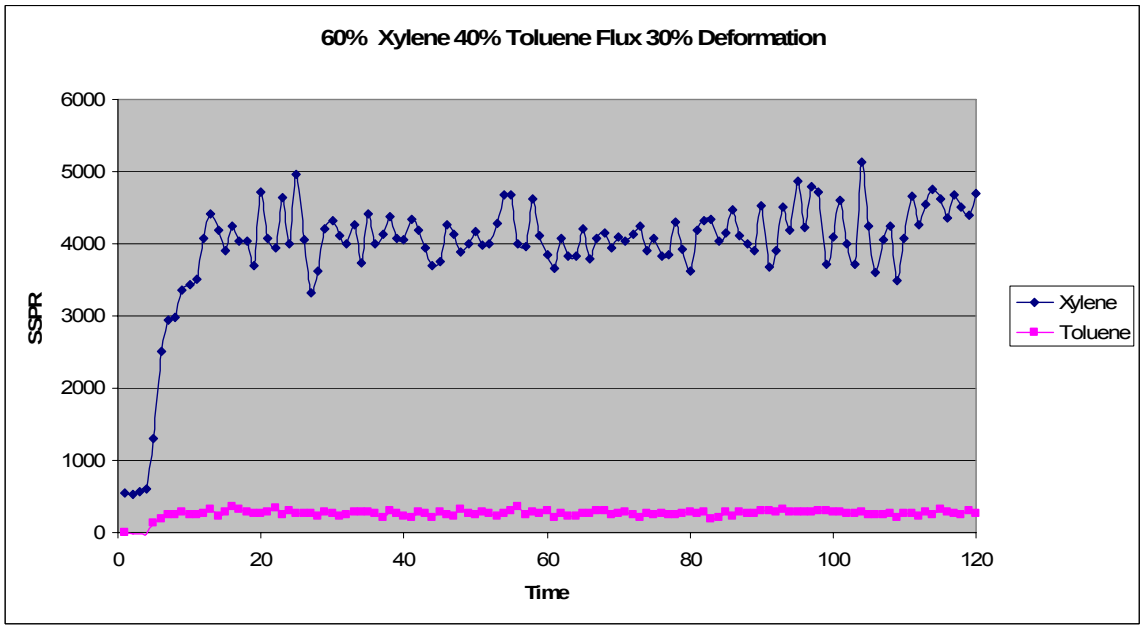

Figure 91: 60% xylene 40% acetone flux 30% deformation

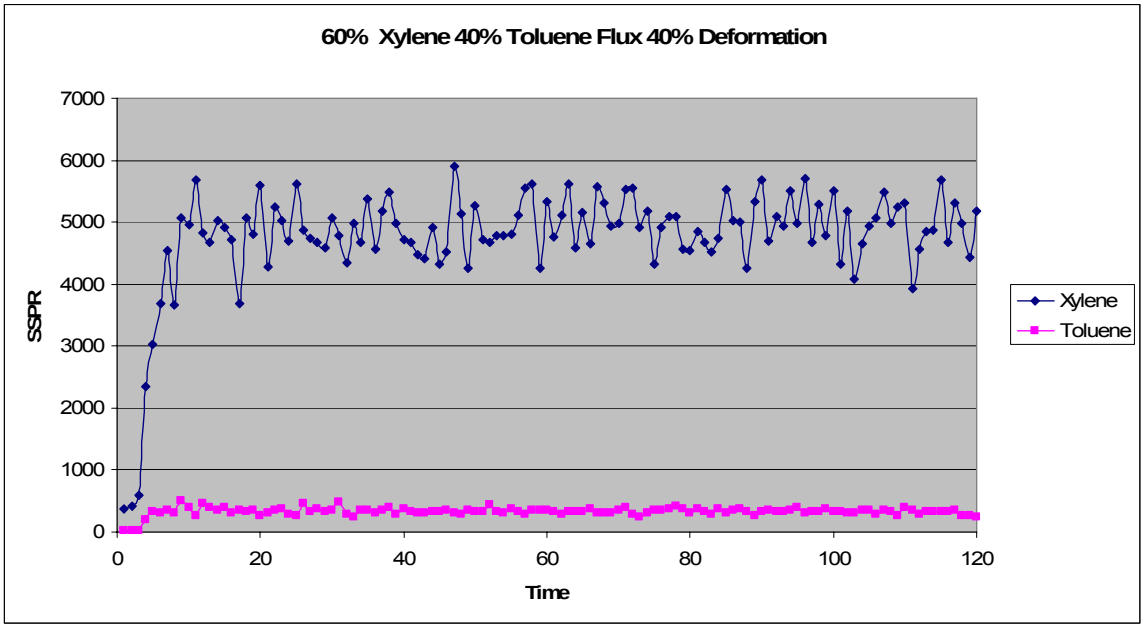

Figure 92: 60% xylene 40% acetone flux 40% deformation

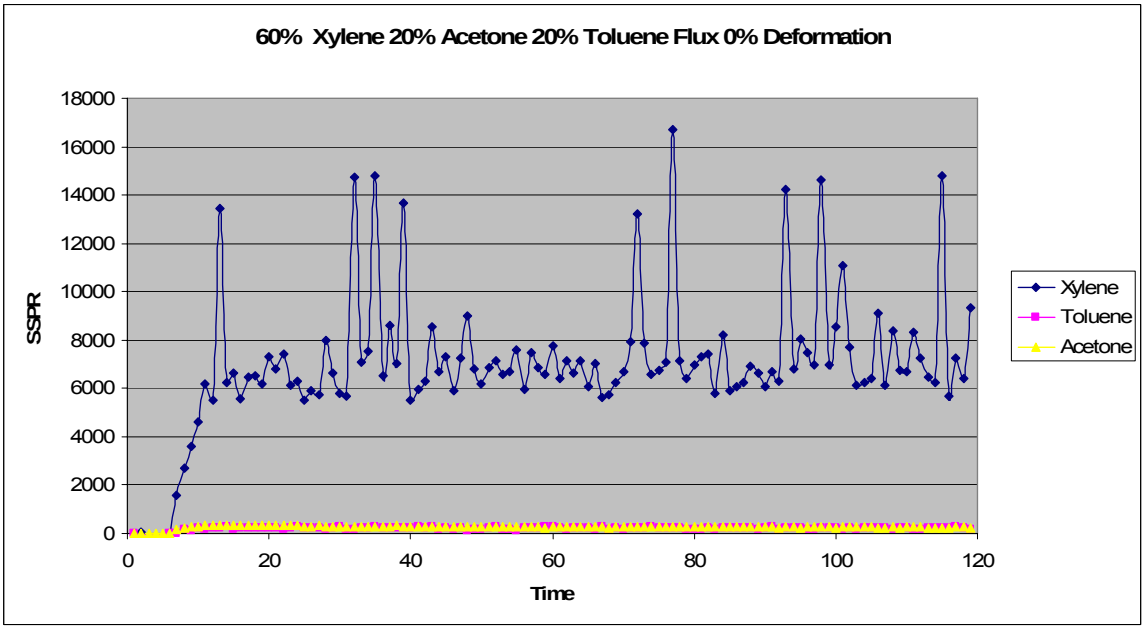

Figure 93: 60% xylene 20% acetone 20% toluene flux 0% deformation

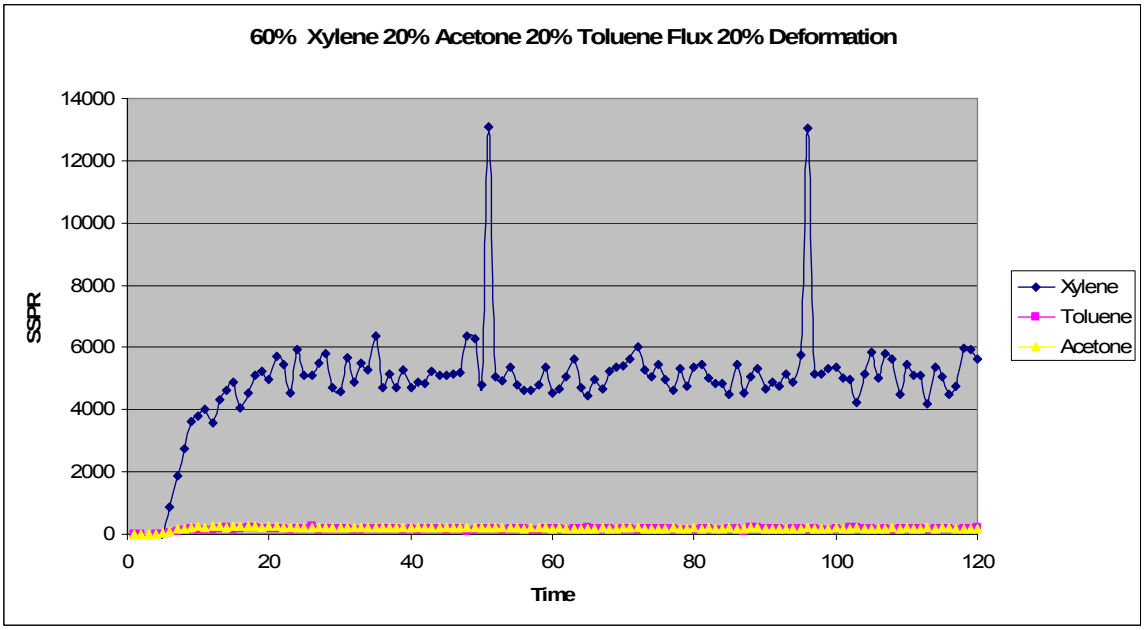

Figure 94: 60% xylene 20% acetone 20% toluene flux 20% deformation

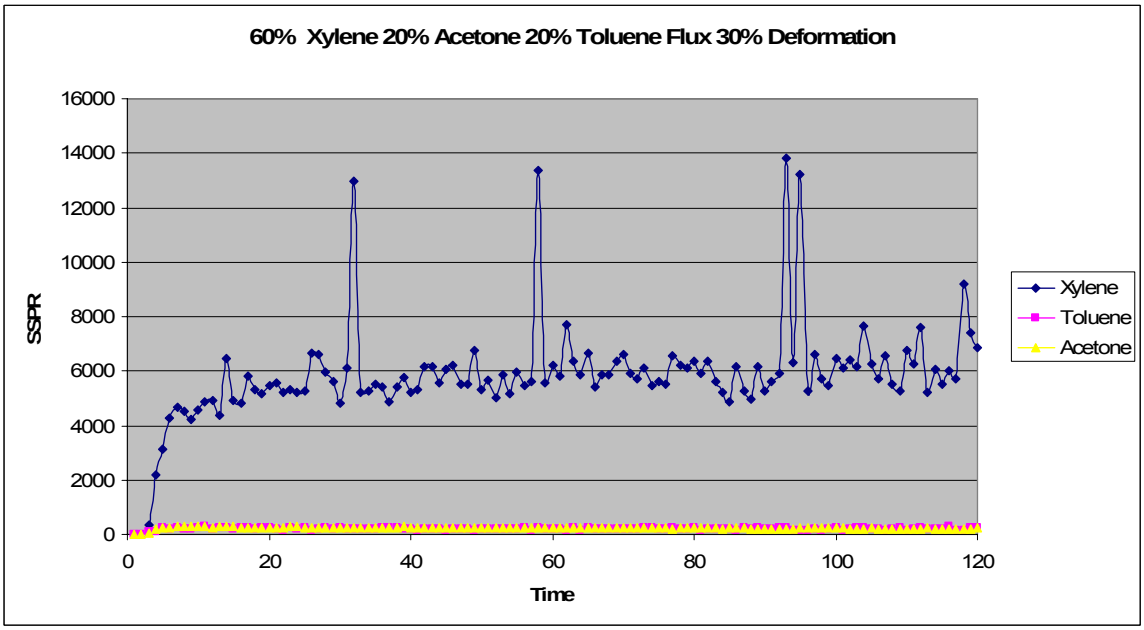

Figure 95: 60% xylene 20% acetone 20% toluene flux 30% deformation

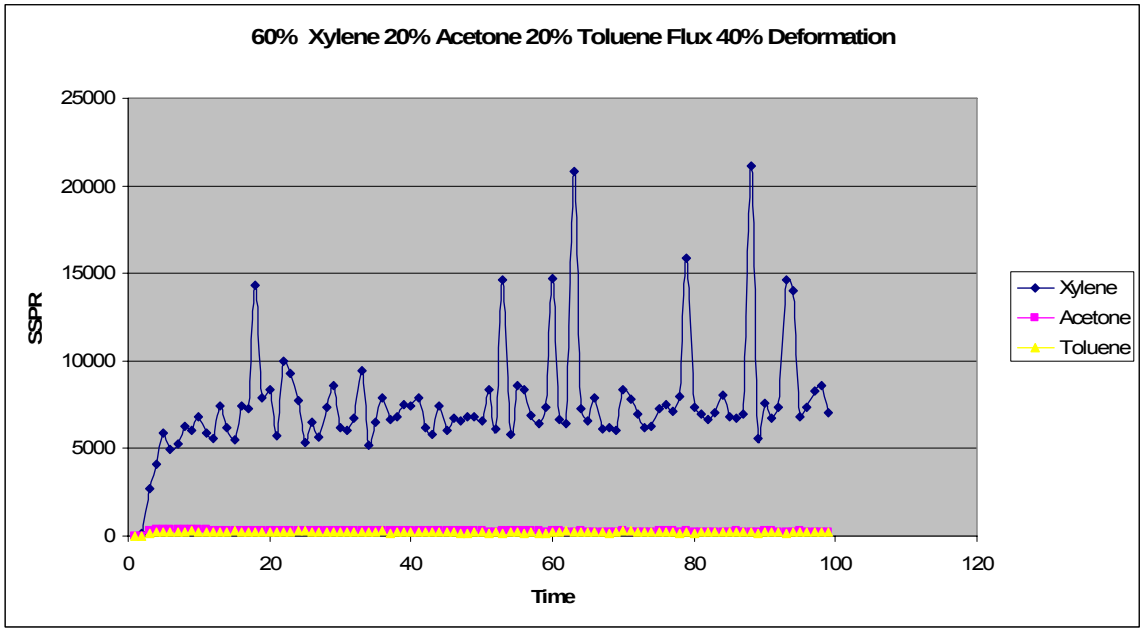

Figure 96: 60% xylene 20% acetone 20% toluene flux 40% deformation

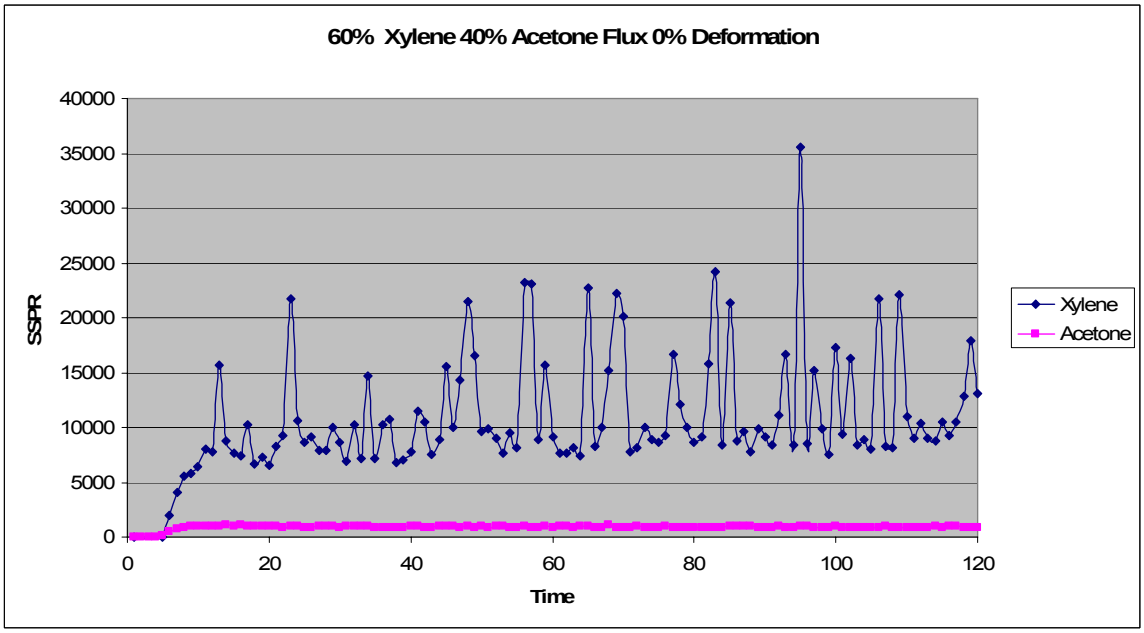

Figure 97: 60% xylene 40% acetone flux 0% deformation

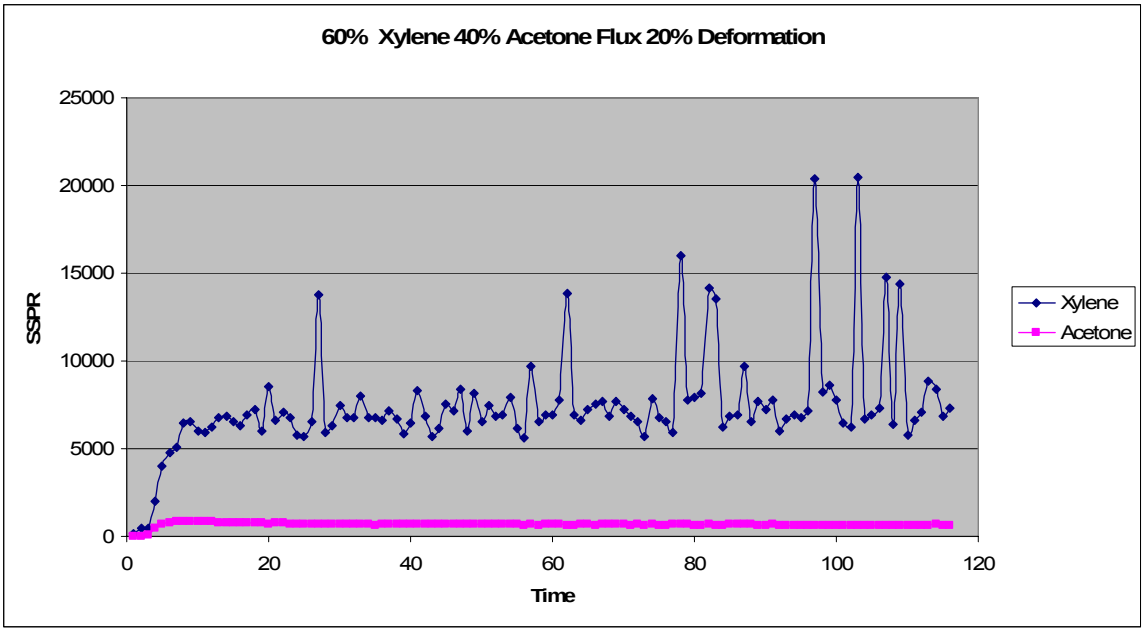

Figure 98: 60% xylene 40% acetone flux 20% deformation

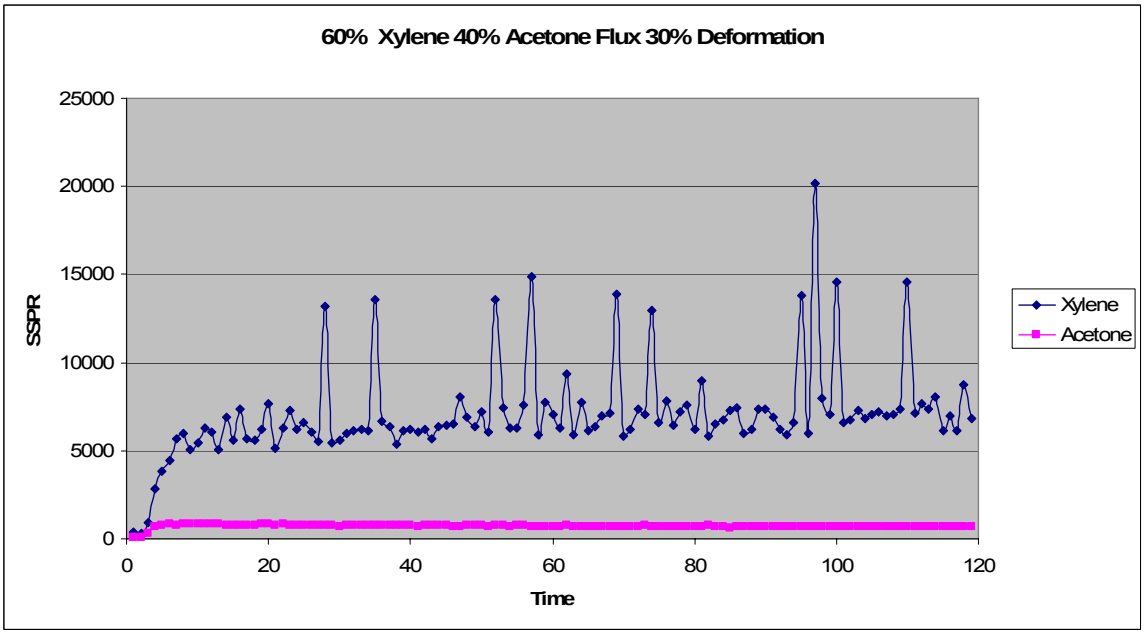

Figure 99: 60% xylene 40% acetone flux 30% deformation

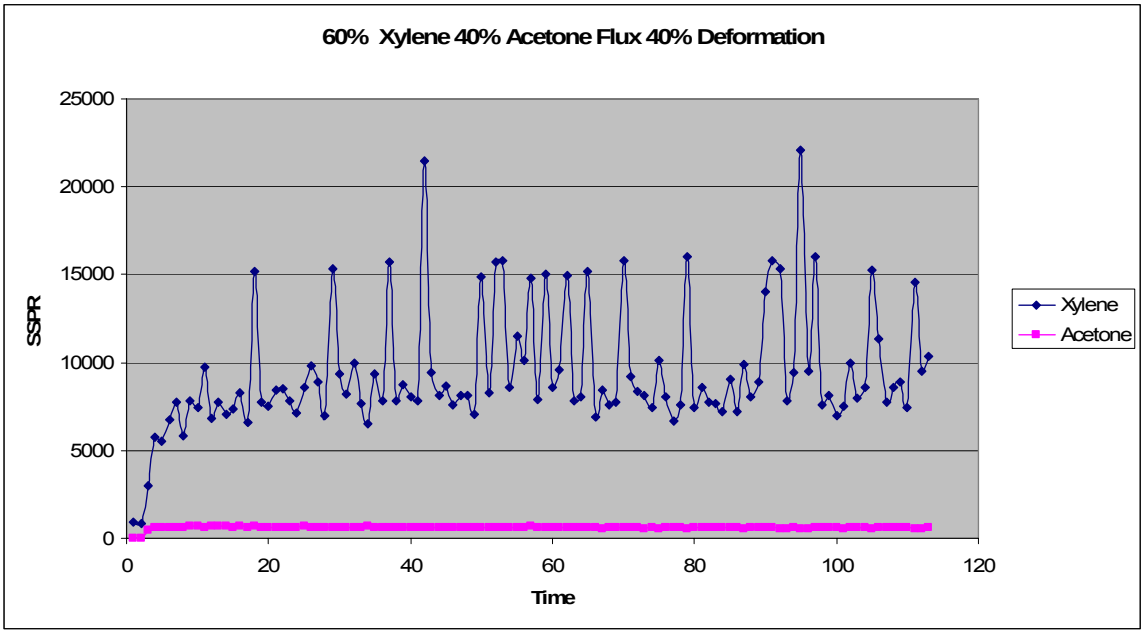

Figure 100: 60% xylene 40% acetone flux 40% deformation

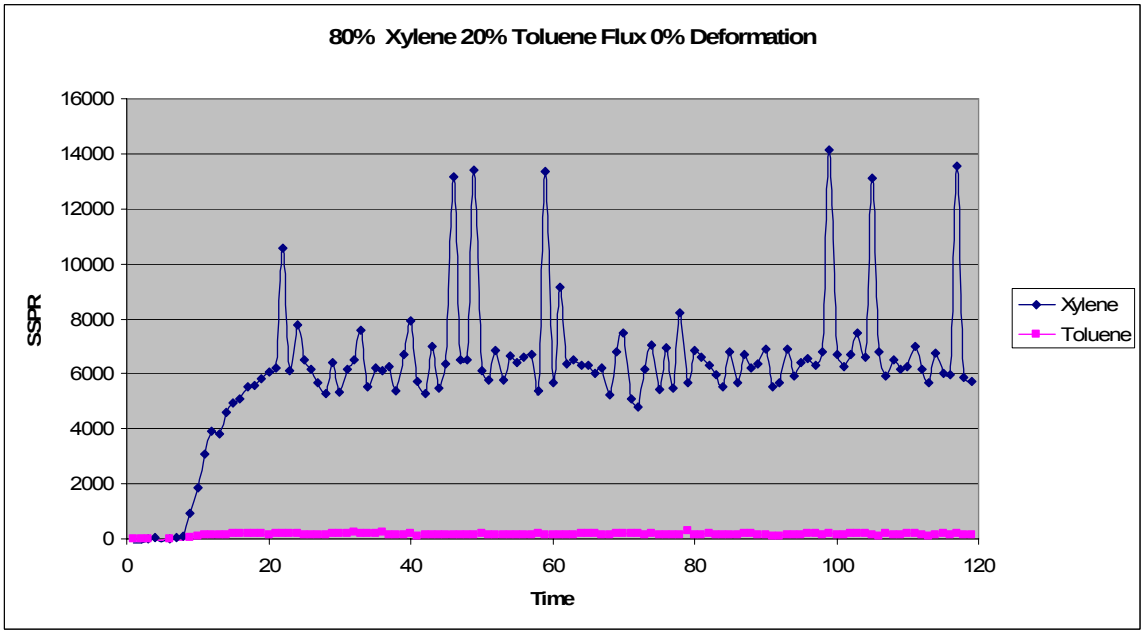

Figure 101: 80% xylene 20% toluene flux 0% deformation

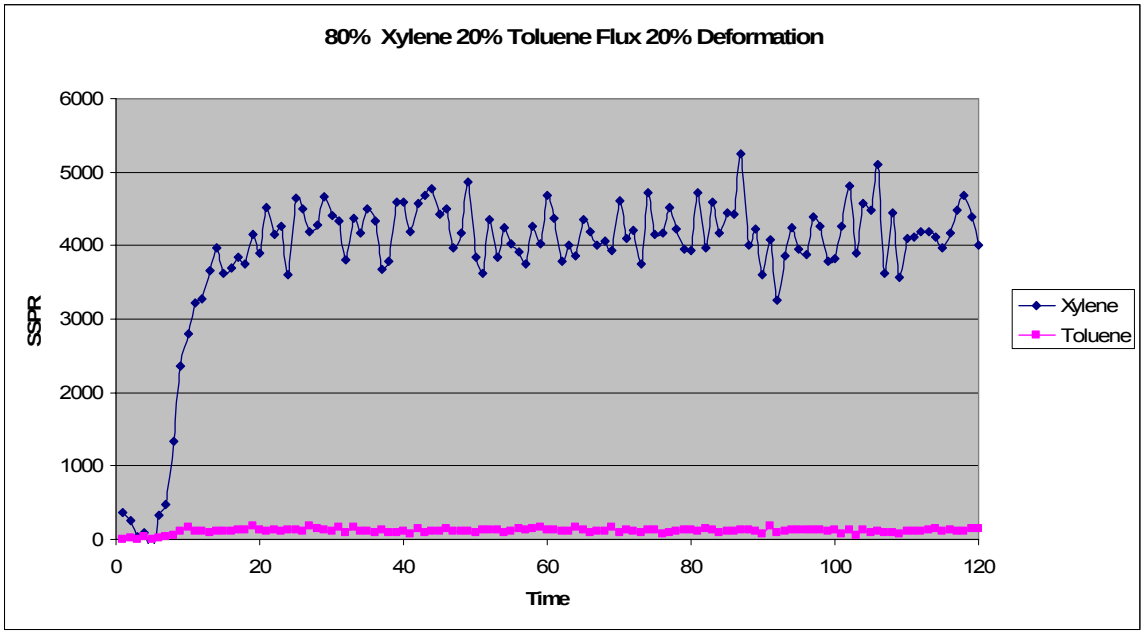

Figure 102: 80% xylene 20% toluene flux 20% deformation

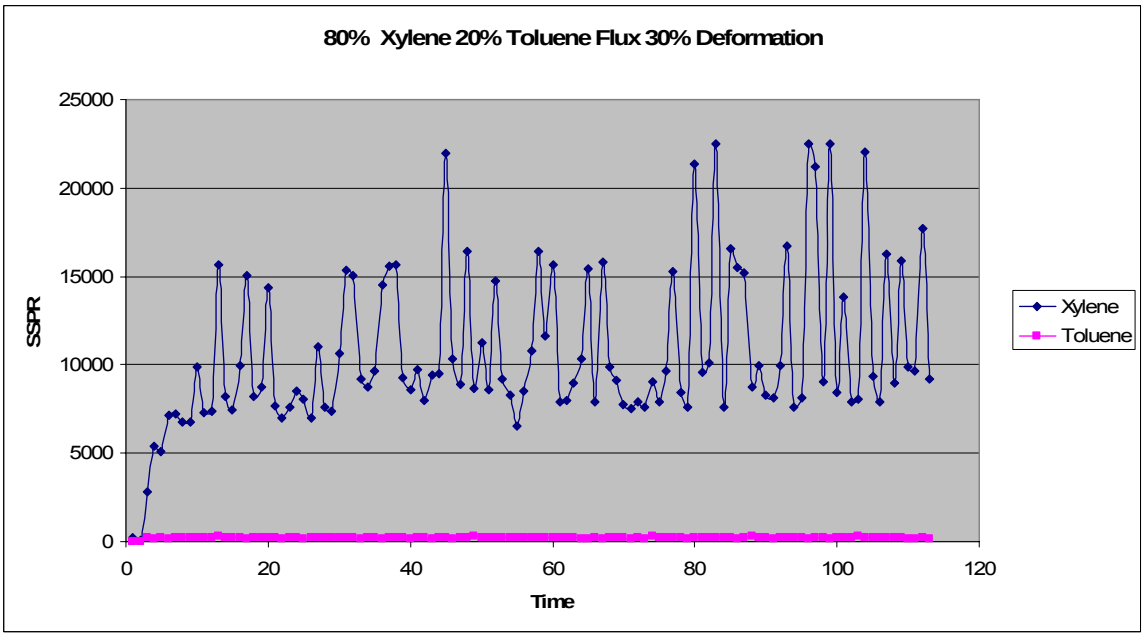

Figure 103: 80% xylene 20% toluene flux 30% deformation

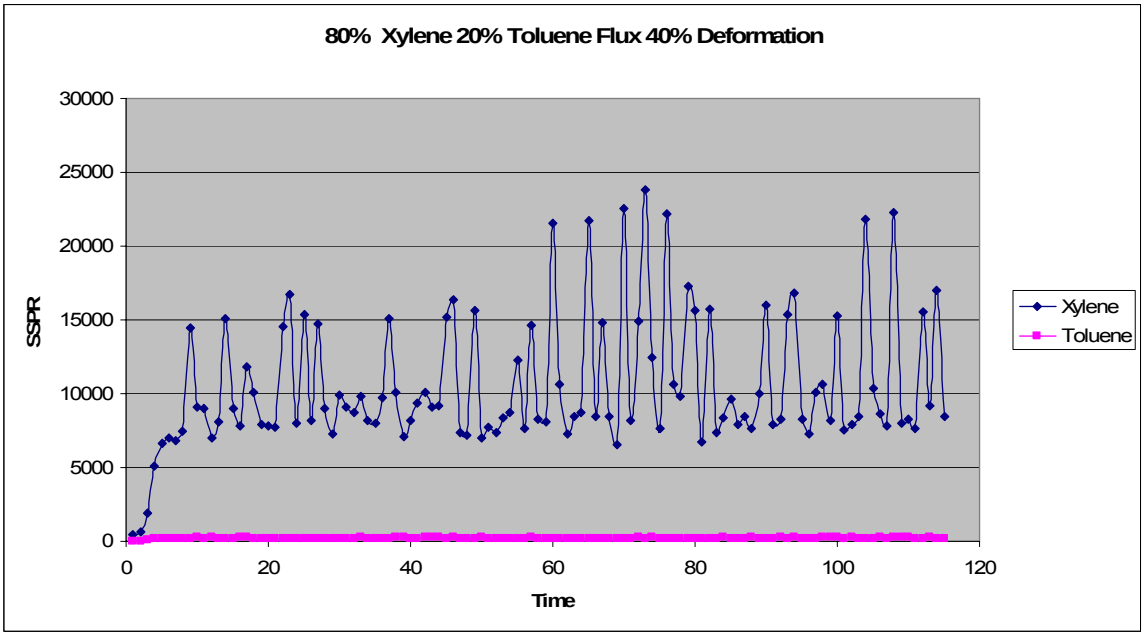

Figure 104: 80% xylene 20% toluene flux 40% deformation

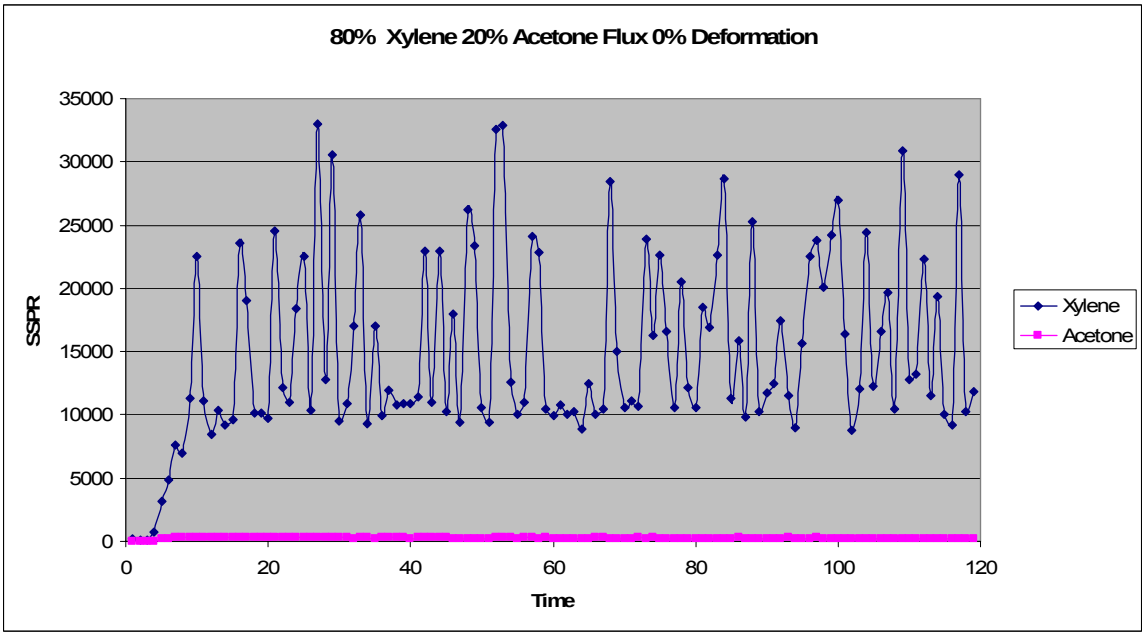

Figure 105: 80% xylene 20% acetone flux 0% deformation

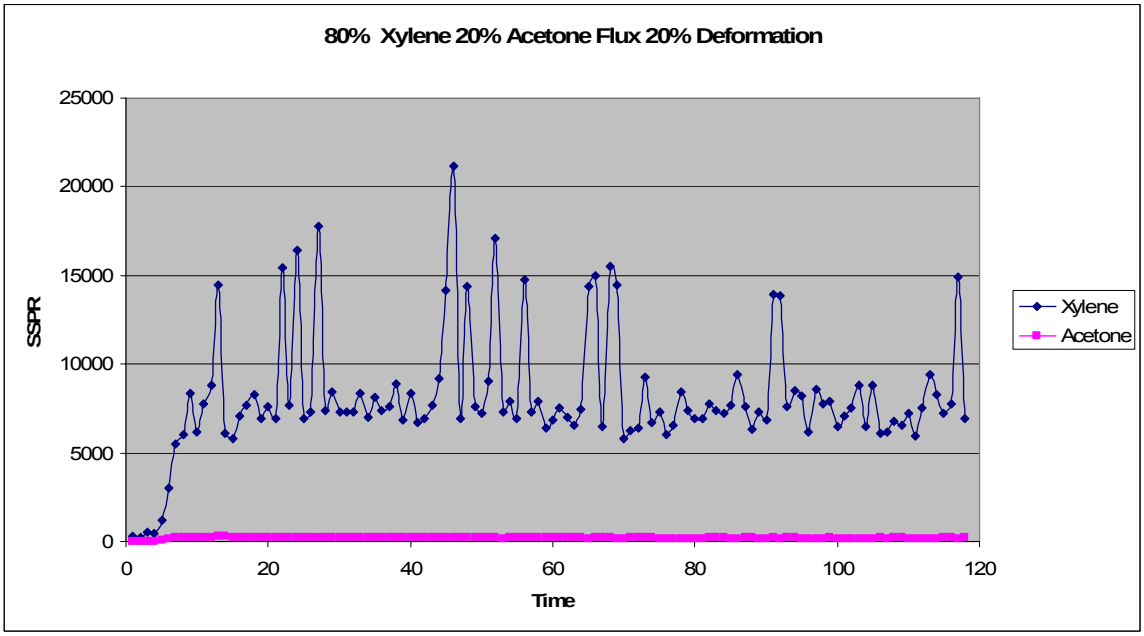

Figure 106: 80% xylene 20% acetone flux 20% deformation

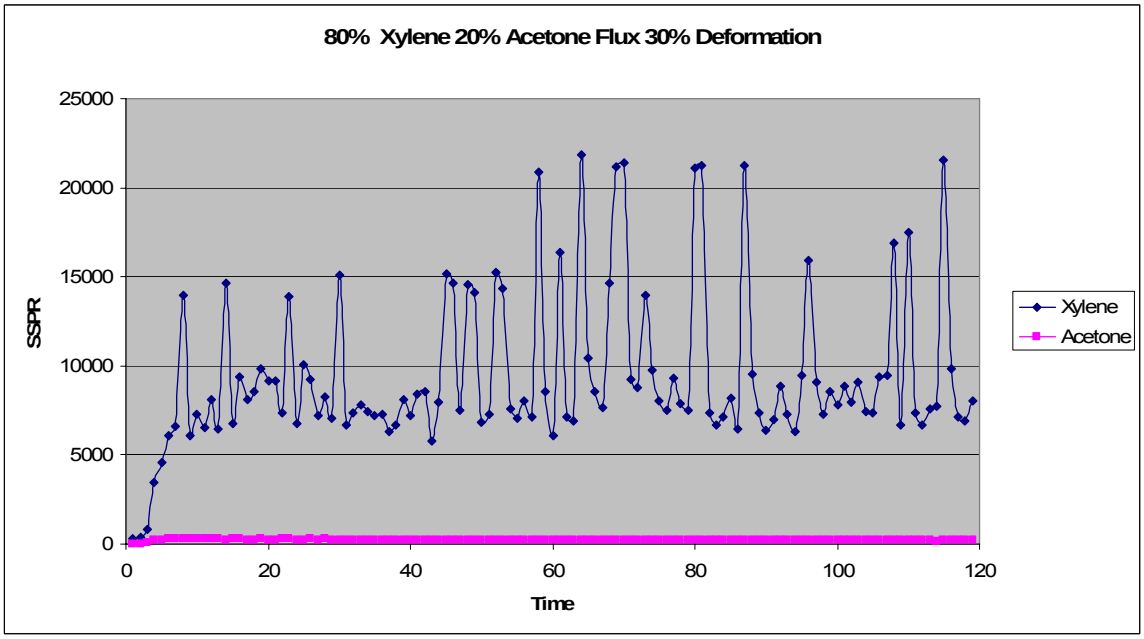

Figure 107: 80% xylene 20% acetone flux 30% deformation

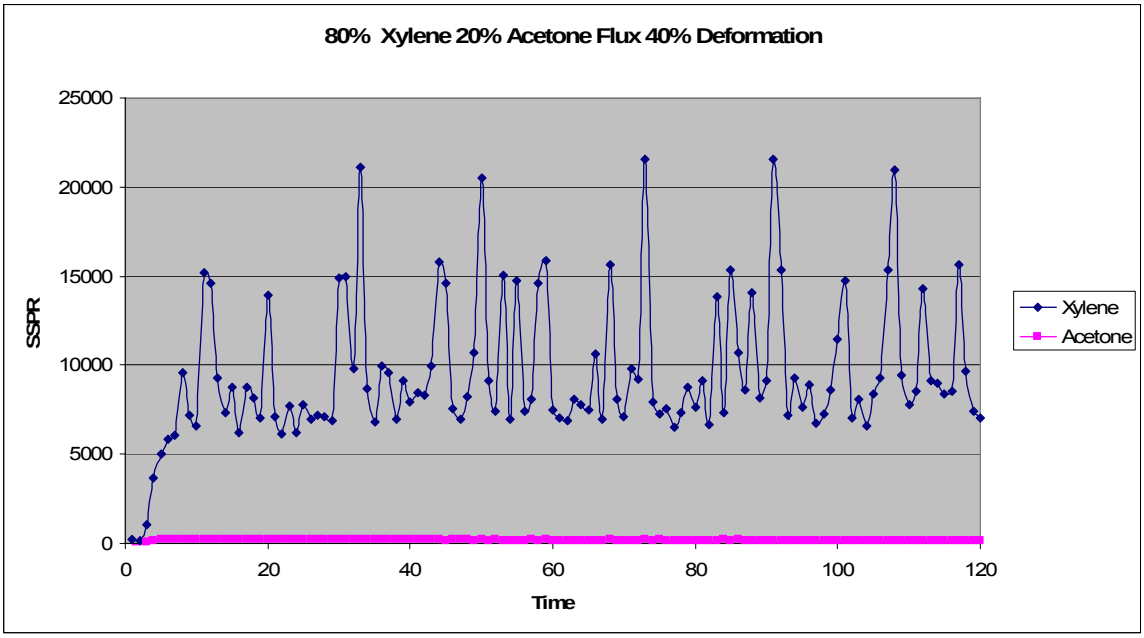

Figure 108: 80% xylene 20% acetone flux 40% deformation

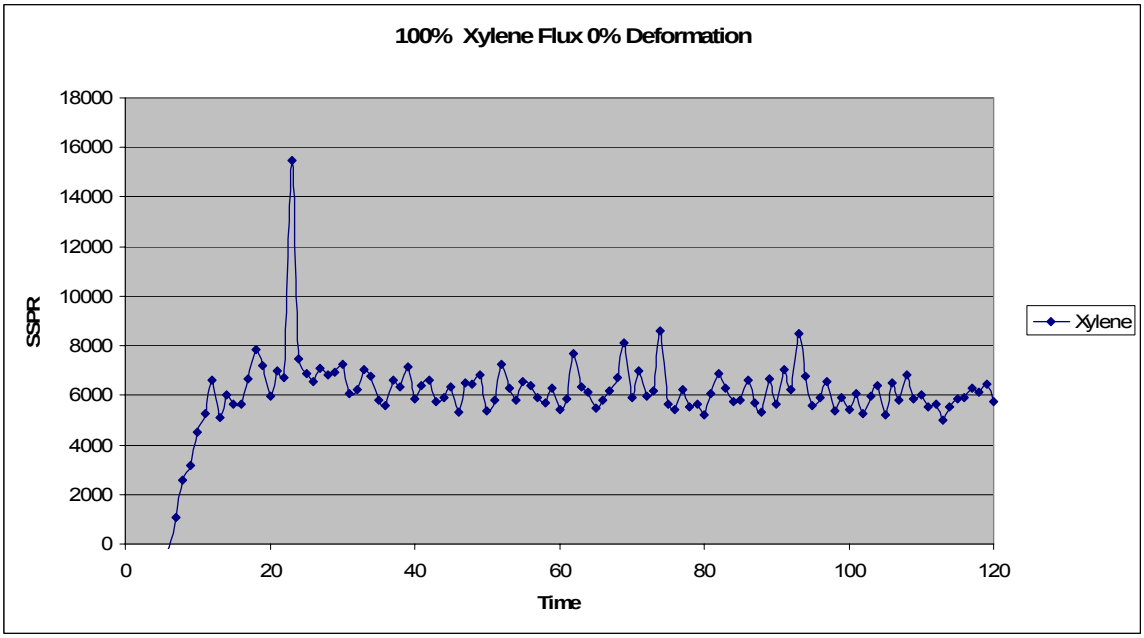

Figure 109: 100% xylene flux 0% deformation

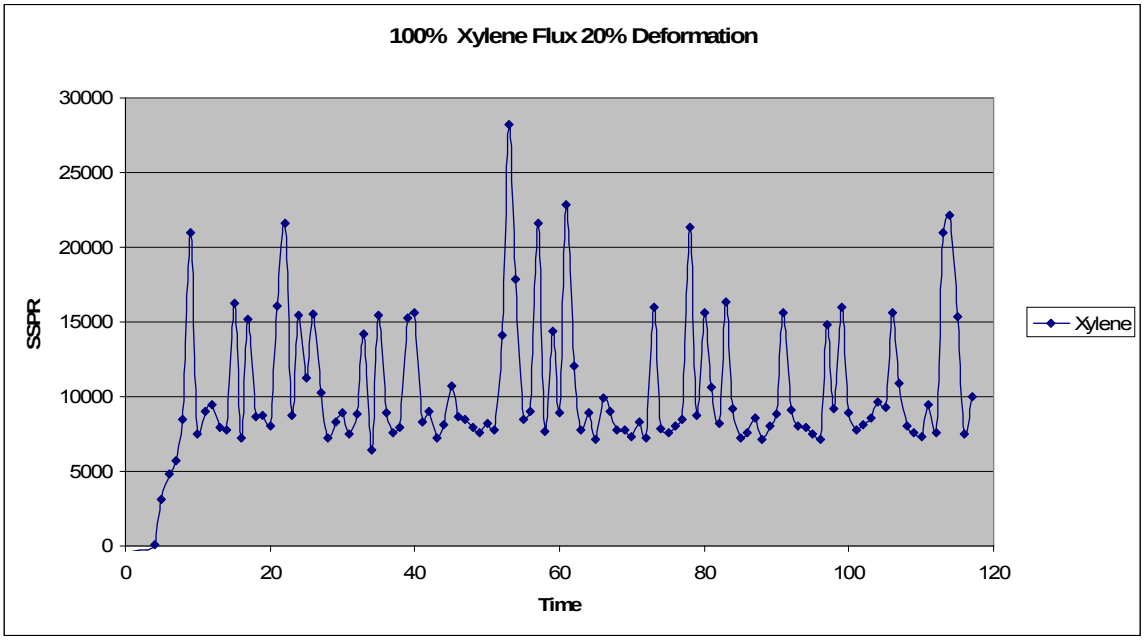

Figure 110: 100% xylene flux 20% deformation

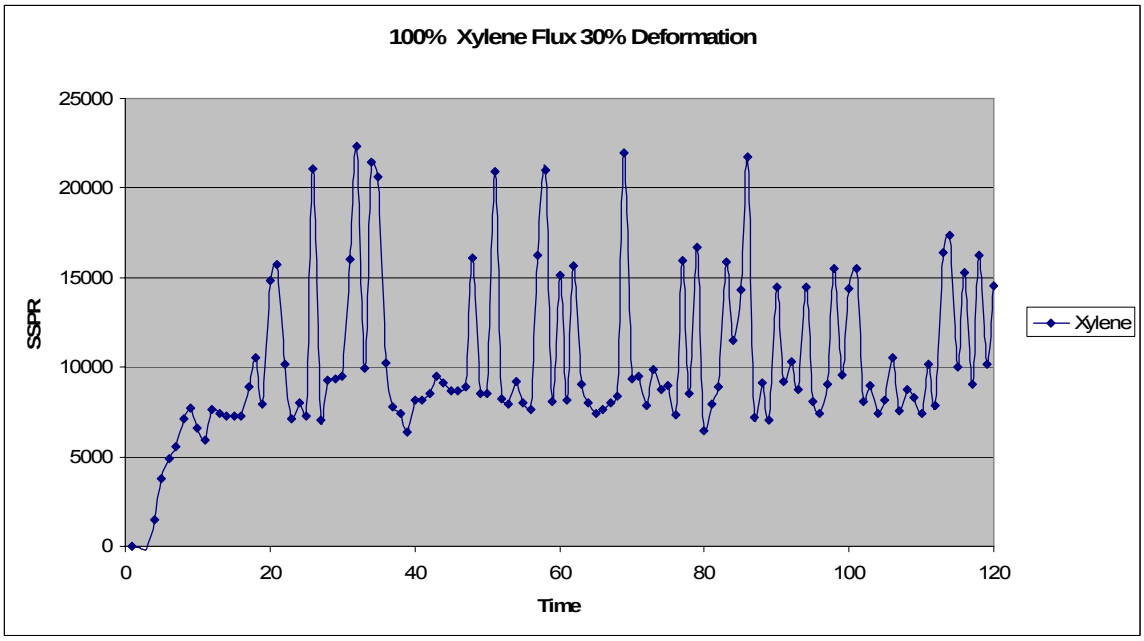

Figure 111: 100% xylene flux 30% deformation

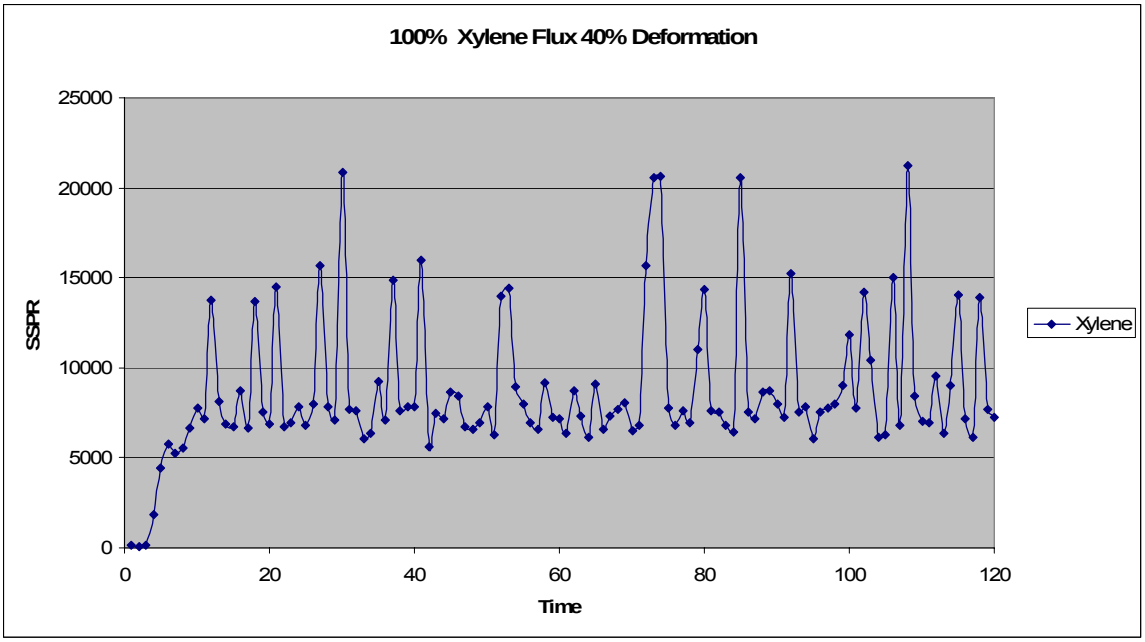

Figure 112: 100% xylene flux 40% deformation